Some aspects of ground station antennas for satellite communication

th e

SOME ASPECTS OF GROUND STATION ANTENNAS FOR SATELLITE COMMUNICATION

by

E.J. Maanders

Technische Hogeschool Eindhoven
Eindhoven Nederland
Afdeling Elektrotechniek

Eindhoven University of Technology
Eindhoven Netherlands
Department of Electrical Engineering

Some aspects of ground station antennas for satellite communication

by

E.J. Maanders

T.H. Report 75-E-60
August 1975

ISBN 90 6144 060

This report has served as a thesis for the degree of Doctor of Applied Science

contents

Summary

Antennas for satellite communication ground stations have to meet very stringent requirements. Apart from the required antenna gain, which in the 4 - 6 GHz band can only be realized with apertures of 25 meter in diameter or more, the need for low noise is essential as well.
In this report the advantages and disadvantages of the front-fed paraboloid and the cassegrain antenna are compared. It appears that the latter has much better noise properties.
In Chapter 3 the problems with regard to blockage in double reflector systems are studied in detail. The influence of the subreflector and its supports on the near-in sidelobes is calculated. Different results may be expected in the $\phi = 0$ and $\phi = 45^0$ plane. Various examples have been worked out with regard to the blockage efficiency.
A theory is further presented indicating that the blockage efficiency may be increased considerably, employing shaped double reflector systems. Shaping both main and subreflector a low subreflector edge illumination may be used, decreasing losses by diffraction and spillover. It further appears that in mismatched shaped systems large first side lobes are to be expected due to over illumination of the edge of the main reflector.
In Chapter 4 the physical optics approximation is discussed as a method to calculate the entire radiation pattern of a reflector antenna. A study has been made of the limitations and errors that occur with this method. Using theoretical truncated feed patterns, the directive gain pattern of the composite antenna system, integrated over the entire sphere does not yield 4π, but more.
In the last chapter the polarization properties of offset antennas are discussed. These properties are very unfavourable with respect to symmetrical front-fed paraboloids and cassegrain antennas.

SAMENVATTING

Op 12 Augustus 1960 bracht de NASA een ballon met een diameter van 30 meter in een baan rond de aarde om na te gaan of telecommunicatie door middel van een dergelijke satelliet mogelijkheden bood. Na de lancering van deze passieve Echo I satelliet heeft de satelliet communicatie zich stormachtig ontwikkeld. De experimenten zijn niet alleen beperkt gebleven tot passieve satellieten,maar ook is onderzoek verricht met aktieve satellieten zoals Courier, Telstar en Relay. Al deze satellieten doorliepen een relatief lage baan rond de aarde in enkele uren.
Aantrekkelijker waren de satellieten die op een hoogte van 35.600 km boven de aarde gebracht konden worden en in precies 24 uur een baan rond de aarde beschreven. Zodoende bewogen ze zich niet t.o.v. een observatiepunt op aarde. Bekend zijn de stationaire satellieten Syncom en vooral Early Bird, welke laatste op 5 april 1965 werd gelanceerd en de eerste commerciele verbinding tot stand bracht tussen Europa en Amerika voor telegrafie, telefonie en televisie. Early Bird wordt tevens beschouwd als de eerste Intelsat satelliet waarvan thans vier generaties zijn gelanceerd.
Ieder land kan deelnemen aan het verkeer via de stationaire satellieten, mits aan een aantal voorwaarden is voldaan. Vooral de eisen die men stelt aan de antenne van het grondstation zijn zeer hoog. Men hanteert hierbij de signaal-ruis verhouding G/T_s, die bij een frekwentie van 4 GHz groter moet zijn dan 40,7 dB. Hierbij stelt G de antennewinst voor en T_s de systeem temperatuur. De antennewinst moet bij 4 GHz tenminste 57 dB bedragen. Een eenvoudige rekensom leert ons dat alleen zeer grote antennes met een apertuur diameter van circa 25 meter hiervoor in aanmerking komen.
De systeem temperatuur T_s is opgebouwd uit twee componenten T_c en T_A. Hierbij is T_c de bijdrage van de microgolf onderdelen, de ontvanger enz., terwijl T_A de antenne temperatuur voorstelt. Omdat T_c meestal tussen 5 en 20 graden Kelvin ligt, afhankelijk van de toegepaste lage ruis ontvanger, is de marge, die overblijft voor T_A om te voldoen aan de eis van $G/T_s > 40,7$ dB bij 4 GHz, erg klein.
Aan de antenne temperatuur T_A wordt vooral bijgedragen door de straling van de hemel die via de hoofdlus van het antenne stralingsdiagram binnen komt, maar tevens straling die via de zijlussen en achteruitstraling van de aarde afkomstig is. De bijdrage van de aarde is erg kritisch, aangezien de aarde beschouwd mag worden als een thermische bron op een temperatuur van circa

290 graden Kelvin, terwijl de hemel op 4 GHz een gemiddelde temperatuur heeft van slechts 15,7^{0}K. Derhalve zal de te ontwerpen antenne zeer lage zijlussen moeten bezitten die de straling van de "warme" aarde zou kunnen ontvangen.
Een van de eerste antennes welke voor een grondstation gebouwd werd,was die in Goonhilly (Engeland). De antenne bestaat uit een paraboloide met een belichter in het brandpunt. Een nadeel van deze opstelling ligt in het feit dat de straling van de belichter, die niet door de parabolische reflector wordt opgevangen ("spillover") gericht is op de "warme" aarde en zodoende aanzienlijk bijdraagt tot T_A. Een ander,meer praktisch nadeel ligt in het feit dat de lage ruis ontvanger direkt achter de belichter in het brandpunt moet worden opgehangen en hierdoor voor service doeleinden moeilijk bereikbaar is. Plaatst men de ontvanger direkt achter de reflector,dan heeft men van de belichter tot de ontvanger lange transmissie leidingen nodig die verliezen hebben en hierdoor extra tot ruis bijdragen. Mede door deze nadelen wordt dit type antenne niet meer gebouwd voor grondstations.
Het eerste grondstation in de Verenigde Staten bevat een zeer grote z.g. hoorn-parabool (Fig. 1.7), een dure constructie, die ondanks de goede antenne eigenschappen uit economische overwegingen niet meer wordt gebouwd.

In Hoofdstuk 2 wordt de cassegrain antenne besproken, een antenne systeem bestaande uit twee reflectoren. De hoofdreflector is een paraboloide en de veel kleinere subreflector een hyperboloide. Het brandpunt van de paraboloide en een van de brandpunten van de hyperboloide vallen samen. Het valt onmiddellijk op dat de cassegrain antenne een belangrijk voordeel heeft boven de parabool antenne die vanuit het brandpunt wordt gevoed. Immers alle "spillover" in het cassegrain systeem is grotendeels gericht op de koude hemel (Fig. 2.4), waardoor dit type antenne belangrijk betere ruis eigenschappen bezit. Bovendien kan de ruisarme ontvanger onmiddellijk achter de hoofdreflector worden gemonteerd met korte transmissieleidingen.
Een nadeel van de cassegrain antenne is de vermindering van de antennewinst doordat de subreflector met de subreflector-steunen een deel van de antenne apertuur blokkeert; bovendien geeft de subreflector aanleiding tot diffractie verliezen die niet meer mogen worden verwaarloosd zolang de diameter van de subreflector niet veel groter is dan de golflengte.
Hoofdstuk 2 geeft allereerst een serie geometrische en optische betrekkingen noodzakelijk voor het ontwerp van een cassegrain antenne. Vervolgens worden enige pagina's gewijd aan de scalaire apertuur methode waarmee de hoofdlus en enige zijlussen van een stralende apertuur c.q. parabool antenne kunnen

worden berekend. Deze methode leent zich ook bijzonder goed voor het berekenen van de antenne winst.
Er wordt aangetoond,dat met behulp van de scalaire apertuur methode tevens de invloed van het stralingsdiagram van de belichter in beschouwing kan worden genomen. Bewezen wordt,dat dit ook mogelijk is in cassegrain antennes. Met behulp hiervan wordt in eerste instantie de invloed op de antenne winst nagegaan van blokkering door de subreflector door middel van een correctieterm. Op analoge wijze kan een correctieterm worden afgeleid,die de invloed op de antennewinst bepaalt, veroorzaakt door diffractie aan de rand van de subreflector. Zodoende is het mogelijk een gesloten betrekking te ontwikkelen waarin het antennerendement beschreven wordt onder invloed van de apertuur belichting, de "spillover", de subreflector blokkering en de subreflector diffractie.
De resultaten van uitgebreide berekeningen tonen aan dat het maximaal haalbare rendement van de cassegrain antenne ongeveer 74% bedraagt. Vergelijkt men dit getal met eerdere berekeningen van Silver voor een parabool antenne met belichter in het brandpunt,dan kan men vaststellen dat de blokkering en diffractie van de subreflector voor practische antenne constructies het antenne rendement met circa 8% verlagen. Bovendien blijkt dat het rendement vrijwel onafhankelijk is van de verhouding brandpuntsafstand/diameter hoofdreflector (F/D) zodat de mechanische constructeur zich op dit punt tamelijk grote vrijheden kan veroorloven.

In hoofdstuk 3 wordt dieper en algemener ingegaan op blokkerings problemen met dubbel reflector antennes, waarbij blijkt dat voor de meeste praktische antenne constructies de invloed van de subreflector steunen niet mag worden verwaarloosd. De steunen, ook wel uithouders genaamd, veroorzaken twee soorten schaduwen op de apertuur,die afkomstig zijn van vlakke en bolvormige golven in het antenne systeem. De schaduwen van de bolgolven hebben hierbij een merkwaardige trapezium-achtige vorm en worden met geometrisch optische methoden bepaald.
Men kan nu de invloed van deze steunen en de subreflector op het antennestralingsdiagram nagaan,door allereerst het stralingsdiagram van de oorspronkelijke,niet geblokkeerde apertuur te berekenen en vervolgens de geblokkeerde delen in tegenfase hierbij op te tellen (het z.g. "zero-field" concept). Het is nu mogelijk met behulp van scalaire methoden na te gaan wat de invloed van de dikte van de uithouders is en de plaats waar deze aan de

hoofdreflector zijn bevestigd, zulks bij verschillende randbelichtingen. Het feit doet zich nu voor, dat de eerste zijlus geen constante waarde heeft en in het $\phi = 0^0$ vlak een hogere waarde heeft dan in het $\phi = 45^0$ vlak. Er is nog onderzoek gaande hoe het gedrag van de eerste zijlus is in andere ϕ vlakken en tevens dat van de tweede zijlus. De resultaten zijn belangrijk omdat men met deze wetenschap, door de antenne om zijn as te laten draaien, in bepaalde richtingen een lager zijlussen patroon kan bewerkstelligen.
In het tweede deel van hoofdstuk 3 wordt een diepgaande theoretische beschouwing over blokkering gegeven. Vooral wordt nagegaan wat er met het vermogen gebeurt, dat geblokkeerd wordt. Men kan dan inzien dat dit vermogen in de zendsituatie van de antenne op willekeurige wijze de apertuur verlaat en zal bijdragen tot verre zijlussen gepaard gaande met een vermindering van het antenne rendement. Vervolgens wordt het begrip relatief blokkerings-rendement gedefinieerd, waarna dan bewezen wordt dat dit voor uniforme apertuur belichting $(1 - B/A)^2$ bedraagt, waarbij A de niet geblokkeerde apertuur voorstelt en B het oppervlak van de geblokkeerde delen.
Een theorie wordt nu ontwikkeld waarbij aangetoond wordt dat het geblok-keerde vermogen P_B, dat normaal gesproken verloren gaat en het zijlusniveau nadelig beïnvloedt, nuttig kan worden toegevoerd aan de stralende antenne apertuur. Bewezen wordt dat het blokkerings rendement dan stijgt tot $(1 - B/A)$ als maximum voor uniforme apertuur belichting.
Inhet laatste deel van hoofdstuk 3 wordt het blokkerings rendement van dubbel reflector systemen behandeld als functie van verschillende variabelen die ook gebruikt zijn bij de zijlus bepaling en levert zodoende voor de praktijk zeer bruikbare gegevens.

Meerdere malen is het antenne stralingsdiagram ter sprake gekomen en is opgemerkt dat scalaire methoden alleenmaar geschikt zijn voor de berekening van de hoofdlus en de nabije zijlussen. Wil men echter de antenne temperatuur juist kunnen voorspellen dan moet men volgens formule 1.8 inzicht hebben in het totale stralingsdiagram $G(\theta,\phi)$.
In hoofdstuk 4 wordt op een van de methodes waarmede men $G(\theta,\phi)$ kan bepalen uitvoerig ingegaan. De keuze is hierbij gevallen op de physisch optische benadering (P.O.) van de stromen op het oppervlak van de reflector. De stroomdichtheid $\bar{K}$ wordt hierbij bepaald door de uitdrukking $\bar{K} = 2(\bar{n} \times \bar{H}_i)$ op het belichte deel van de reflector. $\bar{H}_i$ is hierbij het op de reflector invallend magnetisch veld en $\bar{n}$ de normaalvector op het oppervlak. Op de schaduw-

zijde van de reflector worden de stromen nul verondersteld.
Deze methode is met wisselend sukses door verschillende onderzoekers reeds toegepast hetgeen uitvoerig wordt toegelicht.
Allereerst is een studie gemaakt van de polarisatie eigenschappen van de toe te passen antenne belichters. De keuze is gevallen op een bron van Huygens omdat dit de vergelijkingen sterk vereenvoudigt (dubbele integralen kunnen door middel van Besselse funkties herleid worden tot integralen met een variabele) en ook, omdat vele praktische belichters polarisatie eigenschappen vertonen,die veel overeenkomst vertonen met die van een bron van Huygens.
Men kan nu betrekkingen afleiden die het veld voorstellen dat door de reflector wordt gereflecteerd. Telt men bij dit laatste veld dat van de belichter op dan verkrijgt men het totale diagram $G(\theta,\phi)$, later herleid tot praktische vormen voor computer berekeningen. De methode is geldig voor alle cirkelvormig symmetrische reflectoren.
Enige speciale gevallen kunnen zonder een computer worden nagerekend. Hierbij blijkt dat P.O. voor een uniform belichte parabool antenne niet alleen in de hoofdrichting correcte resultaten oplevert doch tevens voor de achteruitstraling $\theta = \pi$. In deze richting is de straling gelijk aan die van de belichter, waaruit dan volgt dat de z.g. vlek van Poisson alleen afhankelijk is van de openingshoek van de parabool Ψ.
Vervolgens is een literatuur studie gemaakt van de fouten en beperkingen die P.O. geeft. Hier is erg veel over geschreven en de meningen lopen sterk uiteen. Erg veel bezwaar bestaat tegen de wijze waarop de stroomdichtheid aan de reflector rand plotseling naar nul nadert en dit aan de schaduwzijde blijft. Merkwaardig is echter dat ondanks de verkeerde benadering van de stroom aan de rand de berekende stralings diagrammen goede overeenkomst vertonen met gemeten diagrammen. De meesten zijn het er wel over eens dat P.O. betere resultaten oplevert naarmate de reflector diameter veel groter wordt dan de golflengte.
In het navolgende wordt eerst nagegaan onder welke omstandigheden P.O. zeker verkeerde uitkomsten zal opleveren. Hiertoe zijn een aantal mathematische benaderingen van belichter diagrammen toegepast. Het resulterende antenne diagram $G(\theta,\phi)$ blijkt onjuist te zijn indien belichters worden toegepast met afgeknotte stralingsdiagrammen. Per definitie immers, moet $G(\theta,\phi)$ geintegreerd over de gehele bol 4π opleveren. Heel duidelijk wordt de onjuistheid gedemonstreerd bij een door een afgeknotte belichter (Fig. 4.3) uniform belichte parabool antenne. De afwijkingen van 4π bedragen soms meer

dan 10%.
Berekent men nu $G(\theta,\phi)$ van de reflectoren belicht met een cosinus funktie, die maar zeer langzaam afloopt naar nul, dan zijn de afwijkingen van 4π verwaarloosbaar klein.
De invloed van de reflector diameter wordt duidelijk indien deze kleiner wordt. Eerst bij $D \geq 25\lambda$ worden de verschillen t.o.v. 4π aanvaardbaar. De invloed van de reflector randbelichting op de resultaten is nauwelijks merkbaar zelfs niet bij hoge waarden als - 5.5 dB.
Het integreren van het antenne stralingsdiagram over de gehele bol lijkt een machtig wapen te zijn om controle op de berekeningen uit te oefenen. Het is zeer merkwaardig dat dit in de literatuur nergens staat vermeld en dat klaarblijkelijk de meeste onderzoekers deze methode niet toepassen. Echter, indien de integraal 4π oplevert is nog geen bewijs geleverd dat alle verre zijlussen goed zijn uitgerekend, omdat vele zijlussen een dusdanige lage waarde kunnen hebben dat ze niet of nauwelijks tot de integraal $\int_{4\pi} G(\theta,\phi)d\Omega$ bijdragen.
Een definitieve uitspraak lijkt pas mogelijk indien de berekeningen zeer precies vergeleken kunnen worden met metingen. Dit is niet goed realiseerbaar aangezien het gemeten diagram altijd de invloed bevat van blokkerende obstakels, welke invloed op het gehele antenne diagram tot nu toe niet berekend kon worden.

Zoals eerder vermeld,wordt het antennerendement van een cassegrain antenne nadelig beinvloed door blokkering en diffraktie van subreflector en uithouders. Verder wordt de randbelichting meestal zo gekozen,dat de antennewinst maximaal wordt, zodat de apertuurbelichting vaststaat en geen middelen meer aanwezig zijn om het rendement te verhogen of de zijlussen te verlagen. Sedert enige jaren is een methode bekend (Galindo) waarbij men door het toepassen van een aantal optische en geometrische betrekkingen bij dubbel reflector systemen een willekeurige apertuurbelichting kan voorschrijven. In hoofdstuk 5 wordt een voorbeeld uitgewerkt met als voorwaarde uniforme belichting van de apertuur van de hoofdreflector. Tevens wordt aangegeven op welke wijze het subreflector blokkerings rendement kan worden verhoogd zoals theoretisch voorspeld in hoofdstuk 3. Het blijkt dat dit op zeer eenvoudige wijze kan plaatsvinden. De hoofdreflector en de subreflector zijn nu geen zuivere paraboloide resp. hyperboloide meer. De subreflector blijkt bovendien zwak kegelvormig te zijn rondom de symmetrie-as. Indien men geen poging doet het blokkeringsrendement van de subreflector te verhogen,dan is

de subreflector niet kegelvormig.
Om de invloed van de uithouders op de blokkering te verminderen zijn meer ingrijpende vormveranderingen van hoofd- en subreflector noodzakelijk. Theoretisch is het mogelijk de blokkering door bolvormige golven geheel te doen verdwijnen. Dit probleem is nog in studie.
Met behulp van P.O. worden vervolgens de stralingsdiagrammen van aangepaste subreflectoren berekend en vergeleken met die van een hyperboloide. Zoals uit de stralingsdiagrammen blijkt, treedt verlaging van de veldsterkte op in het geblokkeerde centrum van de hoofdreflector apertuur. Deze verlaging is echter afhankelijk van de subreflector diameter en bedraagt voor $D_s = 50\lambda$ bijna 20 dB. Het vermogen, dat door de aangepaste subreflectoren wordt geblokkeerd, blijkt aanzienlijk minder te bedragen dan bij een zuivere hyperboloide, terwijl de kegelvormige subreflector duidelijk favoriet is t.o.v. de niet kegelvormige aangepaste subreflector.
Met als uitgangspunt uniforme belichting over de hoofdreflector apertuur ontstaan subreflectoren die na reflectie een te hoog deel van het vermogen aan de hoofdreflector voorbij stralen (hoofdreflector spillover). Het is daarom verstandiger om althans naar de rand van de hoofdreflector een lagere veldsterkte voor te schrijven. Hoe laag deze randbelichting moet zijn en welk deel van de apertuur men wel uniform mag belichten hangt samen met het zoeken naar een maximale G/T_s verhouding. Dit onderwerp is nog in studie.
In het algemeen kan men vaststellen dat het principe van dubbel reflector systemen met aangepaste reflectoren grote voordelen biedt ten opzichte van de klassieke cassegrain antenne. Spillover en apertuur belichting kunnen onafhankelijk van elkaar gekozen worden. Uniforme of gedeeltelijk uniforme apertuurbelichting zal het rendement doen stijgen terwijl men aan de subreflector zeer weinig spillover verliezen kan verkrijgen door een lage randbelichting aldaar te kiezen. De lage subreflector randbelichting vermindert bovendien de subreflector diffractie verliezen.
Het laatste deel van hoofdstuk 5 behandelt aangepaste dubbel reflector systemen waarin een andere belichter wordt geplaatst dan die waarvoor het antennesysteem is ontworpen. Het blijkt nu, dat het rendement een maximum vertoont voor belichters waarvan de hoofdlus een geringere breedte heeft dan die van de oorspronkelijke belichter. Vermindert men de hoofdlusbreedte nog meer, dan daalt de randbelichting van de hoofdreflector. Indien echter belichters worden toegepast die een bredere hoofdlus hebben dan de oorspronkelijke belichter dan ontstaat het gevaar voor overbelichte hoofdreflector randen met een ongewenste invloed op het

zijlusniveau. Deze theorie is zeer belangrijk voor aangepaste dubbel reflector systemen die een belichter gebruiken met een frekwentie afhankelijk stralingsdiagram.

Alle tot nu toe besproken antenne typen hebben in meer of mindere mate last van blokkering door belichter, subreflector en uithouders. In het laatste hoofdstuk echter,worden asymmetrische antennevormen besproken,die dit euvel niet hebben. De reflector wordt hierbij gevormd door een deel van een paraboloide dat ontstaat na doorsnijding met een kegel. Naast deze open parabool antenne is ook een variant bekend met een subreflector, de open cassegrain antenne. Aan de hand van Fig. 6.2 kan men vaststellen dat de stralengang niet gehinderd wordt door blokkerende obstakels.
Hoofdstuk 6 memoreert allereerst de geometrie van deze antennes en toont tevens aan dat de maximaal bereikbare winstfaktor in dezelfde orde van grootte ligt als bij symmetrische parabool antennes.
Het belangrijkste deel van dit hoofdstuk is echter gewijd aan de kruis-polarisatie eigenschappen van deze antennes. Sedert er plannen bestaan om frekwenties boven 10 GHz tweemaal te gebruiken met orthogonale polarisaties is het onderzoek op dit punt aanzienlijk toegenomen zoals uit de literatuur moge blijken.
In het hier beschreven onderzoek wordt aangetoond dat door het berekenen van elektrische velden in de apertuur van de (hoofd)reflector uitdrukkingen kunnen worden afgeleid voor het polarisatie rendement van de parabool antenne, de klassieke cassegrain antenne, en tevens van de open parabool en open cassegrain antenne. Vooral de laatste antenne geeft aanleiding tot gekompliceerde betrekkingen.
Als belichter zijn zowel de elektrische dipool als de bron van Huygens gebruikt, waarvan bekend is dat de eerste bij een parabool antenne leidt tot zeer slechte polarisatie eigenschappen, terwijl het polarisatie rendement van een parabool antenne belicht met een bron van Huygens gelijk is aan 1.
Na uitvoerige berekeningen blijkt dat het polarisatie rendement van de klassieke cassegrain antenne belicht door een elektrische dipool aanzienlijk beter is dan dat van een parabool antenne en beter wordt naarmate de vergrotingsfaktor M (zie hoofdstuk 2) groter wordt. Belicht door een bron van Huygens wordt ook hier het polarisatie rendement 1.
De asymmetrische antennes gedragen zich totaal anders. Het lijkt dat het polarisatie rendement zeer slecht is en te vergelijken is met een symmetrische parabool antenne belicht door een elektrische dipool. Het is opvallend

dat het type belichter, elektrische dipool of bron van Huygens vrijwel geen een rol speelt en dat het rendement grotendeels bepaald wordt door de z.g. "offset" hoek Ψ_0. Voor satelliet communicatie boven 10 GHz lijken deze asymmetrische antennes nauwelijks bruikbaar.
Een praktisch voorbeeld toont tenslotte aan dat een open golfpijp in de TE_{10} mode polarisatie eigenschappen vertoont die de eigenschappen van een bron van Huygens benaderen. Tevens doet zich het interessante feit voor dat de polarisatie eigenschappen van een symmetrische parabool antenne met dit type belichter aanleiding geeft tot een polarisatie rendement dat afhankelijk is van de frekwentie.

1. GENERAL REVIEW

1.1. Introduction

On August 12, 1960, a 100-foot diameter spherical balloon was placed in orbit around the earth by the National Aeronautics and Space Administration (NASA) to study the feasibility of providing long distance communication by means of reflection from orbiting earth satellites. Since the launch of this Echo I satellite [53], this type of communication has developed tremendously. The Echo I and later on the Echo II satellite [58], launched January 25, 1964, using the spherical balloon as a passive reflector, had as main objectives to demonstrate two-way voice communications between the east and west coast of the USA and to study the propagation of the medium, including effects of the atmosphere, ionosphere and balloon in the microwave band. Several experiments with active satellites had meanwhile been carried out. The first experimental satellite was called Score , launched December 18, 1958, which had a lifetime of only 12 days verifying voice communication and teletyper transmission. The next more advanced satellite was the Courier [107] for voice, data and fascimile transmission and was launched on October 4, 1960. Better known, however, are the experiments carried out by the active satellites Telstar [17] and Relay [61] launched July 10, 1962 and December 13, 1962 respectively, both in an elliptic orbit round the earth. These satellites provided the first experience with wideband active repeaters in orbit and also data on the reliability in space, apart from the communication experiments, including TV transmission.

A satellite in a 35,600 km altitude equatorial orbit completes one orbit in exactly 24 hours. If such a satellite is moving in the direction of rotation of the earth it will remain stationary with respect to an arbitrary point of observation on the earth. The stationary 24-hour communication satellite appeared to be attractive, since it eliminated many ground station problems, such as tracking, hand-over of communication from one satellite to another and coverage, as met with non-stationary satellites.

The first stationary satellite was Syncom [36, p.336] . It was launched July 26, 1963, and followed on April 5, 1965, by the first commercial satellite Early Bird [78], resulting in a commercial telecommunication link between North America and Europe. This link was used for normal telegraphy, telephony and TV purposes.

Since 1969 Early Bird is no longer in use. Early Bird was the first of the generations of Intelsat Satellites [56], four generations of which have now been launched.

The Intelsat satellites are part of a global system of telecommunication on a commercial basis called "International Telecommunication Satellite Consortium" (Intelsat). If a country wants to participate in this type of traffic, it has to meet the requirements of Intelsat's governing body, the Interim Communications Satellite Committee (ICSC). Especially the antennas for the ground stations have to meet very stringent requirements [37]. Apart from the required antenna gain, which in the 4-6 GHz band can only be realized with apertures of 25 m in diameter or more, the need for low noise is essential. Noise is introduced by the microwave receiver itself, and further contributions arise from losses in the waveguide components. Moreover, the noise is increased by external sources such as thermal radiation from the sky and via sidelobes and back radiation, also from the ground. Especially the contribution due to ground radiation is critical, since the ground can usually be regarded as a thermal source of 290 K, while the sky radiates at much lower average temperatures. The sky radiation reaches a minimum at 4 GHz, where the average temperature is only 15.7 K [23]. Therefore, an antenna has to be designed with a gain as high as possible and a noise temperature as low as possible.

A low antenna temperature can be obtained by very low sidelobes, thus receiving only little radiation from the "hot" earth, while the antenna main beam points to the "cold" sky.

It has become common practice in satellite communications to introduce the "figure of merit", which is defined as the ratio of antenna gain and the system noise temperature T_s. This G/T_s ratio therefore depends not only on the reflector system and feed, but also on the environment in which the antenna operates, the elevation of the antenna, and the noise in the remainder of the receiver system.

Owing to the high cost of antennas for ground stations the same antenna is used for reception as well as for transmitting purposes. The remarks made above apply to some extent also to the use of the antenna for transmitting purposes. As a matter of fact, in the latter case a high antenna gain is wanted, while the radiation in unwanted directions must be low to avoid interference with stations operating on the same frequency, such as for radio relay systems.

In the case the antenna gain is too low for transmission, the transmitter power can be increased to some extent, so that the antenna gain is not so critical for transmission as for reception purposes. Naturally, it is almost impossible to increase the transmitter power on board the satellite, when the satellite is in orbit.
The present frequency bands allocated to satellite communication are 3.7 - 4.2 GHz for the reception of satellite signals on earth and 5.925 - 6.425 GHz for transmitting to the satellite. In the near future frequency bands above 10 GHz will also be used for satellite communication, viz. 10.95 - 12.5 GHz for space-to-earth communications and 12.5 - 14.5 GHz for earth-to-space communication. Higher frequency bands have meanwhile been allocated for the purpose of satellite communication as well. Generally, the requirements in these frequency bands are more or less similar to those at 4 and 6 GHz. An exception has probably to be made as to the spurious radiation from the ground. At 4 GHz this contributes considerably to the antenna noise temperature, but at frequencies over 10 GHz the average sky temperature is higher, viz. 20.5 K at 12 GHz compared with 15.7 K at 4 GHz [111], so that the contribution from the ground has less influence. Between 10 GHz and 100 GHz there are a number of frequency bands, where the sky temperature is 290 K [50], so that sidelobes and back radiation are less important in this respect. It must be pointed out, however, that in the future the near angle sidelobes of an antenna ground station for satellite communications may become critical if they point to closely spaced geostationary communication satellites.

1.2. The antenna gain

Two closely related definitions for the antenna gain are known [52].
The directive gain in a given direction θ,ϕ is defined as the ratio of the power $P(\theta,\phi)$ in that direction per unit solid angle to the average power radiated per unit solid angle or

$$G_d(\theta,\phi) = \frac{P(\theta,\phi)}{P_R/4\pi} \tag{1.1}$$

where θ and ϕ are spherical coordinates [Fig. 1.1.] and P_R the total power radiated by the antenna. The directivity of an antenna is its maximum directive gain. The power gain of an antenna in a specified direction

θ,ϕ is 4π times the ratio between the power $P(\theta,\phi)$ in that direction per unit solid angle to the total power P_T accepted by the antenna or

$$G_p(\theta,\phi) = \frac{P(\theta,\phi)}{P_T/4\pi} \tag{1.2}$$

In the direction of the maximum value the power gain is termed "maximum power gain". The radiation efficiency of an antenna is defined by

$$\frac{G_p(\theta,\phi)}{G_d(\theta,\phi)} = \frac{P_T}{P_R} \tag{1.3}$$

For many antennas the antenna dissipation losses may be neglected, giving a radiation efficiency of nearly 100 %, which explains the fact that the term antenna gain is used quite generally. As we concentrate in this work on reflector antennas only, it is useful to mention that, neglecting losses, the maximum gain of a uniformly illuminated paraboloid reflector may be written as

$$G = \left(\frac{\pi D}{\lambda}\right)^2 \tag{1.4}$$

which is explained in any text on antennas [117, p.233]. D is the reflector diameter, λ the wavelength. Generally, the maximum gain will not be obtained and an efficiency factor η will have to be introduced so that

$$G = \eta\left(\frac{\pi D}{\lambda}\right)^2 \tag{1.5}$$

This factor, which is lower than 1, depends on a great number of different contributions, which has been discussed elsewhere [20]. For the Intelsat systems, ICSC [37] has quoted the antenna gain for the 4-6 GHz band

$$10 \log G \geq 57 + 20 \log \frac{f}{4} \quad \text{dB} \tag{1.6}$$

where f has to be expressed in GHz. This means that at 4 GHz $G \geq 57$ dB. A simple calculation shows that this antenna gain may be obtained with an antenna with $\eta = 46\%$, if the diameter of the antenna is 25 m or more. No such specifications are known at this moment for frequencies above 10 GHz.

1.3. The antenna temperature

As explained before, the antenna noise temperature is a very important feature in satellite communications, especially if satellites operate in the frequency band of 4 to 6 GHz. Special radio frequency components are now used, such as masers and cooled parametric amplifiers, which have reduced the receiver noise temperature in this frequency band to about 5, to 20 K. In designing antennas for satellite communications great care has to be taken to keep the antenna noise temperature on the same level. An antenna receiving a signal in a frequency band of B hertz will also receive noise power in that band in accordance with the relation:

$$N = k \cdot T_A \cdot B \ , \tag{1.7}$$

where k = Boltzmann's constant = $1.38.10^{-23}$ Joule/ K, and T_A = the antenna temperature. Therefore, the noise power delivered to the antenna terminals is characterized by a number T_A in degrees Kelvin. Apparently, the antenna noise power is calculated in the same way as the noise power of a resistor at T degrees Kelvin [52].

Noise power received by an antenna may be radiated by any hot body at all frequencies. The distribution of this energy as a function of the frequency for an ideal black body is given by Planck's radiation law and the approximation of Rayleigh-Jeans, which holds reasonably well at microwave frequencies. To derive an expression for the antenna temperature, discrete thermal sources are replaced by equivalent black bodies everywhere in the field of view of the antenna [49]. A single discrete source radiates thermal energy according to the Rayleigh-Jeans law through a small cone of solid angle to all parts of the antenna. An integration has to be carried out over the whole antenna to find the total power available at its terminals from the single discrete source. A second integration has to be performed over the entire antenna pattern to add the contributions from all the discrete sources to the power at the antenna terminals. When the derivation is completed the equation for the noise temperature is:

$$T_A = \frac{1}{4\pi} \int_0^{\pi} \int_0^{2\pi} G(\theta,\phi)\, T(\theta,\phi)\, \sin\theta \, d\phi \, d\theta \ , \tag{1.8}$$

where $T(\theta,\phi)$ = distribution of the sky temperature over all angles about the antenna and

$d\Omega = \sin\theta \, d\phi d\theta$, the element of solid angle

If $P(\theta,\phi)$ from Eq. 1.1 is substituted in Eq. 1.8 and if both $P(\theta,\phi)$ and $T(\theta,\phi)$ are constant within a small solid angle $\Delta\Omega$, the noise contribution from that solid angle can be written as

$$\Delta T_A = \frac{P(\theta,\phi)}{P_T} T(\theta,\phi) \; \Delta \Omega \tag{1.9}$$

The term $P(\theta,\phi) . \Delta \Omega / P_T$ can be considered as the total relative power radiated within the solid angle $\Delta \Omega$ in the direction (θ,ϕ) and presented as the coefficient β_i . If the total antenna volume, 4π, is divided into a number of solid angles having an average temperature of T_i , the antenna temperature will be

$$T_A = \sum_{i=1}^{n} \beta_i \, T_i \tag{1.10}$$

where

$$\sum_{i=1}^{n} \beta_i = 1 \tag{1.11}$$

If for example, part of the radiation pattern of the antenna, comprising 1% of the total power, is pointed towards the direction of a full absorbing medium with a physical temperature of 300 K, the contribution of this quantity to the total noise temperature of the antenna will be 3 K [23].

As mentioned before, the ICSC does not specify a certain antenna temperature but a "figure of merit" or quality factor for the whole antenna system. This "figure of merit" which is a measure of the signal to noise ratio, should be greater than 40.7 dB at 4 GHz at an elevation of the antenna main beam of 5^o and measured at the input of the low noise receiver during dry and clear weather. The factor T_s represents here the total system noise temperature, thus

$$T_S = T_C + T_A \tag{1.12}$$

where, T_C is the contribution of the microwaves components, receiver, etc. Most of the components contributing to this noise have been explained before [20].

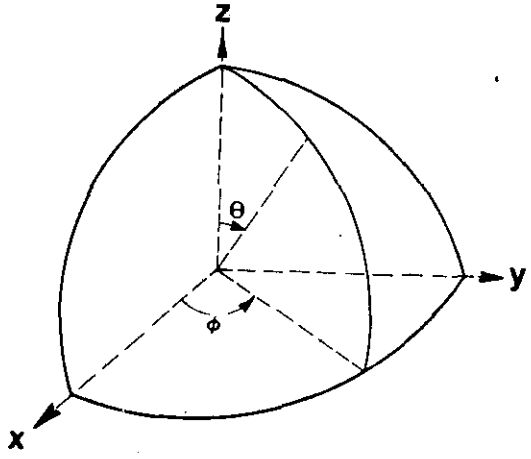

Fig. 1.1.

Spherical coordinates

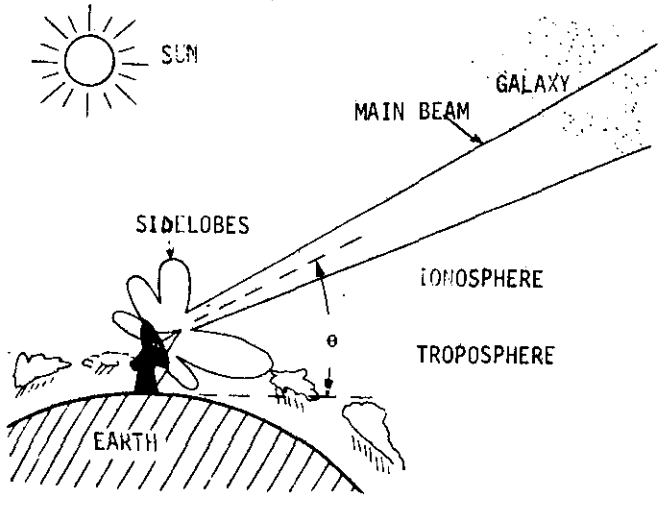

Fig. 1.2. Sources contributing to antenna noise from outside the antenna system

Fig. 1.2 shows the possible contributions to the antenna temperature T_A, and Fig. 1.3 the sky temperature $T(\theta,\phi)$ as a function of the frequency and the elevation angle of the antenna. This sky temperature is mostly independent of the azimuth angle ϕ, so that calculations with $T(\theta)$ are sufficient. It appears [Fig. 1.3] that 4 GHz is a well-chosen frequency for the purpose of satellite communication. At 10^o elevation and at 4 GHz, $T(\theta)$ is equal to 15 K. If the main beam of the antenna points upwards at an elevation angle of 10^o and if this beam comprises

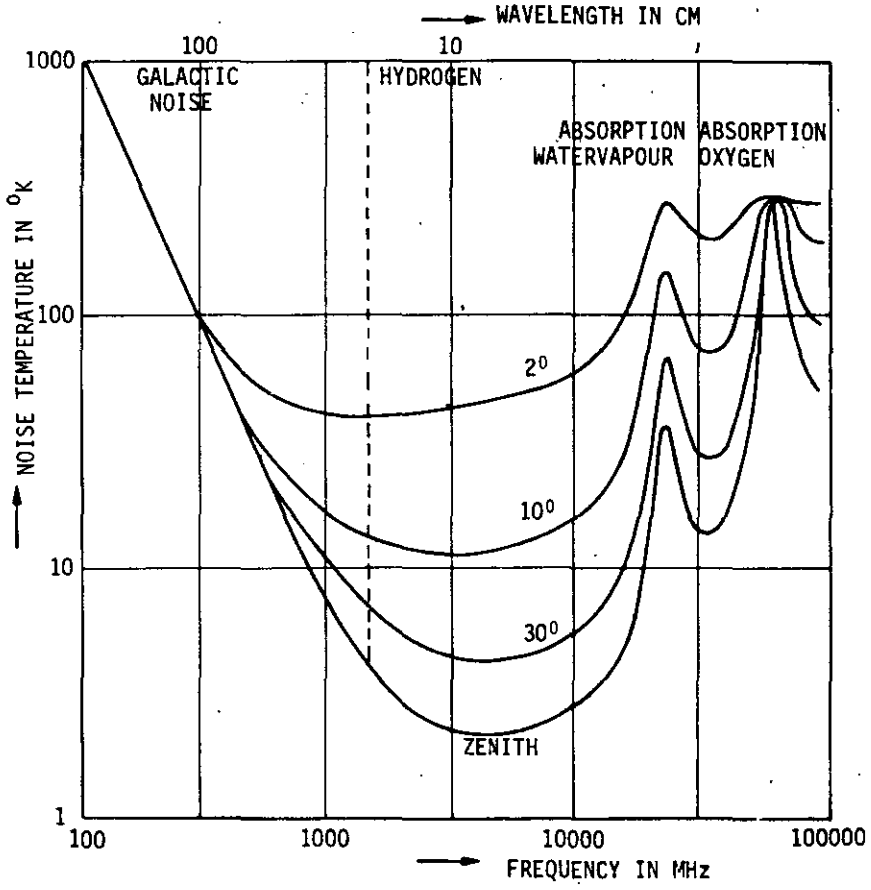

Fig. 1.3. The noise temperature of the sky as a function of the frequency and antenna elevation

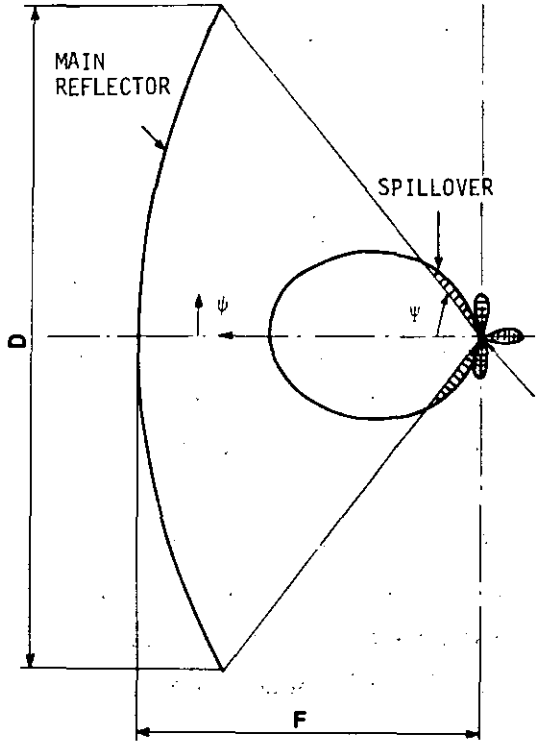

Fig. 1.4 a.
Front-fed paraboloid with antenna feed pattern and spillover

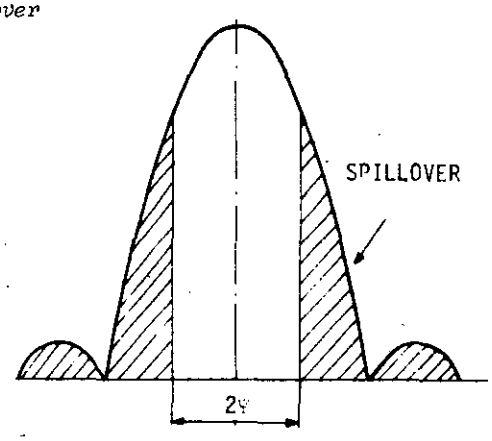

Fig. 1.4.b.

Radiation pattern of antenna feed in rectangular coordinates

90% of all the energy in main beam and sidelobes, the contribution of the main beam to the total noise temperature T_A = 0.9 x 15 K = 13.5 K. A great number of ground stations have been investigated [25] with respect to their gain and antenna noise temperature. Some of the properties of such antenna constructions will briefly be reviewed below and discussed more in detail in the following chapters.

1.4. Some antenna constructions

There are various approaches for satellite communication ground station antennas each having specific advantages and disadvantages. One of the first antennas which was used for a satellite communication ground station was a front-fed paraboloid installed at Goonhilly in 1963. This type of antenna has been known for many years and has been discussed thoroughly by Silver [108, p.415]. The antenna feed, horn of dipole, is located in the focus of the paraboloid. Only part of the power transmitted by the feed is captured by the paraboloid, concentrated and reradiated; that part which is not captured is lost and reduces the antenna efficiency [Fig. 1.4a and 1.4b]. The lost radiation, which is mostly called "spillover" should be minimized because it is directed to earth (T = 290 K) , and will, in cases where the antenna is used for reception purposes, contribute considerably to the antenna noise temperature. Spillover can be decreased if more energy radiated by the feed horn is concentrated on the paraboloid;

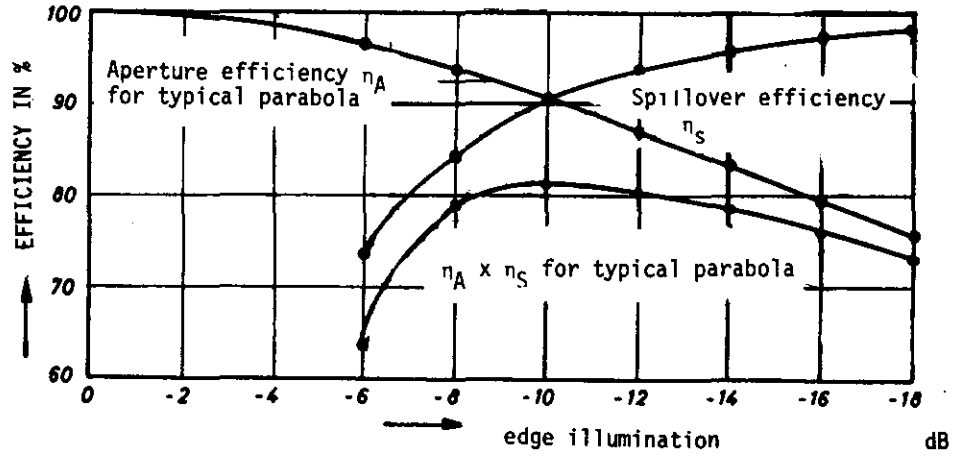

Fig. 1.5. Illumination and spillover efficiency

however, such a solution meets considerable objections. This can be seen from Fig. 1.4b, showing that the centre of the paraboloid is much better illuminated than the edge, decreasing the aperture efficiency.
It has long been known [108, p.177] that a reflector antenna has maximum gain if the aperture of the antenna is uniformly illuminated at constant phase. If the illumination is different, the aperture efficiency will be lower than 100 %.
The illumination efficiency could be increased if tapering towards the edge of the reflector is decreased; however, this would increase the spillover. If the aperture efficiency η_A is multiplied by η_S, being the spillover efficiency, one obtains:

$$\eta_A \cdot \eta_S = \cot^2 \tfrac{1}{2}\Psi \left| \int_0^{\Psi} [G_f(\psi)]^{\frac{1}{2}} \tan \tfrac{1}{2}\psi d\psi \right|^2 \qquad (1.13)$$

where $G_f(\psi)$ is the gain pattern of a circularly symmetrical radiation pattern of a primary feed. Fig. 1.5 shows both η_A and η_S, as well as their product, as a function of the illumination taper towards the edge of the main reflector. It appears that this product is maximum at about -10 dB edge illumination.
At Goonhilly [Fig. 1.6] difficulties as described above have indeed been met [16, 116].
Another practical disadvantage of this type of antenna is the location of part of the low noise receiver directly behind the feed in the focus of the antenna. It is possible to locate the receiver behind the reflector but in that case long transmission lines are required introducing intolerably high losses and noise contributions (0.1 dB loss is equal to an increase in noise of about 7 degrees K). This is the main disadvantage of the front-fed paraboloid; therefore, it is no longer used for satellite ground stations. The ground stations built in England afterwards use a different principle (Chapter 2 and 5).

The first ground station in the USA was a large horn paraboloid antenna located in Andover, developed by the Bell Labs [48]. The first French station at Pleumeur Bodou has been built according to this principle, and is a true copy of the Andover station. The vast dimensions of this antenna are shown in Fig. 1.7. Although it has very good noise properties, it is for economical reasons that it is no longer built.

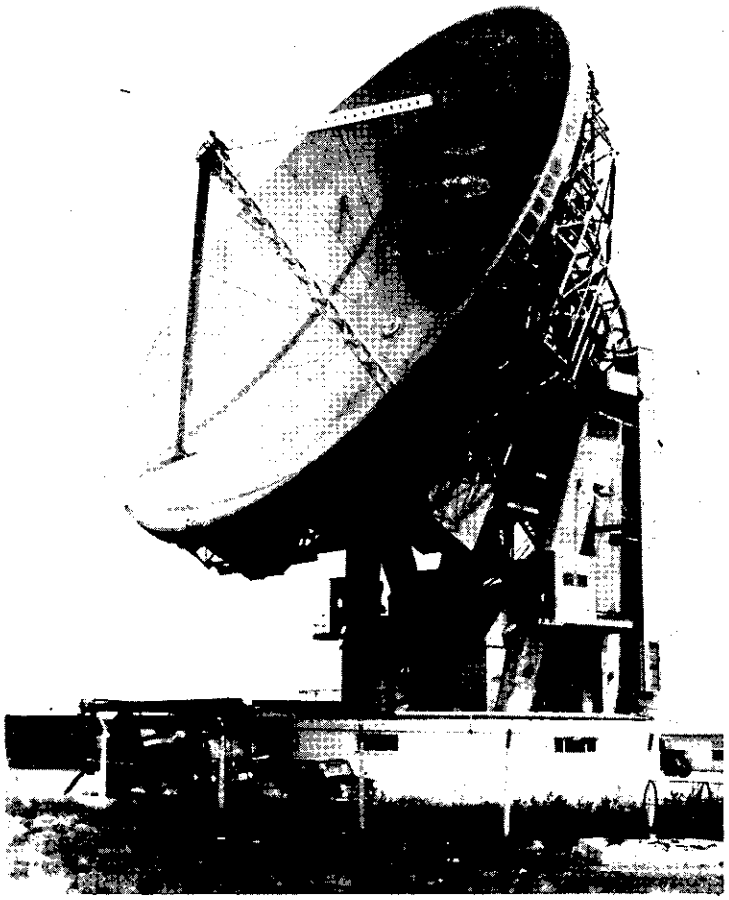

Fig. 1.6 The Goonhilly I ground station.

Nowadays, most ground stations are built in accordance with the modified cassegrain antenna [39,124]. In the future the open cassegrain antenna [67] may become popular. Therefore, we will study the properties of these antennas in detail.

For this purpose, we introduce the classical cassegrain antenna in chapter 2 and shall demonstrate the problems that arise with the blockage and diffraction of the subreflector. In chapter 3 the blockage efficiency of such double reflector antennas is investigated and calculations are carried out of the near-in sidelobes, taking into account the influence of the supports. Chapter 4 pays attention to the physical optics approximation [108, p.144], by which far angle sidelobes of reflector antennas may be calculated. The discussion comprises the validity of this method and the errors that may occur. Finally, Chapter 5 deals with modified cassegrain antennas and Chapter 6 with some aspects of offset paraboloid reflectors and open cassegrain antennas, with special regard to the cross-polarization properties.

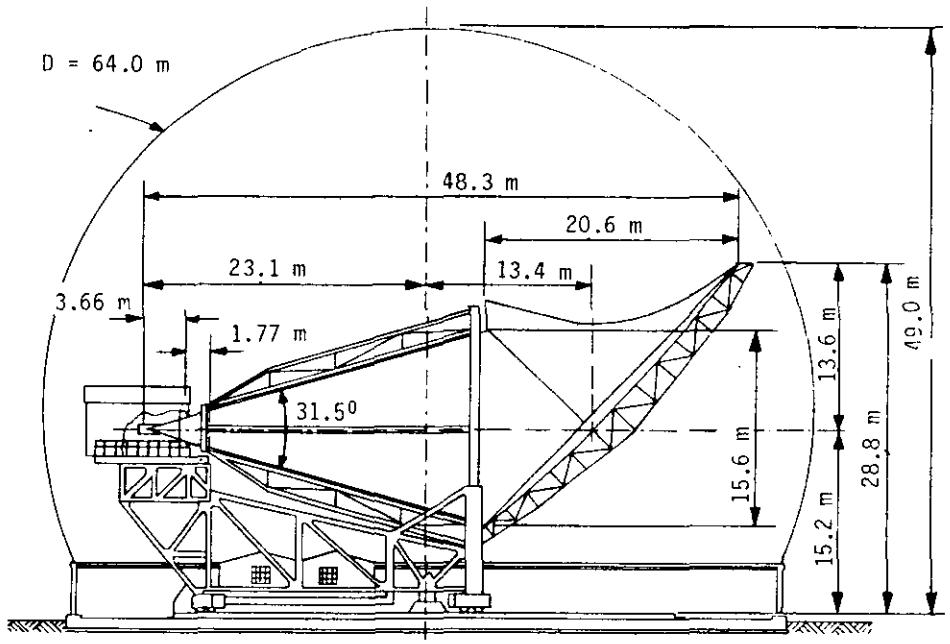

Fig. 1.7. Cross-section of the horn paraboloid antenna with radome at Andover

2. THE CLASSICAL CASSEGRAIN ANTENNA

2.1. Introduction

In 1672, the French optician Cassegrain invented a telescope consisting of two reflectors. This type has been used by astromoners for a long time, and even new telescopes are built according to the same principle [125]. The application of the cassegrain system to microwave antennas is, however, of only recent date [46].

The classical form of the system is shown in Fig.2.1. It employs a main dish, which is a paraboloid, and an auxiliary reflector or subdish with a hyperbolic contour. One of the foci P_1 is the real focal point of the system and is located near the main dish. The other focus, P_2, is a virtual focal point located at the focus of the paraboloid. If the primary feed is situated at the focus P_1 and the secondary reflector is illuminated, the waves are reflected in accordance with ray optics. On reaching the main dish, the waves are again reflected in accordance with ray optics, and because of the antenna geometry employed the rays emerge parallel, with a plane wave front, forming a collimated beam.

Several ground stations have been constructed in accordance with this principle, e.g. Mill Village (Canada) and two Japanese stations [25].A variation of the cassegrain system is found in the first German ground station [Fig. 2.2.], where a horn paraboloid, also known by the name of Hogg horn, is used as a primary source [Fig. 2.3.]. The F/D ratio of the main reflector is only 0.26. The subreflector is located near the aperture of the main reflector. It appears that the antenna system is very well protected against ground radiation resulting in a very low noise temperature; at an elevation angle of 7.5^{o}, the contribution to the system noise temperature is only 7 K at 4 GHz. Deep paraboloids are, however, more expensive than shallows ones. The subreflector is situated in the near field of the primary source. For this reason the shape of the subreflector needs to be a paraboloid. In this way it is possible to illuminate the subreflector over a wide frequency range and with little spillover. The equiphase plane of the horn paraboloid, which should be plane near the subreflector, shows errors near the edge of the subreflector so that

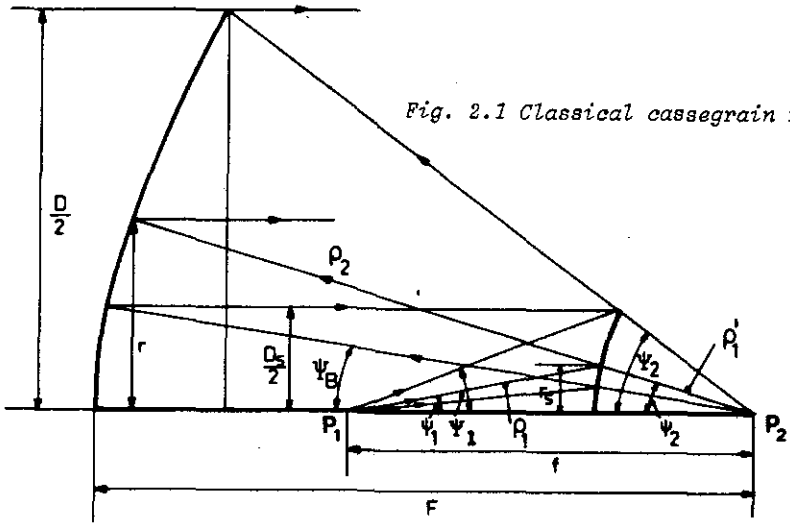

Fig. 2.1 Classical cassegrain reflector system

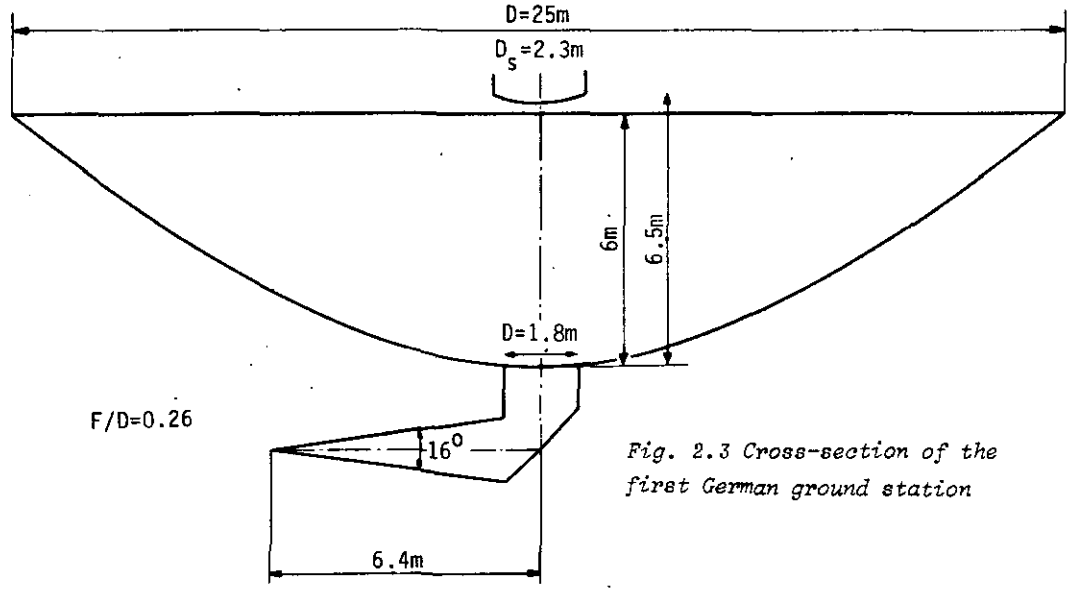

Fig. 2.3 Cross-section of the first German ground station

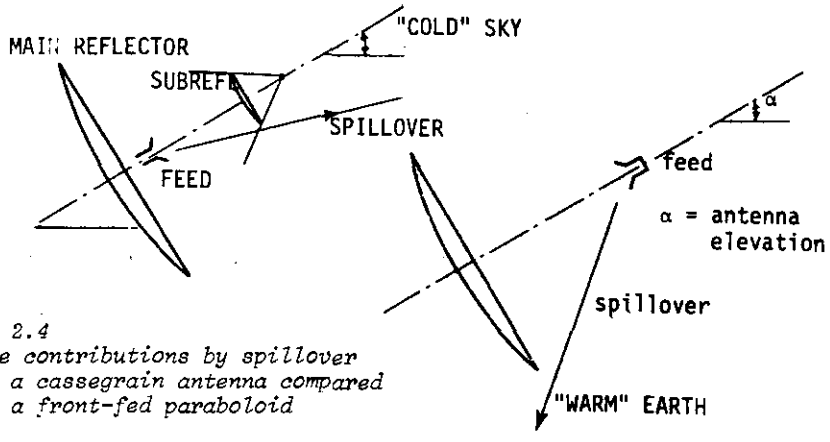

Fig. 2.4
Noise contributions by spillover from a cassegrain antenna compared with a front-fed paraboloid

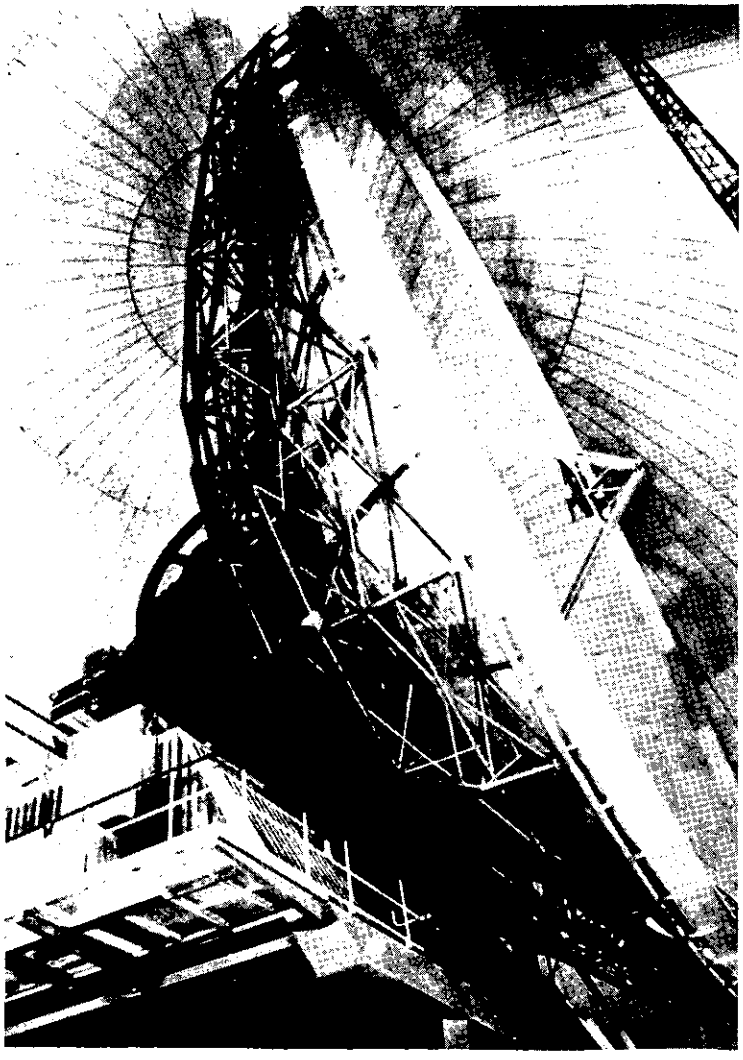

Fig. 2.2 The first German groundstation at Raisting.

corrections at the subreflector surface are required [118]. A disadvantage is the low illumination efficiency of the main reflector [119], which has been improved in the second German ground station [120].

If a comparison is made between a classical cassegrain antenna and a front-fed paraboloid, it appears that in the former the feed can be located much closer to the main reflector than in the latter. The feed lines can then be made much shorter, keeping the losses low. Moreover, feedhorn and low noise receiver can be reached much more conveniently for servicing purposes.

The noise properties of the cassegrain antenna are also better than those of a front-fed paraboloid, since in the latter the greater part of the spillover is directed towards the 'hot' earth, while the cassegrain system has hardly such contribution. There is spillover round the edge of the subreflector of cassegrain antennas; however, the greater part of this spillover is directed towards the cold sky [Fig.2.4]. Further, the subreflector blockage causes sidelobe increase round the main lobe [31]. Spillover and blockage will therefore only contribute to the antenna noise temperature at very low elevation angles, while the front-fed paraboloid receives radiation from the ground at every elevation angle.

A disadvantage of the cassegrain system is the decrease in antenna efficiency by blockage and diffraction introduced by the subreflector.

Diffraction occurs since the dimensions of the subreflector are not much larger than the wavelength. These effects cause a decrease in antenna efficiency. A recent investigation [21] has shown that the subreflector supports have also considerable contributions to the blockage. In the case

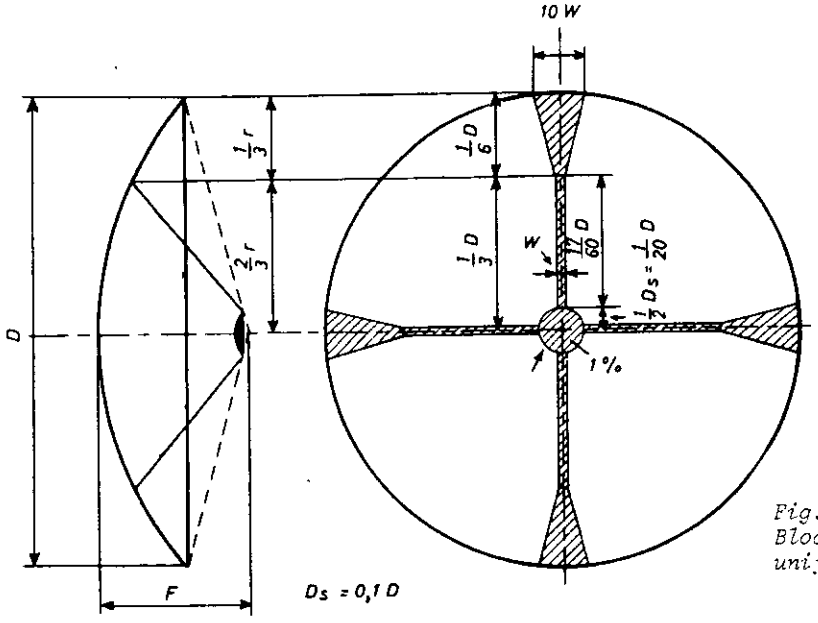

Fig. 2.5
Blockage in a cassegrain antenna with uniform aperture illumination

of cassegrain antennas these supports have to be much thicker than those supporting a feed horn for front-fed paraboloids. Therefore, in front-fed paraboloids this effect may often be neglected.
Fig. 2.5 shows in what way the aperture is blocked by a subreflector and its supports. The shadow of the supports has a peculiar form, which will be discussed in more detail in Chapter 3.
Calculations [Chapter 3] will show that the losses caused by spherical wave shadows are larger than those of the subreflector only. In the present chapter we shall discuss some of the problems related to the subreflector blockage and diffraction, and investigate in particular in what way the antenna efficiency is influenced.

2.2. Geometrical and optical relations

For the purpose of deriving geometrical and optical relations in a cassegrain system, we have illustrated in Fig. 2.1 half a cross-section of this system. The other half has been omitted as the entire system is circularly symmetrical.

The main dish is a paraboloid with the following equation in polar coordinates

$$\rho_2 = \frac{2F}{1 + \cos\psi_2} = \frac{F}{\cos^2 \tfrac{1}{2}\psi_2} \quad , \tag{2.1}$$

where F represents the focal length of the paraboloid with the origin located in the focal point P_2 of the paraboloid and ψ_2 the polar angle. It is readily seen in Fig. 2.1 that

$$\sin\psi_2 = r/\rho_2 \quad , \tag{2.2}$$

r being the distance from the centre of the paraboloid's aperture to an arbitrary point in the aperture. Combining Eqs. 2.1 and 2.2 results in

$$r = 2F \tan\tfrac{1}{2}\psi_2 \quad , \tag{2.3}$$

If Ψ_2 represents the angular aperture of the paraboloid, Eq. 2.3 becomes

$$D = 4F \tan\tfrac{1}{2}\Psi_2 \tag{2.4}$$

D being the diameter of the main reflector.
The equations of the hyperboloid in polar coordinates may be expressed in two ways, depending on the location of the origin. If this is situated in P_2, which is also one of the foci of the hyperboloid, we find

$$\rho_1' = \frac{f(e^2 - 1)}{2e(e\cos\psi_2 + 1)} \tag{2.5}$$

If, however, the origin for describing the hyperboloid is located in P_1, being the second focus of the hyperboloid, we find

$$\rho_1 = \frac{-f(e^2 - 1)}{2e(-e\cos\psi_1 + 1)} \tag{2.6}$$

e being the hyperboloid eccentricity.
From Fig. 2.1 we find also

$$r_s = \frac{-f(e^2 - 1)}{2e\,(-e\cos\psi_1 + 1)}\sin\psi_1 \tag{2.7}$$

and

$$r_s = \frac{f(e^2 - 1)}{2e(e\cos\psi_2 + 1)}\sin\psi_2 \tag{2.8}$$

Hannan [46] has indicated a relationship between the angles ψ_1 and ψ_2 viz.:

$$\tan\tfrac{1}{2}\psi_2 = \frac{e + 1}{e - 1}\tan\tfrac{1}{2}\psi_1 \tag{2.9}$$

The factor $(e + 1)/(e - 1)$ represents the magnification factor M of the cassegrain system.
Another relation may be found directly from Fig. 2.1

$$\cot\Psi_1 + \cot\Psi_2 = 2f/D_s \tag{2.10}$$

where Ψ_1 is the maximum angle from the horizontal axis to the ray from the feed and D_s the diameter of the subreflector.
Potter [87] has found a relation to transform the gain function of the lossless primary feed $G_1(\psi_1)$ into the subreflector gain function $G_2(\psi_2)$ on

a geometrical optics basis:

$$G_1(\psi_1)\ \sin^2\psi_1 = G_2(\psi_2)\ \sin^2\psi_2 \qquad (2.11)$$

where both $G_1(\psi_1)$ and $G_2(\psi_2)$ are circularly symmetrical.
If ψ_1 and ψ_2 are near to zero, we find by means of Eq. 2.9 that Eq. 2.11 becomes $G_1(\psi_1) = M^2\ G_2(\psi_2)$.
It is understood that the feed system comprising the feed horn and subreflector may be replaced by a point source at the focus of the main reflector with the gain function $G_2(\psi_2) = G_1(\psi_1)\ \sin^2\psi_1/\sin^2\psi_2$.
The Eqs. 2.8 , 2.9 , and 2.11 are represented graphically by the figures 2.6 , 2.7 and 2.8 respectively.

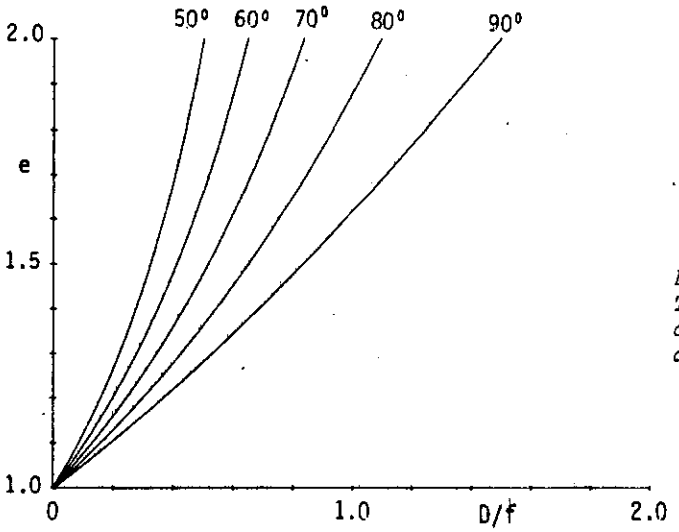

Fig. 2.6
The hyperboloid eccentricity as a function of D_s and f with the angular aperture Ψ_2 as a parameter (Eq. 2.8)

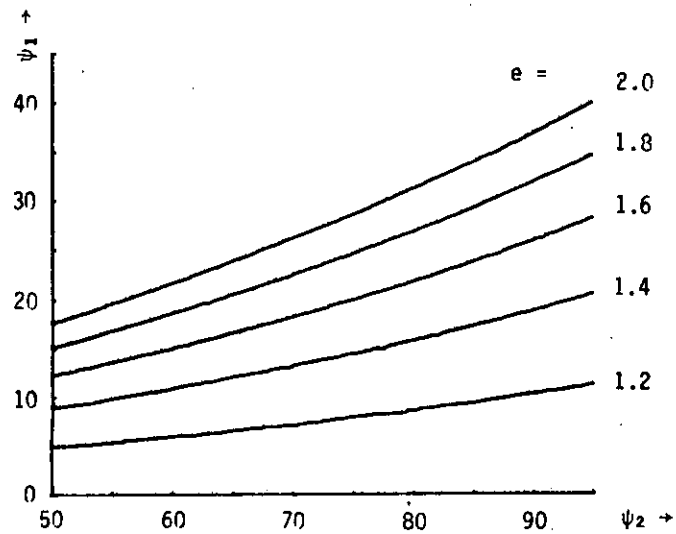

Fig. 2.7 The relationship between direct and reflected rays at hyperboloid subreflector with the eccentricity as a parameter (Eq. 2.9)

2.3. The antenna gain

2.3.1. Calculations by the scalar aperture method

Considering the scalar field of the radiating aperture, Silver [108, p.170] has presented an equation for calculating the diffracted field in a field point starting from the amplitude and phase distribution of the field over the aperture.
Generally, the scalar diffracted field is represented by

$$U_p(\theta,\phi) = \frac{1}{4\pi}\int_A F(x,y)\,\frac{e^{-jkR'}}{R'}\,\left[\left(jk+\frac{1}{R'}\right)\bar{a}_z.\bar{a}_{R'} + jk\bar{a}_z.\bar{a}_s\right]\,dxdy \qquad (2.12)$$

where $\bar{a}_z.\bar{a}_{R'}$ is the cosine of the angle between the normal to the aperture and the $\bar{a}_{R'}$ direction.

The vector $\bar{a}_s$ is the unit vector along a ray. If the phase error over the aperture is small, the $\bar{a}_z.\bar{a}_s$ term may be replaced by unity [108, p. 172]. Further $k = 2\pi/\lambda$, while θ and ϕ are spherical coordinates of a field point [Fig. 2.9].
If the field point is situated in the Fraunhofer or far zone region, Eq. 2.12 may be approximated by [108, p. 173]:

$$U_p(\theta,\phi) \approx \frac{j}{\lambda R}\,e^{-jkR}\int_A F(x,y)\,e^{jk\,\sin\theta(x\cos\phi + y\sin\phi)}\,dxdy \qquad (2.13)$$

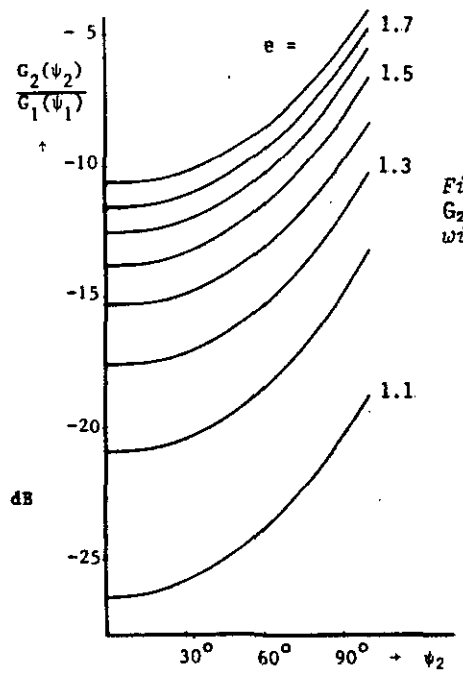

Fig. 2.8
G_2/G_1 as a function of ψ_2 with e as a parameter

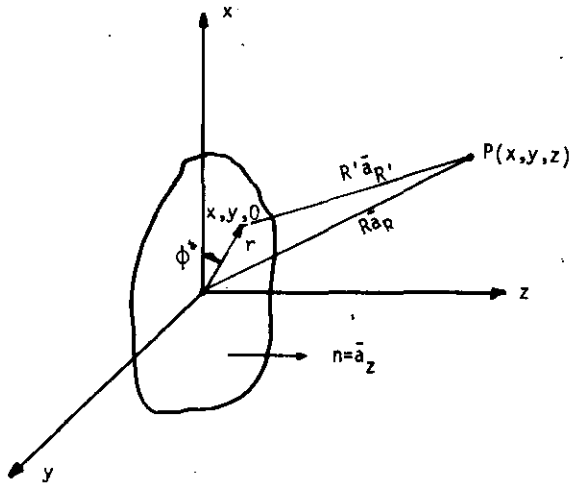

Fig. 2.9.

The radiating aperture.

This equation applies in a small angular region about the z - axis.

Moreover, the following assumptions are required [84]

(1) The field point is in the far zone as explained before

(2) The aperture field is uniformly polarized

(3) The aperture phase distribution must be uniform.

If the aperture is circular and its diameter is D, it is more convenient to use polar coordinates r,ϕ' which are related to x,y by $x = r\cos\phi'$ and $y = r\sin\phi'$.

Neglecting the phase term $\exp(-jkR)$ the field distribution over the aperture now becomes $F(r,\phi')$ and Eq. 2.13 becomes

$$U_p(\theta,\phi) \approx \frac{j}{\lambda R}\int_0^{2\pi}\int_0^{\frac{1}{2}D} F(r,\phi')\, e^{jkr\sin\theta\cos(\phi-\phi')} r\,dr\,d\phi' \qquad (2.14)$$

Generally, the aperture illumination does not depend on ϕ'. Since

$$2\pi J_0(kr\sin\theta) = \int_0^{2\pi} e^{jkr\sin\theta\cos(\phi-\phi')}\,d\phi' \qquad (2.15)$$

the double integral of Eq. 2.14 may be reduced to the single integral

$$U_p(\theta) = \frac{2\pi j}{\lambda R}\int_0^{\frac{1}{2}D} F(r)\, J_0(kr\sin\theta)\, r\,dr \qquad (2.16)$$

If the aperture is illuminated uniformly, $F(r)$ will be a constant and the integration results in

$$U_p(\theta) = \frac{j\pi D^2}{\lambda R} \cdot \frac{J_1(u)}{2u} \qquad (2.17)$$

$J_0(u)$ and $J_1(u)$ being Bessel functions of zero and first order, and $u = \pi D/\lambda \cdot \sin\theta$.

As explained by Silver [108, p.177], the gain calculation by means of Eq. 2.17 leads to

$$G_{max} = (\pi D/\lambda)^2$$

This $J_1(u)/u$ character of the radiation pattern is very well known in antenna engineering; the far field power pattern or field intensity is proportional to the square of the magnitude of the field.

It is found that

$$G(u) :: [J_1(u)/u]^2$$

Apparently the far field scalar integral for the circular aperture

$$F'(u) = 2\pi a^2 \int_0^1 F(r)\, J(ur)\, r\,dr \quad ,$$

where a is the radius of the aperture, is of the form

$$f'(\alpha) = \int_0^\alpha x\, f(x)\, J_\nu(\alpha x)\, dx \quad ,$$

which is the Hankel transform of order ν of the function $f(x)$ [7,p.46]. More especially the far field pattern $F'(u)$ of a circular aperture is the Hankel transform of zero order of the aperture illumination $F(r)$ so that

$$F'(u) = \int_0^1 F(r)\, J_0(ur)\, r\,dr \quad .$$

The inverse relationship becomes

$$F(r) = \int_0^\infty F'(u)\, J_0(ur)\, u\,du \quad ,$$

showing that aperture illumination and far field pattern are related by a transform relationship. However, this pattern only applies very near the

main lobe of the antenna pattern, which according to Silver [108, p.193] is about $\theta = 3\lambda/D$ .For the determination of the main lobe and the near sidelobes this simplified aperture method has become very popular and is easy to carry out. In most cases the aperture is not illuminated uniformly, but tapered towards the edge. This results in a reduction in gain , an increase in beamwidth of the mainlobe, and a decrease in the sidelobe level. A great number of investigators have used this method and have introduced various possible aperture distributions $F(r,\phi')$. As far as important to cassegrain antennas, these distributions will be mentioned further in this chapter or elsewhere.

2.3.2. The scalar aperture method with gain functions

The method described in the previous section has the disadvantage that it does not allow for the influence of the feed pattern with regard to the antenna performance. It will be understood that the feed pattern originates a certain field distribution across the aperture, and, moreover, that always part of the feed pattern will be lost as spillover along the subreflector. Therefore, we shall introduce gain functions of the feed $G_f(\xi,\psi)$ into Eq. 2.16.
If the feed is located in the focus of a paraboloid [Fig. 2.10], the field across the aperture [108, p. 419] is

$$F(r,\phi') = [2(\mu/\varepsilon)^{\frac{1}{2}} P_T/4\pi]^{\frac{1}{2}} \frac{[G_f(\xi,\psi)]^{\frac{1}{2}}}{\rho} \tag{2.18}$$

Substituting Eq. 2.18 in Eq. 2.16 leads to

$$U_p(\theta) = \frac{2\pi j}{\lambda R} \int_0^{\frac{1}{2}D} [2(\mu/\varepsilon)^{\frac{1}{2}} P_T/4\pi]^{\frac{1}{2}} \frac{[G_f(\xi,\psi)]^{\frac{1}{2}}}{\rho} J_0(kr \sin\theta)\, r dr \tag{2.19}$$

In these equations ρ is given by Eq. 2.1. From the geometry in Fig. 2.1 we know that $r = 2F \tan\frac{1}{2}\psi$, $D = 4F \tan\frac{1}{2}\Psi$ and $dr = Fd\psi/\cos^2\frac{1}{2}\psi = \rho d\psi$. Therefore,

$$U_p(\theta) = \frac{2\pi j}{\lambda R} [2(\mu/\varepsilon)^{\frac{1}{2}} P_T/4\pi]^{\frac{1}{2}} \int_0^{\Psi} [G_f(\xi,\psi)]^{\frac{1}{2}} 2F \tan\tfrac{1}{2}\psi \cdot J_0(k.2F \tan\tfrac{1}{2}\psi \sin\theta)\, d\psi \tag{2.20}$$

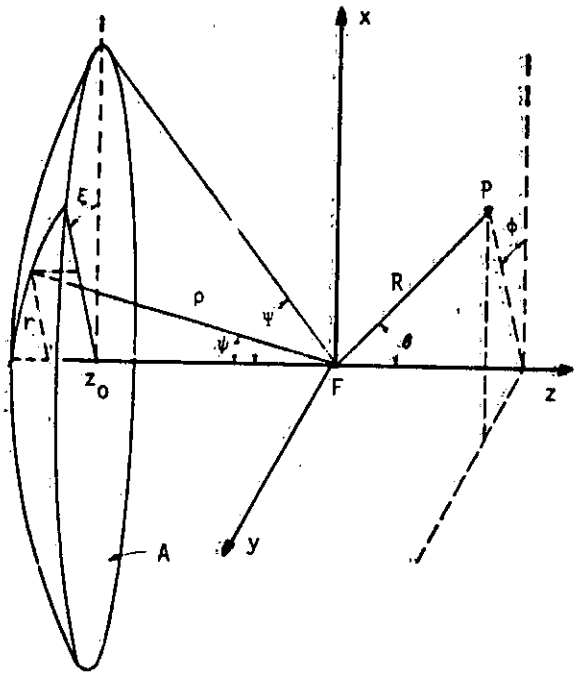

Fig. 2.10
Geometrical parameters for the paraboloidal reflector

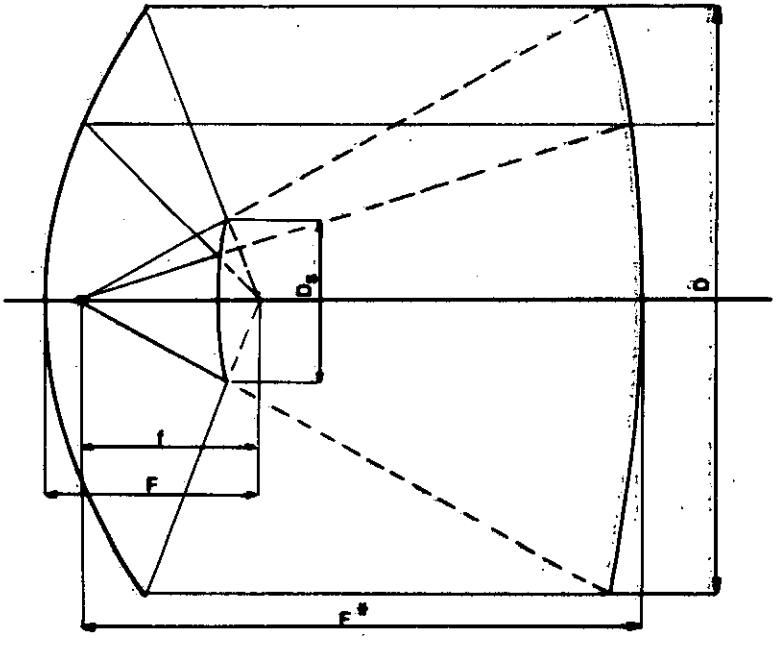

Fig. 2.11. Equivalent parabola concept.

and, if we assume that the feed pattern is no function of ξ,

$$U_p(\theta) = j\frac{\pi D}{\lambda R}\,[2(\mu/\varepsilon)^{\frac{1}{2}}\,P_T/4\pi]^{\frac{1}{2}}\,\cot\tfrac{1}{2}\Psi \int_0^{\Psi} [G_f(\psi)]^{\frac{1}{2}}\,\tan\tfrac{1}{2}\psi\,\cdot J_0\left(\frac{\pi D}{\lambda}\cot\tfrac{1}{2}\Psi\,\tan\tfrac{1}{2}\psi\,\sin\theta\right) d\psi \qquad (2.21)$$

The maximum field intensity for $\theta = 0$ is now found to be

$$U_p(0) = \frac{j}{R}[2(\mu/\varepsilon)^{\frac{1}{2}} P_T/4\pi]^{\frac{1}{2}} \frac{\pi D}{\lambda} \cot\tfrac{1}{2}\Psi \int_0^{\Psi} [G_f(\psi)]^{\frac{1}{2}} \tan\tfrac{1}{2}\psi \, d\psi \tag{2.22}$$

The power radiated per unit solid angle in the forward direction is now given by [108, p.177]

$$P(0) = \tfrac{1}{2}R^2(\varepsilon/\mu)^{\frac{1}{2}}|U_p(0)|^2 \tag{2.23}$$

and the antenna gain by

$$G = \frac{4\pi \, P(0)}{P_T} \tag{2.24}$$

An equation for the antenna gain is now found to be identical to that of Silver [108, p.425],

$$G = (\frac{\pi D}{\lambda})^2 \cot^2\tfrac{1}{2}\Psi \; \left| \int_0^{\Psi} [G_f(\psi)]^{\frac{1}{2}} \tan\tfrac{1}{2}\psi \, d\psi \right|^2 \tag{2.25}$$

The factor $(\pi D/\lambda)^2$ is the gain of a uniformly illuminated constant phase aperture, the remainder is the antenna efficiency η_1

$$\eta_1 = \cot^2\tfrac{1}{2}\Psi \; \left| \int_0^{\Psi} [G_f(\psi)]^{\frac{1}{2}} \tan\tfrac{1}{2}\psi \, d\psi \right|^2 \tag{2.26}$$

Eq. 2.22 may also be used successfully for calculations of the forward gain and near sidelobes of a cassegrain antenna. In that case we have to replace ψ by ψ_2, Ψ by Ψ_2 and G_f by G_2.
As demonstrated by Hannan [46], the cassegrain system consisting of main and subdish may be replaced by an equivalent focussing surface with a parabolic contour. This equivalent parabola has a focal length equal to the distance from its vertex to the real focal point [Fig. 2.11].
Apparently we may replace the cassegrain antenna by a "normal" front-fed paraboloid having a focal length

$$F^* = F \frac{e + 1}{e - 1} = MF, \tag{2.27}$$

explaining the term magnificator ratio M.
Substituting Eqs. 2.11 and 2.9 in Eq. 2.21, we obtain, at unit distance

$$U_p(0) = j[2(\mu/\varepsilon)^{\frac{1}{2}} P_T/4\pi]^{\frac{1}{2}} \pi D/\lambda \cot\tfrac{1}{2}\psi_1 \int_0^{\psi_1} [G_1(\psi_1)]^{\frac{1}{2}} J_0(\pi D/\lambda \cot\tfrac{1}{2}\psi_1 \tan\tfrac{1}{2}\psi_1 \cdot \sin\theta) \tan\tfrac{1}{2}\psi_1 \, d\psi_1 \qquad (2.28)$$

whose maximum intensity for $\theta = 0$ is

$$U_p(0) = j[2(\mu/\varepsilon)^{\frac{1}{2}} P_T/4\pi]^{\frac{1}{2}} \frac{\pi D}{\lambda} \cot\tfrac{1}{2}\psi_1 \int_0^{\psi_1} [G_1(\psi_1)]^{\frac{1}{2}} \tan\tfrac{1}{2}\psi_1 \, d\psi_1 \qquad (2.29)$$

Similarly to Eq. 2.26 we find [Appendix 2.1]

$$\eta_1 = \cot^2\tfrac{1}{2}\psi_1 \left| \int_0^{\psi_1} [G_1(\psi_1)]^{\frac{1}{2}} \tan\tfrac{1}{2}\psi_1 \, d\psi_1 \right|^2 \qquad (2.30)$$

Silver [108, p. 426] has published a graph of Eq. 2.26 using feed patterns defined by

$$\begin{aligned} G_f(\psi) &= 2(n+1)\cos^n\psi \qquad 0 < \psi \leq \tfrac{1}{2}\pi \\ &= 0 \qquad\qquad\qquad\quad \psi > \tfrac{1}{2}\pi \end{aligned} \qquad (2.31)$$

for values of n between 2 and 8. In cassegrain antennas the angular aperture of the subreflector is much smaller than that of a front-fed paraboloid. Consequently, the subreflector has to be illuminated by a narrower beam, resulting in far higher values of n in Eq. 2.31. In Fig. 2.12, Eq. 2.30 is graphically represented for two values of η higher than 20. It appears that the maximum efficiency is of the same order as that of Silver found for lower values of n.
If blockage and diffraction of the subreflector have to be taken into account, Eqs. 2.29 and 2.30 will have to be modified, which will decrease antenna gain and efficiency.

2.4. Factors decreasing the antenna gain

2.4.1. Subreflector blockage

As will be explained in more detail in Chapter 3, the cassegrain antenna system has a serious limitation with regard to aperture blockage by

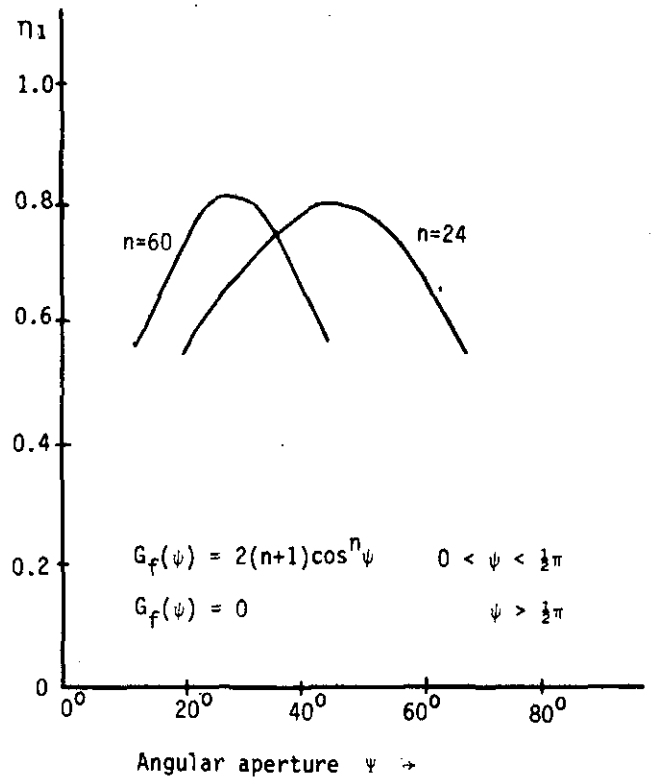

Fig. 2.12. Dependance of the efficiency on angular aperture and primary feed pattern for higher values of n.

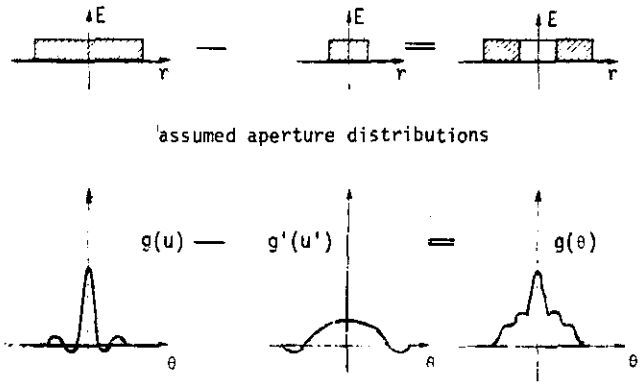

Fig. 2.13 Radiation patterns corresponding to assumed aperture distributions

subreflector and subreflector supports. In this section we shall only pay attention to the contribution of the subreflector blockage to the decrease in antenna gain and we shall calculate this using gain functions discussed in Sec. 2.3.2. A more detailed description of aperture blockage calculated by means of the scalar aperture method is found in Chapter 3.
If the aperture of a circularly symmetrical antenna is illuminated uniformly in phase and amplitude, the generalized secondary circularly symmetrical pattern near the main axis [108, p.194] becomes

$$g(u) = \frac{\pi D^2}{2} \cdot \frac{J_1(u)}{u} \tag{2.32}$$

where D is the diameter of the aperture, $J_1(u)$ a Bessel function of the first order, and

$$u = \frac{\pi D}{\lambda} \sin\theta \tag{2.33}$$

The angle θ constitutes part of a spherical coordinate system [Fig. 1.1.] and for $\theta = 0$ the position of the antenna axis is found. The pattern is independent of ϕ. Silver [108, p. 190-192] assumed that over the exposed area the presence of an obstacle would not alter the amplitude distribution $F(r,\phi')$ [Fig. 2.9], which would exist in its absence, therefore, the obstacle can be regarded as producing a field equal in amplitude but 180^o out of phase with the original field distribution over the area it covers. In this way zero illumination is obtained over the blocked parts of the aperture. This principle is often called the "zero field concept". Therefore, if the aperture is blocked by a subreflector with a diameter D_s in a cassegrain system, the generalized circularly symmetrical pattern of this subreflector may be represented by

$$g'(u') = \frac{\pi D_s^2}{2} \cdot \frac{J_1(u')}{u'}$$

where

$$u' = \pi D_s/\lambda \sin\theta$$

The modified pattern is then

$$g_t(\theta) = g(\theta) - g'(\theta) \tag{2.34}$$

This principle will be used to investigate the influence of the blocking obstacles within a cassegrain antenna system on the sidelobes of the secondary pattern. This means that the contribution of the subreflector is found by subtracting the aperture field between 0 and $\frac{1}{2}D_s$ from the original field [Fig. 2.13].

Apparently all radiation between $0 < \psi_2 < \Psi_B$ from the feed is blocked and scattered. Using the same constants as in Sec. 2.3, the pattern to be subtracted from the main pattern is

$$U_B(\theta) = \underbrace{j\,[2(\mu/\varepsilon)^{\frac{1}{2}}\,P_T/4\pi]^{\frac{1}{2}}}_{\text{constant}} \cdot \frac{\pi D_s}{\lambda}\cot\tfrac{1}{2}\Psi_B \int_0^{\Psi_B} [G_2(\psi_2)]^{\frac{1}{2}}\, J_0\left(\frac{\pi D_s}{\lambda}\cot\tfrac{1}{2}\Psi_B \tan\tfrac{1}{2}\psi_2 \cdot \sin\theta\right) \tan\tfrac{1}{2}\psi_2\, d\psi_2 \tag{2.35}$$

In the main direction ($\theta = 0$) we obtain

$$U_B(0) = \text{constant}\,\frac{\pi D_s}{\lambda}\cot\tfrac{1}{2}\Psi_B \int_0^{\Psi_B} [G_2(\psi_2)]^{\frac{1}{2}}\, \tan\tfrac{1}{2}\psi_2\, d\psi_2 \tag{2.36}$$

In accordance with the zero field concept, the total field in the main direction is now expressed by

$$U_{tot} = U_P - U_B \tag{2.37}$$

or by Eq. 2.29

$$U_{tot} = \text{constant}\,\frac{\pi D}{\lambda}\left[\cot\tfrac{1}{2}\Psi_1 \int_0^{\Psi_1} [G_1(\psi_1)]^{\frac{1}{2}}\, \tan\tfrac{1}{2}\psi_1 d\psi_1 - \frac{D_s}{D}\cot\tfrac{1}{2}\Psi_B \cdot \int_0^{\Psi_B} [G_2(\psi_2)]^{\frac{1}{2}}\, \tan\tfrac{1}{2}\psi_2\, d\psi_2\right] \tag{2.38}$$

and the antenna gain by

$$G_{tot} = (\pi D/\lambda)^2 \left|\cot\tfrac{1}{2}\Psi_1 \int_0^{\Psi_1} [G_1(\psi_1)]^{\frac{1}{2}}\, \tan\tfrac{1}{2}\psi_1\, d\psi_1 - \frac{D_s}{D}\cot\tfrac{1}{2}\Psi_B \cdot \int_0^{\Psi_B} [G_2(\psi_2)]^{\frac{1}{2}} \tan\tfrac{1}{2}\psi_2\, d\psi_2\right|^2 \tag{2.39}$$

or in terms of relative blockage efficiency [40], [Ch.3],

$$\frac{\eta_B}{\eta_1} = \left| 1 - \frac{D_s}{D\sqrt{\eta_1}} \cot\tfrac{1}{2}\psi_B \int_0^{\psi_B} [G_2(\psi_2)]^{\frac{1}{2}} \tan\tfrac{1}{2}\psi_2 \, d\psi_2 \right|^2 \qquad (2.40)$$

where $G_1(\psi_1)$ and $G_2(\psi_2)$ are related by Eq. 2.11.
The relative blockage coefficient as a function of the edge illumination is shown in Fig. 2.14.

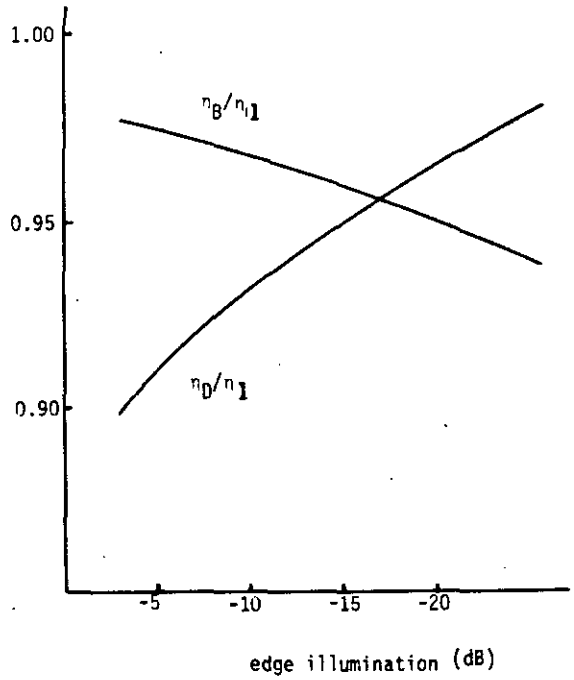

Fig. 2.14. Relative blockage and diffraction efficiency of the subreflector as a function of the edge illumination of the subreflector; $D_s = 33\ \lambda$, $n = 60$, $\psi_2 = 75^o$

2.4.2. Diffraction

2.4.2.1 Diffraction phenomena introduced by the subreflector

The cassegrain system was originally designed for use at optical frequencies. At radiofrequencies however, the dimensions of the subreflector are not always large compared with the wavelength, resulting in diffraction which cannot be explained by geometrical optics. This means that not all the power reflected by the subreflector is captured by the main reflector, so that some power is lost. The result is that not only does the antenna efficiency de-

crease, but also the power which is scattered contributes to higher sidelobes. Several handbooks are available [4, Ch. 8] which treat diffraction effects in detail. We would mention here the approximation which can be obtained by using the principle of stationary phase [108, p. 119]. By this principle it was found that only stationary phase areas yield contributions to the electric field, while contributions of other parts of the surface are negligible.

The principle of stationary phase has been applied by Gillitzer [40], who has found that the field reflected from the subreflector is partly characterized by small oscillations which can be described by Fresnel integrals. Near the edge of the subreflector, however, the field decreases monotonically and reaches a value of -6 dB at the edge of the subreflector in the direction of the angular aperture Ψ_2 (Fig. 2.15). If the angle at which the monotonic decrease towards the edge starts is called Ψ_D, (Fig. 2.16), Gillitzer [40] found that

$$\Psi_D = \Psi_2 - 0.65 \sqrt{\frac{\lambda \sin\Psi_2}{D_s}} \tag{2.41}$$

We shall now use these results to determine the decrease in antenna gain by the diffraction phenomena of the subreflector. For that purpose we approximate the field reflected by the subreflector as shown in Fig. 2.15. Therefore, we split the gain function $G'(\Psi_2)$ of this field into two parts:

$$G'(\psi_2) = G_2(\psi_2) \qquad \text{for} \quad 0 < \psi_2 < \Psi_D \tag{2.42}$$

and

$$G'(\psi_2) = G_2(\psi_2)\, e^{-2\gamma(\psi_2 - \Psi_D)} \qquad \text{for} \quad \Psi_D < \psi_2 < \Psi_2 \tag{2.43}$$

The field expressed by Eq. 2.42 is determinated by geometrical optics and if $G_1(\psi_1)$ is known, it can easily be found by means of Eq. 2.11.

The field expressed by Eq. 2.43 demonstrates the monotonic decrease in the amplitude of the reflected wave near the edge of the subreflector. As the fieldstrength at the edge reaches a value of -6dB, $G'(\psi_2)$ becomes $0.25 \times G_2(\psi_2)$ for $\psi_2 = \Psi_2$ and, in consequence,

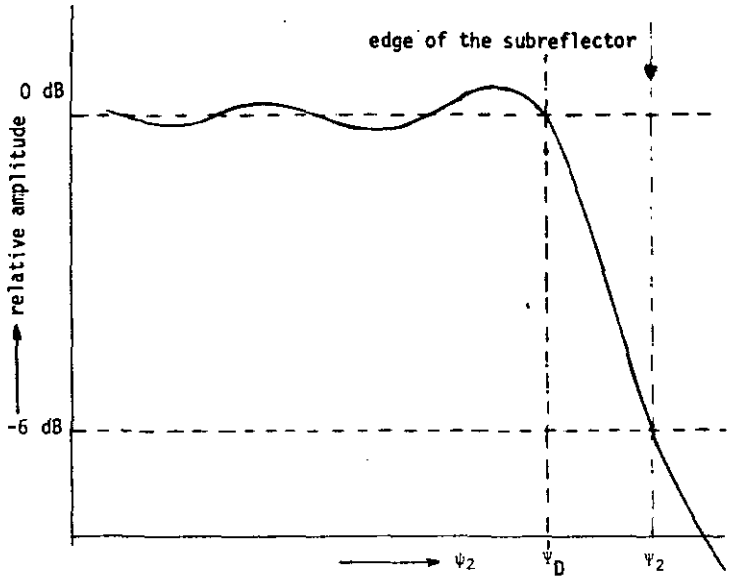

Fig. 2.15 Decrease of amplitude caused by diffraction

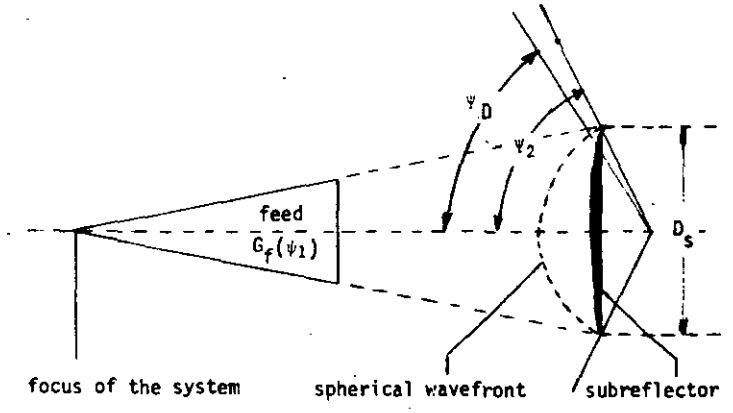

Fig. 2.16 Geometry of feed and subreflector

$$\gamma = 1.07 \sqrt{\frac{D_s}{\lambda \sin \Psi_2}} \tag{2.44}$$

The value of -6 dB has also been reported by Potter [88] and by Rusch [96]. The field obtained by the stationary phase method as described above yields good results for the capturing area of the main reflector. For values $\psi_2 > \Psi_2$, Eq. 2.43 becomes rapidly very inaccurate. If the radiation pattern has to be known in this area as well, other methods are in favour [96]. These calculations are far more accurate compared with the stationary phase method, although under certain circumstances errors may be made. In chapter 4 this subject will be discussed in detail. If we now want to calculate the decrease in antenna gain we have to correct Eq. 2.21 in the interval $\Psi_D < \psi_2 < \Psi_2$.

Thus, the correction term is

$$U_D(\theta) = \text{constant } \pi D/\lambda \cot\tfrac{1}{2}\Psi_2 \int_{\Psi_D}^{\Psi_2} [G_2(\psi_2)]^{\frac{1}{2}} [1 - e^{-\gamma(\psi_2 - \Psi_D)}] \cdot J_0(\pi D/\lambda \cot\tfrac{1}{2}\Psi_2 \tan\tfrac{1}{2}\psi_2 \sin\theta) \tan\tfrac{1}{2}\psi_2 d\psi_2 \quad (2.45)$$

In the forward direction, where $\theta = 0$, we obtain

$$U_D(0) = \text{constant } \pi D/\lambda \cot\tfrac{1}{2}\Psi_2 \int_{\Psi_D}^{\Psi_2} [G_2(\psi_2)]^{\frac{1}{2}} [1 - e^{-\gamma(\psi_2 - \Psi_D)}] \tan\tfrac{1}{2}\psi_2 \, d\psi_2 \quad . \quad (2.46)$$

2.4.2.2. The diffraction efficiency of the subreflector

Let η_1 be the efficiency of a paraboloid reflector antenna (Eq. 2.26); the relative diffraction efficiency of a cassegrain antenna then becomes

$$\frac{\eta_D}{\eta_1} = \left|1 - \frac{U_D(0)}{U_p(0)}\right|^2 \quad (2.47)$$

where $U_D(0)$ is found from Eq. 2.46 and $U_p(0)$ from Eq. 2.22. [40].
As the integration region is limited, Eq. 2.46 can be simplified by using

$$[G_2(\psi_2)]^{\frac{1}{2}} \tan\tfrac{1}{2}\psi_2 = [G_2(\Psi_2)]^{\frac{1}{2}} \tan\tfrac{1}{2}\Psi_2 \, , \quad (2.48)$$

which results after some calculation in

$$U_D(0) = 0.18 \text{ constant. } \pi D/\lambda \left[G_2(\Psi_2) \frac{\lambda \sin\Psi_2}{D_s}\right]^{\frac{1}{2}} \quad (2.49)$$

Substitution of Eq. 2.22 and Eq. 2.49 in Eq. 2.47 yields

$$\eta_D/\eta_1 = (1 - \Delta)^2 \quad (2.50)$$

where

$$\Delta = 0.18 \left[G_2(\Psi_2) \frac{\lambda \sin\Psi_2}{\eta_1 D_s} \right]^{\frac{1}{2}} \qquad (2.51)$$

The relative diffraction efficiency as a function of the edge illumination is shown in Fig. 2.14. Fig. 2.17 shows the relative diffraction efficiency as a function of Ψ_2, keeping $D_s = 33\lambda$, $n = 60$ and the edge illumination -10 dB.

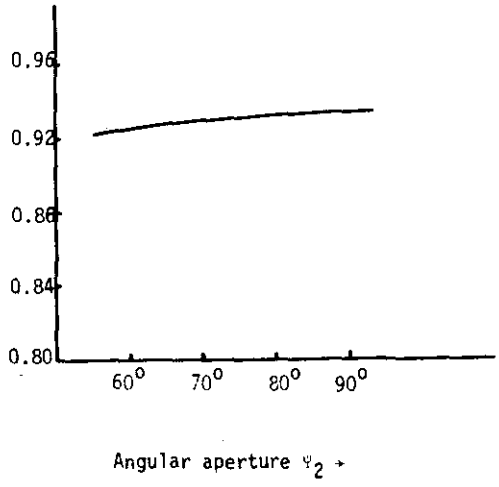

Fig. 2.17. The relative diffraction efficiency as a function of the angular aperture. $D_s = 33\ \lambda$, edge illumination subreflector -10 dB, $n = 60$.

2.4.2.3. Diffraction and scattering of the subreflector supports

Not only the subreflector but also the subreflector supports will scatter power in various directions which are difficult to prodict. Presenting the first German ground station, Trentini et al. [119] also discussed the influence of subreflector and supports on the antenna efficiency and sidelobes.

The amplitude of the first near side lobe has been estimated for uniform illumination and for the aperture illumination $F(r) = 1 - r^2$. Also some estimates have been carried out on farther sidelobes. However, Trentini has carried out his calculations for $0 < \theta < 5^\circ$. As he has used the scalar aperture method [Sec. 2.2.1], which is considered to give only reliable results for $0 < \theta < 3\lambda/D$ [108, p. 193], his results are disputable since the diameter of the main reflector is 350 λ.

Wested [123] in his study on blockage also places some remarks on diffraction in a cassegrain system and states that diffraction by the spars is

unimportant to the calculation of the blockage effect. He recommends, however, to use deep reflectors to protect the antenna against ground noise. Experimental work has been reported by Sheftman [105] and Hartsuijker, Baars et al. [47] but predicting the entire diagram caused by struts does not seem feasible. Apparently, here lies a problem for further study. Some progress has been made in the calculation of the near side lobes in a cassegrain system, which we will discuss in chapter 3.

2.4.3. The antenna gain as a function of the system parameters

Using the equations 2.22, 2.36 and 2.46 it is possible to obtain the effects of blockage and diffraction of a subreflector in one equation:

$$G_t = (\pi D/\lambda)^2 \Big| \cot\tfrac{1}{2}\psi_1 \int_0^{\psi_1} [G_1(\psi_1)]^{\frac{1}{2}} \tan\tfrac{1}{2}\psi_1 \, d\psi_1 - D_s/D \, \cot\tfrac{1}{2}\psi_B \int_0^{\psi_B} [G_2(\psi_2)]^{\frac{1}{2}} \cdot \tan\tfrac{1}{2}\psi_2 d\psi_2 - \cot\tfrac{1}{2}\psi_2 \int_{\psi_D}^{\psi_2} [G_2(\psi_2)]^{\frac{1}{2}} \left[1 - e^{-\gamma(\psi_2 - \psi_D)}\right] \tan\tfrac{1}{2}\psi_2 \Big|^2 \quad (2.52)$$

In Eq. 2.52 a large number of parameters is present influencing the gain of a cassegrain system. Calculations have been carried out to find out the relationship between the antenna efficiency η and

(1) the ratio F/D or angular aperture ψ_2;
(2) the diameter of the subreflector D_s;
(3) the tapering towards the edge of the subreflector;
(4) the radiation pattern of the primary feed $G_1(\psi_1)$.

The feed patterns considered are cosine patterns as explained by Eq. 2.31. These theoretical feed patterns are very similar to the main lobes of most available feeds. The chosen values of n are 60, 40, 24, 16, 12 and 10; the higher the value of n the narrower the main lobe of the feed pattern. The edge tapers -6 dB, -8 dB, -10 dB, -15 dB, -20 dB and the diameters of the subreflector 21λ, 24λ, 27λ, 30λ, 33λ, and 36λ. The diameter of the main reflector was kept constant in all calculations (D = 330λ).

2.5. Results and conclusions

The results of these investigations have been laid down in a number of figures (Figs. 2.18 to 2.21). Some very important conclusions can be drawn from them. Using the cosine shaped feed pattern, it appears that the maximum antenna efficiency that can be reached is about 74%. Comparing this value with Silver [108, p. 426] who used similar feed patterns as primary radiators for front-fed paraboloids and with Fig. 2.12, the antenna efficiency is about 8% lower. The difference is entirely determined by the influence of the subreflector. Figs. 2.18 and 2.19 answer the question if the antenna efficiency is a function of the angular aperture Ψ_2. It is clear from these figures that there is practically no relationship. Using a subreflector diameter of 33λ, it appears that the highest efficiencies are found at F/D = 0.25, the efficiency decreasing very slowly at increasing F/D. As the curves are very close to each other, only curves for F/D = 0.25 and F/D = 0.48 are given. The slight dependance of the final result on F/D may be explained by the behaviour of the diffraction efficiency as a function of the angular aperture Ψ_2. A maximum of 74.2% was found at an F/D ratio of 0.25, an edge illumination of -10.5 dB, and a subreflector diameter of 24λ. The maximum efficiency at an F/D ratio of 0.48 was 73.3% at an edge illumination of -10 dB and a subreflector diameter of 27λ. Although the differences are very small, a low F/D ratio seems somewhat favourable. Fig. 2.20 shows the maximum efficiency that can be reached with different primary gain functions. These curves show that the primary feed pattern $G_1(\psi_1)$ is not critical, because for practically all values of n from 10 to 60 in $G_1(\psi_1) = 2(n+1)\cos^n\psi_1$, an efficiency of about 74% was reached although under slightly different circumstances, such as edge illumination and subreflector diameters.

In Fig. 2.21, using the primary gain function mentioned above with different values of n as parameter, the efficiency is found as a function of the subreflector diameter. It appears that an optimum value of the efficiency can be reached. A maximum may be expected since the losses due to the blocking increase at increasing D_s, while conversely, the losses caused by diffraction decrease if D_s is increased. The maximum in the curves, however, is very flat; therefore, the choice of diameter D_s of the subreflector often depends on other factors such as the influence of the noise temperature.

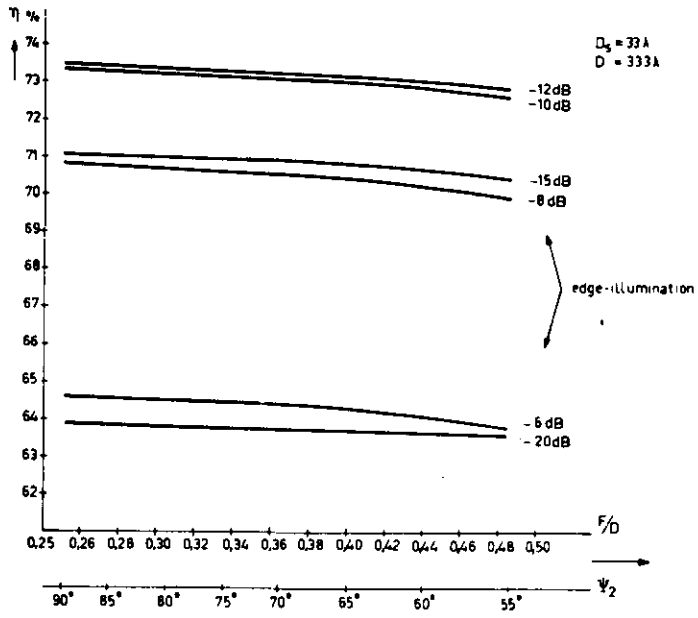

Fig. 2.18 The antenna efficiency η as a function of F/D with the edge illumination of the subreflector as a parameter; gain function of the feed: $G(\psi_1) = 122 \cos^{6.0}\psi_1$

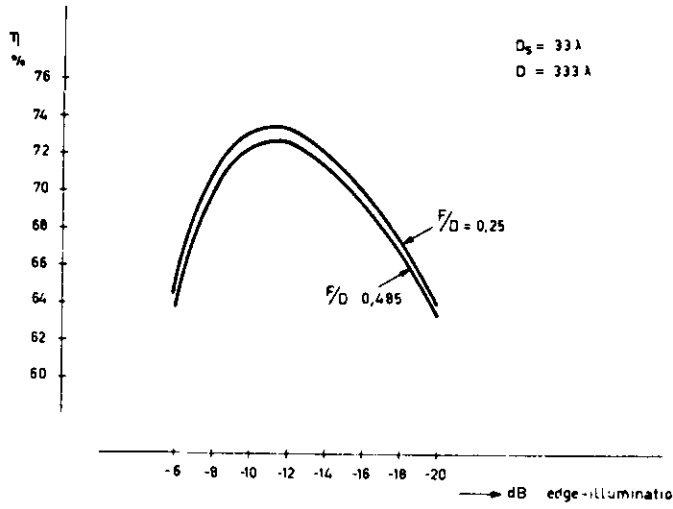

Fig. 2.19 The antenna efficiency η as a function of the edge illumination with the ratio F/D as a parameter. Gain function $G(\psi_1) = 122 \cos^{6.0}\psi_1$

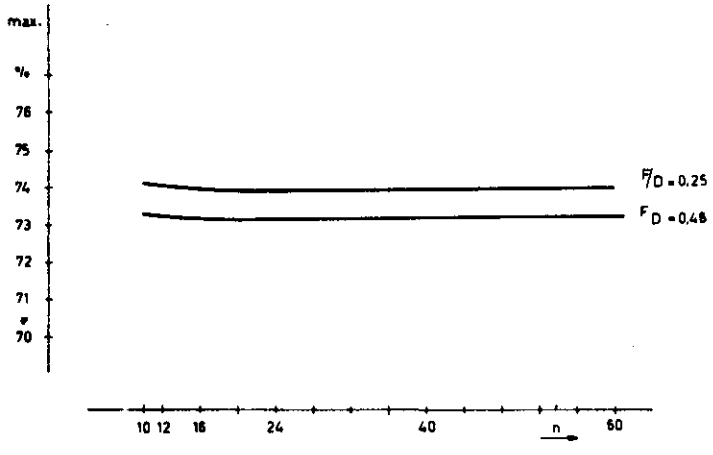

Fig. 2.20 The maximum efficiency as a function of the primary feed pattern $G(\psi_1) = 2(n+1)\cos^n\psi_1$

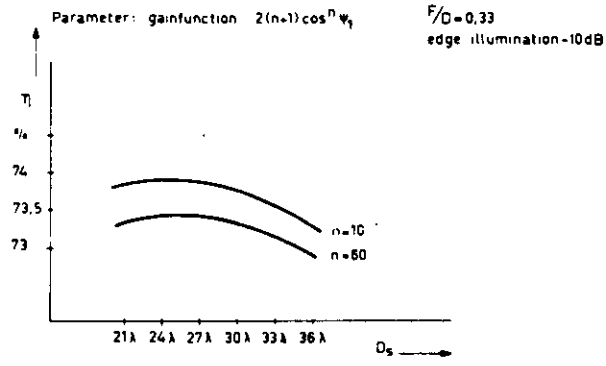

Fig. 2.21 The antenna efficiency as a function of the subreflector diameter

Appendix 2.1. Derivation of Eq. 2.30 from Eq. 2.26

From $\tan\frac{1}{2}\psi_2 = M \tan\frac{1}{2}\psi_1$, where $M = (e + 1)/(e - 1)$ we find $\frac{1}{2}d\psi_2/\cos^2\frac{1}{2}\psi_2 = \frac{1}{2}Md\psi_1/\cos^2\frac{1}{2}\psi_1$ or

$$d\psi_2 = M \frac{\cos^2\frac{1}{2}\psi_2}{\cos^2\frac{1}{2}\psi_1} d\psi_1 = M \frac{1 + \cos\psi_2}{1 + \cos\psi_1} d\psi_1 \tag{1}$$

As, generally

$$\tan\tfrac{1}{2}z = (\sin z)/(1 + \cos z) \tag{2}$$

it follows that

$$M \frac{1 + \cos\psi_2}{1 + \cos\psi_1} = \frac{\sin\psi_2}{\sin\psi_1} \tag{3}$$

Combining Eqs. 1 and 3 we obtain

$$d\psi_2 = \frac{\sin\psi_2}{\sin\psi_1} d\psi_1 \tag{4}$$

From Sec. 2.3.2. we know that

$$\eta_1 = \cot^2\tfrac{1}{2}\Psi_2 \left| \int_0^{\Psi_2} [G_2(\psi_2)]^{\frac{1}{2}} \tan\tfrac{1}{2}\psi_2 \, d\psi_2 \right|^2 \tag{2.26}$$

and

$$G_2(\psi_2) = G_1(\psi_1) \frac{\sin^2\psi_1}{\sin^2\psi_2} \tag{2.11}$$

If we substitute Eqs. 2.9, 2.11 and 4 in Eq. 2.26, we obtain

$$\eta_1 = \frac{1}{M^2} \cot^2\tfrac{1}{2}\Psi_1 \left| \int_0^{\Psi_1} [G_1(\psi_1)]^{\frac{1}{2}} \frac{\sin\psi_1}{\sin\psi_2} M \tan\tfrac{1}{2}\psi_1 \frac{\sin\psi_2}{\sin\psi_1} d\psi_1 \right|^2$$

which is identical with Eq. 2.30.

3. APERTURE BLOCKAGE IN DUAL REFLECTOR ANTENNA SYSTEMS

3.1. Introduction

A limitation of most double reflector antennas, such as cassegrain antennas, is the blockage of the aperture by the subdish and the support legs. Usually, the shadow of the obstacles on the aperture is determined by ray optics. The optical shadows must be weighted by the aperture illumination to calculate the influence on antenna efficiency and sidelobes.
However, as Ruze [101] has already pointed out, the radio frequency shadows are wider than optical shadows; therefore, optical shadows form only an approximation. The problem may be solved if we know in what way the field from the subreflector is scattered by the support legs as regards amplitude and phase, as well as the results of this on the currents induced on the main reflector.
Then by using the current distribution or aperture field methods [108,p.144] the secondary pattern of the reflector may be calculated. However, there is interaction between obstacle and source system, resulting in multiple scattering processes [108,p.129]. This effect may not be neglected here, because the support legs extend from the subreflector to the surface of the main reflector. A calculation of the current distribution over the main reflector seems very difficult. An approach may be found in the geometrical optical theory of diffraction [60]. Therefore, only approximate methods and experiments will give an answer relating to the influence of the support legs on the radiation pattern. It appears that, in accordance with Trentini [119], Kay [59], and Mei and van Bladel [79], diffraction may be neglected and that geometrical optical methods can be used very well, providing the thickness of the support legs $2W > \lambda$.
Recently, Cornbleet [14] has carried out calculations of the radiation pattern of apertures with structural shadows; however, his shadows are not very realistic for cassegrain antennas.
It is common knowledge that in a cassegrain system plane and spherical wavefronts are found. It is also known that shadows due to obstacles depend on the type of wavefront. Shadows in the aperture result in the following effects:

(a) Decrease in antenna gain; this effect can be expressed by the relative blockage coefficient η_B/η_0 where η_0 is the efficiency of the unblocked aperture.

(b) Increase in the sidelobes of the directive gain pattern; different contributions are introduced by the obstacles. Near sidelobes that are to change, are investigated in this chapter. The contribution by the subreflector will be circularly symmetrical, while that by the subreflector support legs is more typically the radiation of a rectangular aperture distribution. There is also wide-angle scattering due to the power blocked by the obstacles. No calculations on this phenomenon will be included.

(c) If sidelobes are directed towards sources with high noise temperature, increase in the noise temperature of the antenna will be noticed because energy is spread from the main beam to the sidelobes.

It is the purpose of this chapter to introduce a method of calculating the influence of blockage on the near sidelobes, as illustrated by several examples, and to discuss several methods of blockage calculation.
The influence of the implantation and thickness of the supports with various edge illuminations will be discussed. Blockage will be investigated theoretically and possibilities of obtaining maximum blockage efficiency will be described.

3.2 Influence of obstructions on the directive gain pattern

Generally, [108, p.173] the relative far field directive gain pattern of a rectangular aperture near the main axis [Fig. 3.1] may be represented by the scalar equation:

$$g(\theta,\phi) = \int_A F(x,y)\, e^{jk \sin\theta(x\cos\phi + y\sin\phi)}\, dxdy \qquad (3.1)$$

and that of a circular aperture [108, p.192] by

$$g(\theta,\phi) = \int_A F(r,\phi')\, e^{jkr \sin\theta \cos(\phi - \phi')}\, rdr\, d\phi' \qquad (3.2)$$

If we want to know the true field pattern $g(\theta,\phi)$, we first calculate $g_0(\theta,\phi)$, being the pattern of the unblocked aperture and subtract from it the contribution $g_1(\theta,\phi)$ of the subreflector and the contributions $g_2(\theta,\phi)$ and $g_3(\theta,\phi)$, being shadows of the supports caused by plane and

spherical waves, respectively. In this way the zero-field concept as discussed in Chapter 2 is met. We shall use the aperture illumination function

$$F(r) = 1 - ar^2 \ , \ 0 \leq r \leq \tfrac{1}{2}D \ , \quad 0 \leq a \leq (2/D)^2 \tag{3.3a}$$

which is circularly symmetrical and shown in Fig. 3.2.
The directive gain pattern of the unblocked circular aperture now becomes

$$g_0(\theta,\phi) = \int_0^{\frac{1}{2}D} r\,dr \int_0^{2\pi} e^{jkr\sin\theta\cos(\phi - \phi')}\,d\phi' - a\int_0^{\frac{1}{2}D} r^3\,dr \int_0^{2\pi} e^{jkr\sin\theta\cos(\phi - \phi')}\,d\phi' \tag{3.4}$$

or

$$g_0(\theta) = 2\pi(\tfrac{1}{2}D)^2(1 - \tfrac{1}{4}aD^2)\,\frac{J_1(u)}{u} + 4\pi a(\tfrac{1}{2}D)^4\,\frac{J_2(u)}{u^2} \ , \tag{3.5}$$

$J_0(u)$, $J_1(u)$ and $J_2(u)$, being Bessel functions of zero, first and second order, and $u = \frac{1}{2}kD\sin\theta$.
As, in accordance with Abramowitch [1, p.390]

$$\lim_{u\to 0} \frac{J_1(u)}{u} = 0.5 \tag{3.6}$$

and

$$\lim_{u\to 0} \frac{J_2(u)}{u^2} = 0.125 \ ,$$

in the main direction, where $\theta = 0$, Eq. 3.5 becomes

$$g_0(0) = \pi(\tfrac{1}{2}D)^2[1 - \tfrac{1}{2}a(\tfrac{1}{2}D)^2] \tag{3.7}$$

This value for $g_0(0)$ will be employed in the following as reference value for the relative pattern of the blocked parts of the aperture.

3.2.1. Contribution by the subreflector

The calculation of the contribution of the subreflector to the radiation pattern is carried out in a similar way as that of $g_0(\theta,\phi)$. This contribution is circularly symmetrical, therefore,

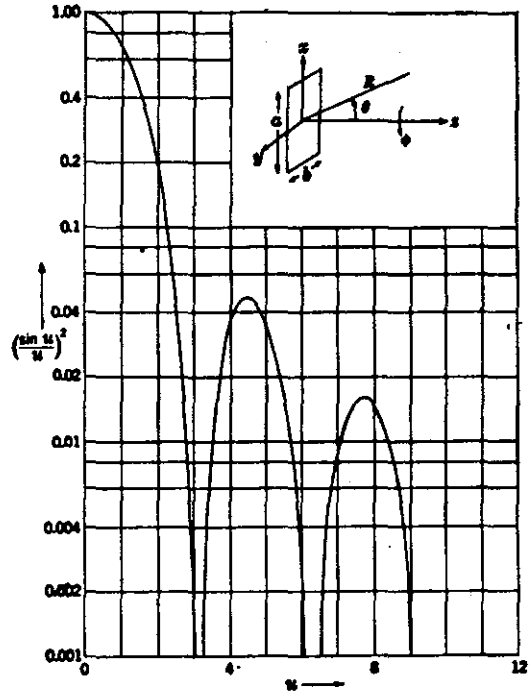

Fig. 3.1 Secondary pattern of a uniformly illuminated rectangular aperture

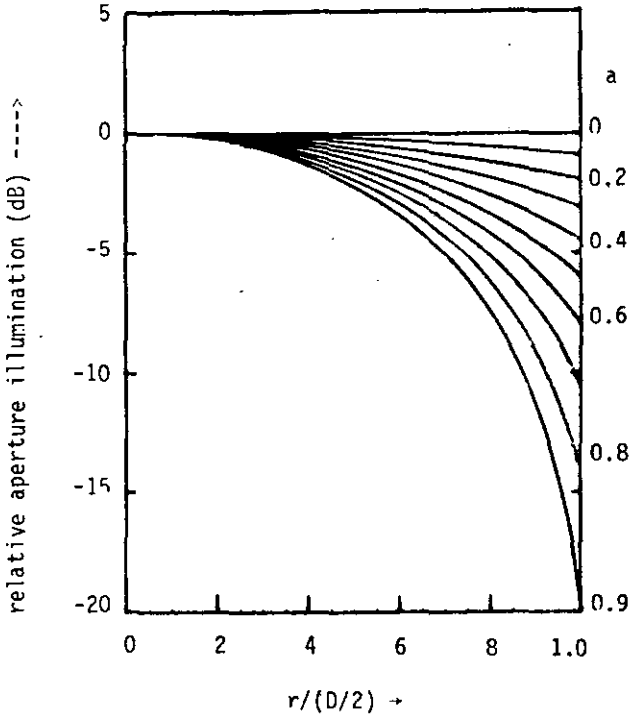

Fig. 3.2.

Aperture illumination function

$F(r) = 1 - ar^2$,

$a_1 = (\frac{D}{2})^2 a$, *being*

a parameter

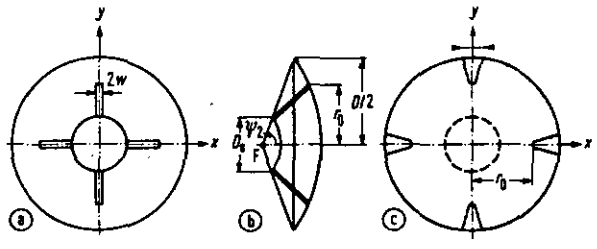

Fig. 3.3 Shadowing by plane and spherical waves in cassegrain antenna systems with four struts
a. Shadow by a plane wave
b. Geometry of the antenna
c. Shadow by a spherical wave

$$g_1(\theta) = 2\pi(\tfrac{1}{2}D_s)^2[1 - a(\tfrac{1}{2}D_s)^2]\frac{J_1(u')}{u'} + 4\pi a(\tfrac{1}{2}D_s)^4 \frac{J_2(u')}{u'^2} \qquad (3.8)$$

where $u' = \frac{1}{2}kD_s \sin\theta$.
On the main axis $\theta = 0$ we find

$$g_1(0) = \pi(\tfrac{1}{2}D_s)^2[1 - \tfrac{1}{2}a(\tfrac{1}{2}D_s)^2] \qquad (3.9)$$

Similarly to Eq. 3.5, Eq. 3.8 is independent of ϕ.
The results of this section are similar to those obtained in Sec. 2.4.1, because the aperture-field distribution $F(r,\phi')$ is related to the primary pattern of an antenna feed by means of Eq. 2.18. A rapid check may be carried out by introducing uniform illumination [108, p.433] over the aperture by taking $a = 0$ in Eq. 3.9 and

$$G_2(\psi_2) = \cot^2\tfrac{1}{2}\Psi_B / \cos^4 \tfrac{1}{2}\psi_2 \qquad (3.10)$$

in Eq. 2.36.

3.2.2. Contribution by the supports due to plane waves

The shadows in the aperture of the supports, resulting from the interception of plane waves, have a rectangular shape [Fig. 3.3].
To calculate the contribution of these shadows to the total directive gain pattern, we shall use Eq. 3.1, while it is convenient to express Eq. 3.3a in rectangular coordinates:

$$F(x,y) = 1 - ax^2 - ay^2,\ 0 < x < \tfrac{1}{2}D,\ 0 < y < \tfrac{1}{2}D,\ 0 \leqslant a \leqslant (2/D)^2 \qquad (3.3b)$$

The contribution is then

$$g_2(\theta,\phi) = \iint (1 - ax^2 - ay^2)\, e^{jk\sin\theta(x\cos\phi + y\sin\phi)}\, dxdy \qquad (3.11)$$

It is convenient to introduce the new variables $u = k\sin\theta\sin\phi$ and $v = k\sin\theta\cos\phi$.

Eq. 3.11 then becomes

$$g_2(u,v) = \int e^{jvx}dx \int e^{juy}dy - \int ax^2 e^{jvx}dx \int e^{juy}dy - \int e^{jvx}dx \int ay^2 e^{juy}dy \text{ or}$$

$$g_2(u,v) = g_2'(u,v) - g_2''(u,v) - g_2'''(u,v). \tag{3.12}$$

After introducing the integration limits we obtain

$$g_2'(u,v) = \int_{-w}^{+w} e^{jvx}dx \left[\int_{-r_0}^{+r_0} e^{juy}dy - \int_{-\frac{1}{2}D_S}^{+\frac{1}{2}D_S} e^{juy}dy \right] + \int_{-w}^{+w} e^{juy}dy \left[\int_{-r_0}^{+r_0} e^{jvx}dx - \int_{-\frac{1}{2}D_S}^{+\frac{1}{2}D_S} e^{jvx}dx \right] \tag{3.13a}$$

$$g_2''(u,v) = \int_{-w}^{+w} ax^2 e^{jvx}dx \left[\int_{-r_0}^{+r_0} e^{juy}dy - \int_{-\frac{1}{2}D_S}^{+\frac{1}{2}D_S} e^{juy}dy \right] + \int_{-w}^{+w} e^{juy}dy \left[\int_{-r_0}^{+r_0} ax^2 e^{jvx}dx - \int_{-\frac{1}{2}D_S}^{+\frac{1}{2}D_S} ax^2 e^{jvx}dx \right] \tag{3.13b}$$

$$g_2'''(u,v) = \int_{-w}^{+w} e^{jvx}dx \left[\int_{-r_0}^{+r_0} ay^2 e^{juy}dy - \int_{-\frac{1}{2}D_S}^{+\frac{1}{2}D_S} ay^2 e^{juy}dy \right] + \int_{-w}^{+w} ay^2 e^{juy}dy \left[\int_{-r_0}^{+r_0} e^{jvx}dx - \int_{-\frac{1}{2}D_S}^{+\frac{1}{2}D_S} e^{jvx}dx \right] \tag{3.13c}$$

Carrying out the integration leads to long expressions which have been discussed elsewhere [28].

If uniform aperture distribution is used ($a = 0$), only Eq. 3.13a is left. In the direction of the main lobe, where $\theta = 0$, we find if $a \neq 0$

$$g_2(0,0) = 8w(r_0 - \tfrac{1}{2}D_S) - 8aw[\tfrac{1}{3}r_0^3 - \tfrac{1}{3}(\tfrac{1}{2}D_S)^3] - 8aw^3(\tfrac{1}{3}r_0 - \tfrac{1}{6}D_S). \tag{3.14}$$

3.2.3. Contribution by the supports due to spherical waves

As observed before [22, 123], the shadows from the supports due to spherical waves are very similar to trapezoids. We shall introduce this approximation because it reduces calculation work and makes possible a convenient solution of the integrals. From Fig. 3.3 it is found that for the trapezoid lying in the area indicated by $r_0 < x < \frac{1}{2}D$, y as a function of x is given by $y(x > 0) = \beta x + w - \beta r_0 = \beta x + \gamma$ with $\beta = w(D/D_s - 1)/(\frac{1}{2}D - r_0)$ and $\gamma = w - \beta r_0$
For $-\frac{1}{2}D < x < -r_0$ we find $y(x<0) = -\beta x + \gamma$.
For the trapezoid parts along the y axis, x is written as a function of y: $x(y>0) = \beta y + \gamma$, $x(y<0) = -\beta y + \gamma$. If $u = k\sin\theta\sin\phi$ and $v = k\sin\theta\cos\phi$, the complete expression for the contribution of spherical waves is then

$$
\begin{aligned}
g_3(u,v) = &\int_{-y(x>0)}^{+y(x>0)} \int_{r_0}^{\frac{1}{2}D} (1 - ax^2 - ay^2)\, e^{jvx}\, e^{juy}\, dxdy + \\
&+\int_{-y(x<0)}^{+y(x<0)} \int_{-\frac{1}{2}D}^{-r_0} (1 - ax^2 - ay^2)\, e^{jvx}\, e^{juy}\, dxdy + \\
&+\int_{-x(y>0)}^{+x(y>0)} \int_{r_0}^{\frac{1}{2}D} (1 - ax^2 - ay^2)\, e^{jvx}\, e^{juy}\, dxdy + \\
&+\int_{-x(y<0)}^{+x(y<0)} \int_{-\frac{1}{2}D}^{-r_0} (1 - ax^2 - ay^2)\, e^{jvx}\, e^{juy}\, dxdy
\end{aligned}
\qquad (3.15)
$$

This integration may be carried out although it is very time consuming [28]. For $\theta = 0$ we find in the main direction

$$
\begin{aligned}
g_3(0,0) = &\, 8\gamma(1 - \tfrac{1}{3}a\gamma^2)(\tfrac{1}{2}D - r_0) + 4\beta(1 - a\gamma^2)(\tfrac{1}{4}D^2 - r_0^2) - \tfrac{8}{3}a\gamma(\beta^2 + 1) \\
&\cdot[(\tfrac{1}{2}D)^3 - r_0^3)] - 2\alpha\beta(\tfrac{1}{3}\beta^2 + 1)[(\tfrac{1}{2}D)^4 - r_0^4].
\end{aligned}
\qquad (3.16)
$$

3.2.4. Total directive gain pattern $g_t(\theta,\phi)$

The expressions found above enable us to find the total pattern $g_t(\theta,\phi)$ in the Fraunhofer zone in accordance with the "zero field concept". As has

been explained before [2], the results only apply for the main lobe and the near sidelobes. We shall find that

$$g_t(\theta,\phi) = g_0(\theta) - g_1(\theta) - g_2(u,v) - g_3(u,v) \qquad (3.17)$$

where $g_0(\theta)$ represents the pattern of an unblocked aperture given by Eq. 3.4; $g_1(\theta)$ the contribution to the pattern by the subreflector [Eq.3.8]; $g_2(u,v)$ the contribution to the pattern due to plane wave shadows [Eq.3.13]; and $g_3(u,v)$ the contribution to the pattern due to spherical wave shadows [Eq.3.15].

In this way the radiation pattern of a cassegrain antenna near the main lobe may be found as a function of several variables, such as the edge illumination of the main reflector, the thickness of the subreflector supports, the ratio D_s/D, the F/D ratio, and the strut implantation. Some examples, particularly for satellite communication ground station antennas are shown in Figs. 3.4 and 3.5 with uniform illumination ($a = 0$), $2w = 2\lambda$, and $\phi = 0$ or $\phi = 45^0$. The position of the first, second, and third sidelobes and their intensity with respect to that of the main lobe are shown. Figs. 3.4a and 3.5a show main and sidelobes of the blocked and unblocked aperture in dB, and Figs. 3.4b and 3.5b the relative pattern of the contributors to the blockage.

The main part of the results for other edge illuminations or different widths of the supports is shown in two tables, one for $\phi = 0^0$ and one for $\phi = 45^0$ [Tables 3.1 and 3.2].

Table 3.1 $D = 330\lambda$; $D/D_s = 10$; $r_0 = 1/3\ D$; $\phi = 0^0$; $a_1 = 0$ (uniform illumination)

		main lobe		1st side lobe		2nd side lobe		3rd side lobe	
	2w	θ in ^{0}	dB	θ in ^{0}	dB	θ in ^{0}	dB	θ in ^{0}	dB
G_0	0	0.00	0.00	0.283	-17.6	0.465	-23.8	0.642	-28.0
G_t	1λ	0.00	-0.26	0.286	-16.5	0.469	-27.0	0.647	-25.2
G_t	2λ	0.00	-0.41	0.288	-16.1	0.473	-29.2	0.652	-24.2
G_t	3λ	0.00	-0.59	0.290	-15.7	0.477	-31.9	0.657	-23.4
G_t	4λ	0.00	-0.76	0.293	-15.3	0.482	-35.3	0.662	-22.8
G_t	5λ	0.00	-0.94	0.296	-14.9	0.487	-39.8	0.667	-22.3

a_1 = 0.7 (edge illumination -10dB)

		main lobe		1st sidelobe		2nd sidelobe		3rd sidelobe	
	2w	θ in ^{0}	dB	θ in ^{0}	dB	θ in ^{0}	dB	θ in ^{0}	dB
G_o	-	0.00	0.00	0.314	-22.4	0.489	-29.6	0.662	-34.1
G_t	1λ	0.00	-0.28	0.316	-20.2	0.494	-38.6	0.666	-28.3
G_t	5λ	0.00	-0.86	0.324	-17.8	-	-	0.690	-24.4

a_1 = 0.9 (edge illumination -20dB)

G_o	-	0.00	0.00	0.336	-24.3	0.515	-32.8	0.688	-38.3
G_t	1λ	0.00	-0.29	0.338	-21.3	0.521	-64.8	0.693	-29.7
G_t	5λ	0.00	-0.82	0.345	-18.8	-	-	0.720	-25.3

Table 3.2 D = 333λ; D/D_s = 10; r_o = 1/3D; φ = 45^0

a_1 = 0 (uniform illumination)

		main lobe		1st sidelobe		2nd sidelobe		3rd sidelobe	
		θ in ^{0}	dB	θ in ^{0}	dB	θ in ^{0}	dB	in ^{0}	dB
G_o	-	0.00	0.00	0.283	-17.6	0.465	-23.8	0.642	-28.0
G_t	1λ	0.00	-0.25	0.283	-17.8	0.460	-25.8	0.635	-25.4
G_t	2λ	0.00	-0.42	0.283	-18.7	0.456	-26.5	0.629	-24.5
G_t	3λ	0.00	-0.59	0.283	-19.7	0.449	-27.0	0.624	-23.7
G_t	4λ	0.00	-0.76	0.283	-20.8	0.443	-27.3	0.620	-23.0
G_t	5λ	0.00	-0.94	0.283	-22.0	0.438	-27.4	0.616	-22.3

a_1 = 0.7 (edge illumination -10dB)

G_o	-	0.00	0.00	0.314	-22.4	0.489	-29.6	0.662	-34.1
G_t	1λ	0.00	-0.28	0.314	-21.7	0.484	-35.7	0.651	-29.1
G_t	5λ	0.00	-0.86	0.317	-26.0	0.460	-39.7	0.631	-26.5

a_1 = 0.9 (edge illumination -20dB)

G_o	-	0.00	0.00	0.336	-24.3	0.515	-32.8	0.688	-38.3
G_t	1λ	0.00	-0.29	0.337	-22.8	0.511	-46.9	0.676	-31.1
G_t	5λ	0.00	-0.82	0.340	-26.3	-	-	0.651	-29.3

3.2.5. Results and conclusions

Studying Fig. 3.4 in the $\phi = 0$ plane, it appears that $g_1(\phi)$ varies only little within the region under discussion. Comparison of $g_1(\theta)$ with $g_0(\theta)$ shows that $g_1(\theta)$ relative to $g_1(0)$ has a similar pattern as $g_0(\theta)$ relative to $g_0(0)$; however, the θ scale of $g_1(\theta)$ has been extended by a factor nearly 10. This is due to the fact that the relation $D/D_s = 10$ has been used and that $\sin\theta \approx \theta$.

The contributions of $g_2(u,v)$ and $g_3(u,v)$ in the $\phi = 0$ plane [Fig. 3.4] are positive within the entire region under discussion. This fact is explained by considering that the contributions of an array of two supports located in the $\phi = 90^0$ plane to the final pattern are almost constant, and that those in the $\phi = 0^0$ plane are alternating but not in such a way that the amplitude of g_2 plus g_3 becomes negative.
The situation in the $\phi = 45^0$ plane [Fig. 3.5] differs entirely from that in the $\phi = 0^0$ plane because now the amplitudes of the patterns g_2 and g_3 are alternatively positive and negative. This is due to the fact that the supports are located symmetrically round the $\phi = 45^0$ plane.

This phenomenon is noticed in all investigations independent of the edge illumination and of the width of the struts.
If we study the results from tables 3.1 and 3.2, it appears that the peak intensity of the main lobe of a blocked aperture is somewhat less than that of an unblocked aperture. In the case of $\phi = 0$, the intensity of the first sidelobe increases with increasing width of the supports. This is noticed for all edge illuminations. However, if $\phi = 45^0$, the opposite occurs and the peak intensity of the first sidelobes decreases with increasing edge illumination; only for small values of w, e.g. $2w = \lambda$, little or no increase or decrease is noticed. The differences are largest when thick supports are employed.
Similar phenomena have been observed earlier in experiments [47, 105], while recent measurements carried out with the 10-metre dish of the Dutch PTT antenna at Nederhorst den Berg confirm the differences in the $\phi = 0$ and $\phi = 45^0$ planes with regard to the first sidelobe [90] [Fig. 3.6] . This effect may be used with advantage for the location of the supports of reflector antennas to obtain lower sidelobes in particular directions.

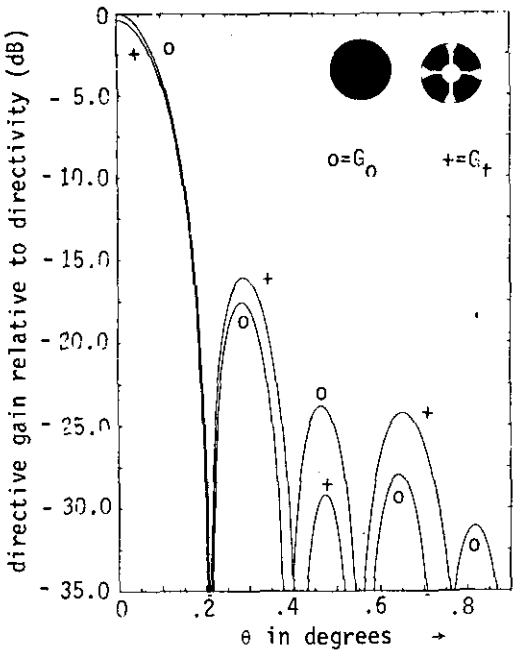

Fig. 3.4a
Directive gain pattern relative to directivity, uniform illumination
$\phi = 0$ $D = 330\lambda$ $D_s = 33\lambda$ $r_o = 110\lambda$ $2w = 2\lambda$

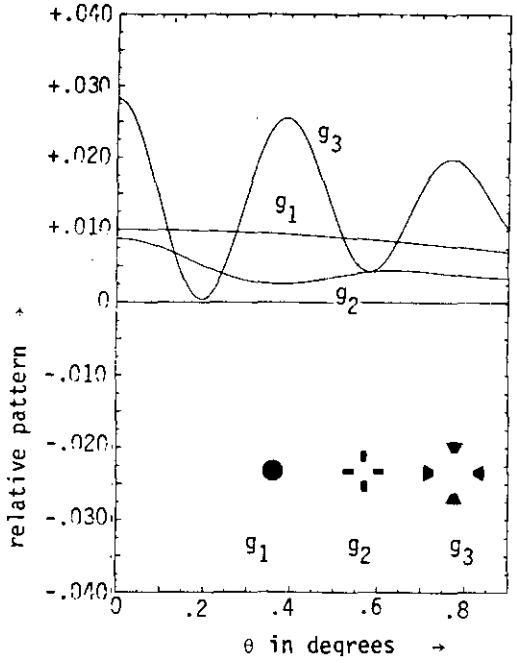

Fig. 3.4b
Relative patterns g_1, g_2 *and* g_3, *uniform illumination*

$$G_o = 10 \log \left| \frac{g_o(\theta)}{g_o(0)} \right|^2 \qquad G_t = 10 \log \left| \frac{g_t(\theta)}{g_o(0)} \right|^2$$

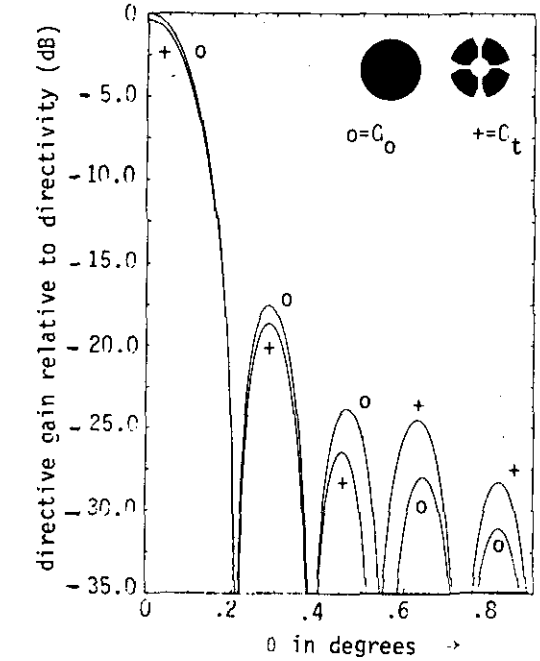

Fig. 3.5a
Directive gain pattern relative to directivity, uniform illumination.
$\phi = 45^0$ $D = 330\lambda$ $D_s = 33\lambda$ $r_o = 110\lambda$ $2w = 2\lambda$

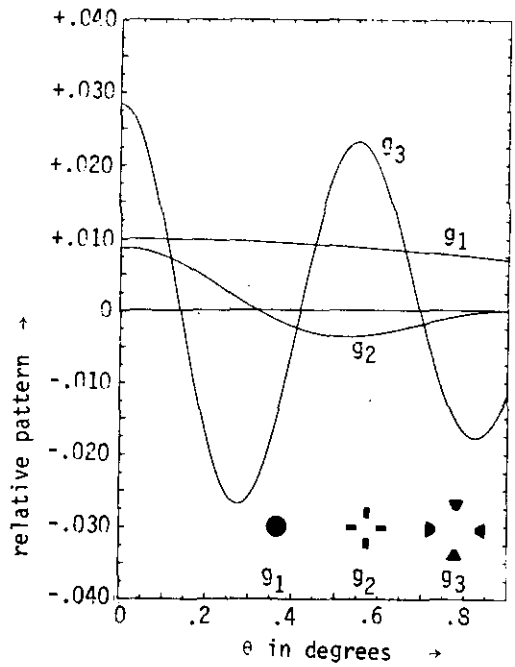

Fig. 3.5b
Relative patterns g_1, g_2 *and* g_3.

$$G_o = 10 \log \left| \frac{g_o(\theta)}{g_o(0)} \right|^2 \qquad G_t = 10 \log \left| \frac{g_t(\theta)}{g_o(0)} \right|^2$$

If the width of the supports $2w < \lambda$, the above method is no longer applicable, as described before [79].

3.3. Power balance of the blocked aperture

If there is no spillover round the edge of the subreflector and the total power P_T radiated by the feed is intercepted by the subreflector, the effective power reradiated by the aperture is found by subtracting the power P_B blocked by the obstacles from the total power P_T.
Let the coordinates of a point in the aperture be x,y and the electric field over the aperture $F(x,y)$. The total power radiated by the non-blocked aperture is, according to Silver [108, p. 177].

$$P_T = \tfrac{1}{2}(\varepsilon/\mu)^{\frac{1}{2}} \int_A |F(x,y)|^2 \, (\bar{a}_z.\bar{a}_s) \, dxdy \tag{3.18}$$

In this equation $\bar{a}_s$ is the unit vector along a ray [108, p. 170] and $\bar{a}_z$ the unit vector perpendicular to the aperture along the z-axis. For $\theta = 0$, in the case that the phase of $F(x,y)$ is constant over the aperture, the rays are parallel to the z-axis so that $\bar{a}_z.\bar{a}_s = 1$.
If the aperture is blocked by a number of obstacles [Fig. 3.7] totalized by

$$B = \sum_{n=1}^{n=m} B_n$$

the blocked power becomes

$$P_B = \tfrac{1}{2}(\varepsilon/\mu)^{\frac{1}{2}} \int_B |F(x,y)|^2 \, dxdy \tag{3.19}$$

This part of the total power P_T is radiated by the primary feed but it cannot be reradiated by the blocked aperture in the normal way, because it will be scattered arbitrarely by the feed support, feed cone, subdish and main dish.
The directive gain function of the lossless antenna is expressed by $G(\theta,\phi)$, where θ and ϕ are spherical coordinates illustrated in Fig. 1.1. This function must also satisfy the relation

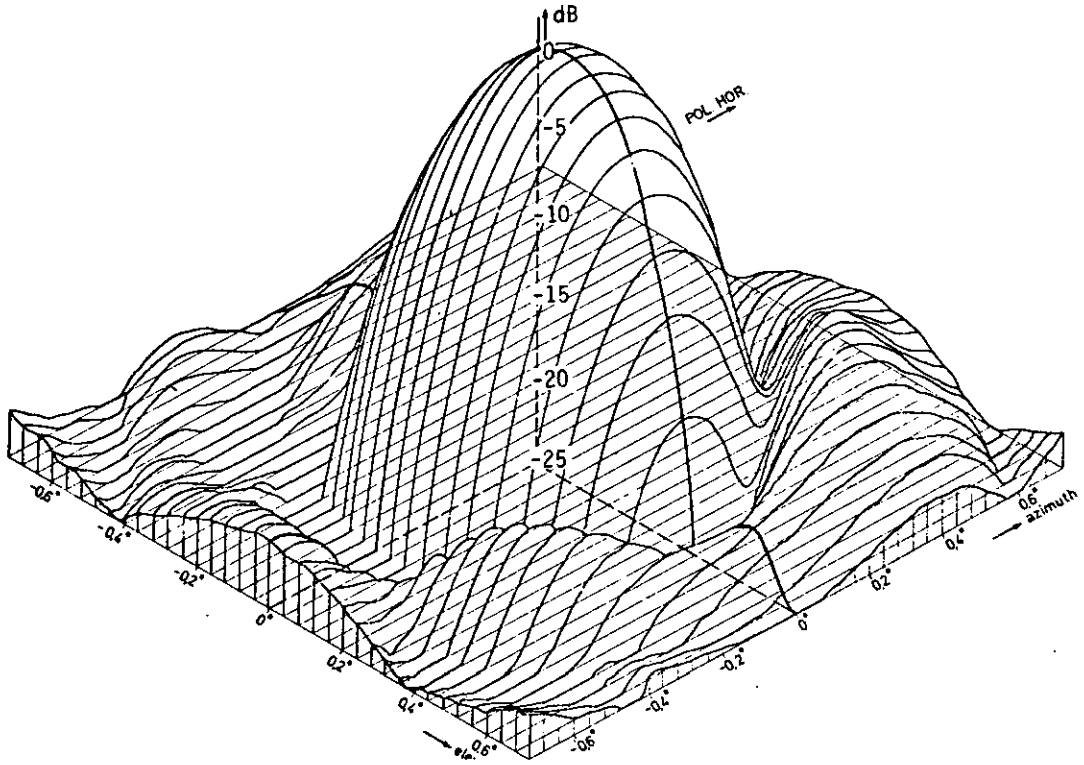

Fig. 3.6 Radiation pattern of the 10 metre antenna at Nederhorst den Berg
f = 12 GHz

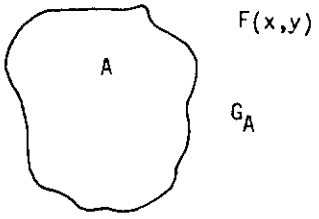

Fig. 3.7a Aperture A without blocking

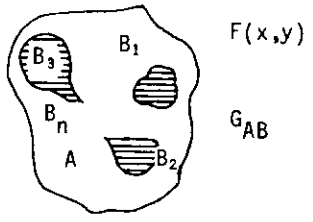

Fig. 3.7b Aperture A blocked by obstacles B

$$\int_{4\pi} G(\theta,\phi)\, d\Omega = 4\pi \tag{3.20}$$

$d\Omega$ being the element of solid angle.

If $P(\theta,\phi)$ is the power radiated by the antenna per unit solid angle in the direction θ,ϕ, and P_T the total power radiated, the gain is defined as

$$G(\theta,\phi) = \frac{P(\theta,\phi)}{P_T/4\pi} \tag{1.1}$$

The power reradiated by the aperture less the blocked areas will now be equal to

$$P_T - P_B = \tfrac{1}{2}(\varepsilon/\mu)^{\frac{1}{2}} \int_{A-B} |F(x,y)|^2\, dxdy \tag{3.21}$$

This equation shows that the surface integral extends over the aperture surface A less the blocked surfaces B. A new gain function

$$G'(\theta,\phi) = \frac{P'(\theta,\phi)}{P_T/4\pi}$$

will now be formed depending on the power $P'(\theta,\phi)$ radiated per unit solid angle, whereas

$$\int_{4\pi} P'(\theta,\phi)\, d\Omega = P_T - P_B \tag{3.22}$$

This new gain function, in which the blocked power is not transported correctly to the aperture, is now determined by

$$\int_{4\pi} G'(\theta,\phi)\, d\Omega \neq 4\pi$$

or

$$\int_{4\pi} G'(\theta,\phi)\, d\Omega = 4\pi(1 - P_B/P_T)$$

or

$$\int_{4\pi} G'(\theta,\phi)\, d\Omega = 4\pi - \frac{2\pi}{P_T}(\varepsilon/\mu)^{\frac{1}{2}} \int_B |F(x,y)|^2\, dxdy \qquad (3.23)$$

The power P_B is scattered by the subreflector, main reflector support legs, feed and feed cone, and adds new contributions to the antenna pattern $G'(\theta,\phi)$, so that the power balance is restored. This scattered power radiates in various directions, which are difficult to predict. The antenna pattern $G'(\theta,\phi)$ with supplementary contributions from the scattered power P_B may increase the noise temperature of the antenna if these contributions are directed towards noise sources at high temperatures [23]. Apparently, the blocked power increases the sidelobe level and the antenna noise temperature as well. Therefore, the total influence of blocking parts on the aperture results in a double effect, viz.,

(1) a decrease in the relative blockage efficiency η_B/η_0 and an increase in the sidelobe level, with the possibility of a higher antenna temperature; in this chapter this effect is studied in detail for the region near the main axis of the antenna.

(2) an increase in the sidelobe level, owing to the blocked power P_B being scattered, and hence higher noise temperatures. This effect is difficult to calculate and will not be discussed in this report.

3.4. Blockage efficiency in general

3.4.1. Basic expressions

Let A be a non-blocked aperture and the coordinates of an aperture field be x,y. Let the aperture field be $F(x,y)$. If the phase is constant over the aperture, the gain obtained for $\theta = 0$ is, according to Silver [108, p. 177],

$$G_A = \frac{4\pi}{\lambda^2} \frac{\left|\int_A F(x,y)\, dxdy\right|^2}{\int_A |F(x,y)|^2\, dxdy} \qquad (3.24)$$

where dxdy represents an elementary area of the aperture.

From Eq. 3.1 it follows that for $\theta = 0$

$$\int_A F(x,y)\, dxdy = g_A(0,0) \tag{3.25}$$

If the aperture illumination is uniform in amplitude and phase, $F(x,y)$ will be a constant. In that case, we find from Eqs. 3.24 and 3.25 that

$$G_{max} = 4\pi A / \lambda^2 \tag{3.26}$$

and $g_A(0,0) :: A$, being the geometrical surface of the aperture.
We also may introduce the effective aperture A_{eff} by

$$G_A = 4\pi A_{eff}/\lambda^2 \tag{3.27}$$

where

$$A_{eff} = \frac{\left| \int_A F(x,y)\, dxdy \right|^2}{\int_A |F(x,y)|^2\, dxdy} \tag{3.28}$$

The illumination efficiency η_0 of this non-blocked aperture will now be defined by the relation

$$\eta_0 = \frac{1}{A} \frac{\left| \int_A F(x,y)\, dxdy \right|^2}{\int_A |F(x,y)|^2\, dxdy} = \frac{A_{eff}}{A} \tag{3.29}$$

The integral

$$\int_A |F(x,y)|^2\, dxdy$$

is a measure of the power radiated by the primary feed and intercepted by the main reflector if no spillover is present. The integral Eq. 3.25 is proportional to the field intensity on the main axis.
For circularly symmetrical aperture field distributions, $dxdy$ of Eq. 3.29 may be replaced by $2\pi r dr$, where r is the radial distance of the elementary

area from the centre of the aperture. Eq. 3.24 then becomes

$$G_A = \frac{8\pi^2}{\lambda^2} \frac{\left| \int_0^{\frac{1}{2}D} F(r)\, r\,dr \right|^2}{\int_0^{\frac{1}{2}D} |F(r)|^2\, r\,dr} \tag{3.30}$$

and Eq. 3.29

$$\eta_0 = \frac{2\pi}{A} \frac{\left| \int_0^{\frac{1}{2}D} F(r)\, r\,dr \right|^2}{\int_0^{\frac{1}{2}D} |F(r)|^2\, r\,dr} \tag{3.31}$$

if D is the diameter of this circular aperture.
Let the aperture be blocked by a number of obstacles B_1, B_2, B_3, -------B_n [Fig. 3.7] with

$$g_B(0,0) = \int_{B_n} F(x,y)\, dxdy \ ,$$

where B_n is the effective aperture surface of the blocked parts, and let G_T be the gain of the aperture A containing the blocking obstacles B. The efficiency η_B of the blocked aperture is now defined by $\eta_B = G_T/G_{max}$ or

$$\eta_B = \frac{1}{A} \frac{\left| \int_{A-B} F(x,y)\, dxdy \right|^2}{\int_A |F(x,y)|^2\, dxdy} \tag{3.32}$$

Comparing the efficiency of the blocked and non-blocked apertures, we obtain the relative blockage efficiency

$$\frac{\eta_B}{\eta_0} = \frac{\left| \int_{A-B} F(x,y)\, dxdy \right|^2}{\int_A |F(x,y)|^2\, dxdy} \cdot \frac{\int_A |F(x,y)|^2\, dxdy}{\left| \int_A F(x,y)\, dxdy \right|^2}$$

or

$$\frac{\eta_B}{\eta_0} = \left| \frac{{}_{A-B}\int F(x,y)\ dxdy}{{}_{A}\int F(x,y)\ dxdy} \right|^2 = \left| \frac{g_{A-B}(0,0)}{g_A(0,0)} \right|^2 \tag{3.33}$$

so that

$$\frac{\eta_B}{\eta_0} = \left| 1 - \frac{{}_{B}\int F(x,y)\ dxdy}{{}_{A}\int F(x,y)\ dxdy} \right|^2 = \left| 1 - \frac{g_B(0,0)}{g_A(0,0)} \right|^2 \tag{3.34}$$

In the same way the blockage efficiency for a circularly symmetrical aperture with circularly symmetrical illumination may be expressed by

$$\frac{\eta_B}{\eta_0} = \left| 1 - \frac{{}_{B}\int F(r)\ rdr}{{}_{A}\int F(r)\ rdr} \right|^2 \tag{3.35}$$

In the case of uniform illumination, $F(x,y)$ is a constant. Therefore,

$$\frac{\eta_B}{\eta_0} = \left| 1 - \frac{B}{A} \right|^2 \tag{3.36}$$

A and B being geometrical surfaces. Calculations with tapered illumination are presented in Sec. 3.5.3.

3.4.2. Optimizing the blockage efficiency

In Sec. 3.3 it was already found that part of the total power P_T radiated by the feed will not be reradiated by the blocked aperture in the proper way, as it does not reach the aperture in the correct direction and phase. The result is that this power is scattered randomly, decreasing antenna gain and blockage efficiency.

If the antenna is used for receiving purposes it is easily shown that power of the incoming waves is intercepted by the obstacles. This intercepted power is always wasted and can never be supplied to the feed of the antenna system properly, as it has not the correct phase. In the remaining part of

this section it will be proved that the blockage efficiency may be increased considerably.

On the ground of considerations which are not of interest here, let $F(x,y)$ be a preferred function for the distribution of the field over an aperture, part of which is inoperative owing to blockage. If it is possible to distribute the total power available for transmission over the unblocked portion of the aperture, such that a new function $c.F(x,y)$ is obtained, the loss of power due to blocking will be partly eliminated. Factor c is here a constant.

The power P_T radiated by the non-blocked aperture is given by Eq. 3.18. Applying the field distribution $F'(x,y) = c.F(x,y)$ over the unblocked portion of the aperture $A-B$, which should radiate P_T as well, leads to

$$P_T = \tfrac{1}{2}(\varepsilon/\mu)^{\frac{1}{2}}\, c^2 \int_{A-B} |F(x,y)|^2 \, dxdy \tag{3.37}$$

so that by means of Eq. 3.18 and 3.21

$$c^2 = \frac{\int_{A} |F(x,y)|^2 \, dxdy}{\int_{A-B} |F(x,y)|^2 dxdy} = \frac{P_T}{P_T - P_B} \tag{3.38}$$

Since the illumination has now been multiplied by a factor c, Eq. 3.33 for the new blockage coefficient can now be written

$$\left(\frac{n_B}{n_0}\right)_{max} = \left| \frac{\int_{A-B} cF(x,y)\, dxdy}{\int_{A} F(x,y) dxdy} \right|^2 = c^2 \, \frac{n_B}{n_0} \tag{3.39}$$

Substituting Eq. 3.38 in Eq. 3.39 we obtain

$$\left(\frac{n_B}{n_0}\right)_{max} = \left| \frac{\int_{A-B} F(x,y)\, dxdy}{\int_{A} F(x,y)\, dxdy} \right|^2 \cdot \frac{\int_{A} |F(x,y)|^2 \, dxdy}{\int_{A-B} |F(x,y)|^2 \, dxdy} \tag{3.40}$$

Comparison of Eq. 3.40 with Eq. 3.33 shows only a little difference in the denominator. In Eq. 3.40 we find the expression

$$\int_{A-B} |F(x,y)|^2 \, dxdy \tag{3.41}$$

as compared with

$$\int_{A} |F(x,y)|^2 \, dxdy \tag{3.42}$$

in Eq. 3.33 .

Eq. 3.41 can be explained as being the power radiated by the blocked aperture with the original aperture field $F(x,y)$. This power is less than that radiated according to Eq. 3.42. This also means that the blocking efficiency η_B/η_0 will increase as compared with the blocking efficiency presented by Eq. 3.33. In the case of uniform illumination, $F(x,y)$ is a constant.

Hence Eq. 3.40 is written as

$$\left(\frac{\eta_B}{\eta_0}\right)_{max} = 1 - \frac{B}{A} \tag{3.43}$$

The improvement compared with Eq. 3.36 shows that the gain and surface are directly proportional to each other, which is normal for antenna systems. Apparently no power transmitted by the feed is lost by scattering through the obstacles blocking the aperture.

In chapter 5 it will be shown that the relative blockage efficiency η_B/η_0 can be increased to a maximum of

$$\frac{\eta_B}{\eta_0} = 1 - \frac{\sum B_{plane}}{A} \quad . \tag{3.44}$$

If the aperture is illuminated uniformly, and ΣB_{plane} represents the parts blocked by plane waves, then Eq. 3.38 becomes

$$c^2 = \frac{A}{A - B_{plane}} \quad . \tag{3.45}$$

3.5 Typical examples of calculations of aperture blockage efficiency

3.5.1. Introduction

The shadows of obstacles within a cassegrain antenna such as subreflector and struts may be treated by geometrical optics, if they are of the same order of magnitude as or larger than the wavelength [59,119]. Although struts of different constructions are known and applied, this paper will only deal with struts of cylindrical cross-section, as frequently used in practice. Moreover, not much difference is noticed if rectangular struts are used [79,101].

It has been indicated before [21] that three major areas of shadowing are known [Figs. 3.3], assuming no feed blockage.

(1) The centre obstacle or the subreflector shows a shadow on the aperture obtained by projecting the subreflector by a plane wave (B_1).

(2) The portion of the plane wave obstructed by the struts is found by projecting the struts on the main reflector aperture (B_2) by a plane wave.

(3) The third shadow (B_3) is formed by projecting the support legs on the aperture by a spherical wave with its phase centre in the focus [Fig. 3.3c]. In the case of shaped systems this wave is nearly spherical.

The last shadow starts from the point where the supports have been fixed to the main reflector, indicated in Fig. 3.3b by the distance r_0. Owing to the mechanical difficulties the supports are very seldom fixed at the rim of a large reflector. Several investigators [21, 101, 119, 123] have made calculations with respect to these shadows more or less approximatedly. The best possible approximation up till now was presented by Ruze [101] and his method will now partly be followed. From the geometry shown in Fig. 3.3, it will be seen that the geometrical surface of the central part B_1 is $\frac{1}{4}\pi D_s^2$ and that the geometrical surface of the shadow of the supports is $B_2 = 8w(r_0 - \frac{1}{2}D_s)$, where it is assumed that the supports are attached to the subreflector, and that four supports will be used. The calculation of the shadow surface from the support legs caused by spherical waves is somewhat more complicated. The projections of the support legs by spherical waves are very similar to trapezoids. Wested [123], however, indicated that the sides of this "trapezoid" are not straight lines, but arcs.

In spite of the small amount of inaccuracy, Wested used the trapezoid

approximation. It does, indeed, simplify the calculations and it is to some extent used in this report to discuss the sidelobes caused by blockage. A calculation without approximation is carried out in Appendix 3.1. It is found there that for four supports the geometrical surface equals to

$$B_3 = \frac{8W}{AB}\left[\tfrac{1}{8}D^2 - \tfrac{1}{2}r_0^2 - (\tfrac{1}{2}D - r_0)\,F\tan\alpha + \frac{\tan\alpha}{12F}(\tfrac{1}{8}D^3 - r_0^3)\right] \qquad (3.46)$$

3.5.2 Uniform illumination

If the field over the aperture has uniform amplitude and phase distribution, the blockage efficiency η_B/η_0 is readily calculated from

$$\frac{\eta_B}{\eta_0} = \left[1 - \frac{B_1 + B_2 + B_3}{A}\right]^2 = \left[1 - \frac{g_1(0,0) + g_2(0,0) + g_3(0,0)}{g_0(0,0)}\right]^2 \qquad (3.47)$$

A being the unblocked geometrical aperture and $\eta_0 = 1$. A numerical example has already been discussed in a previous paper [20].
The blockage efficiency has been calculated for uniform field distribution in the aperture as a function of the width of the support legs with the distance r_0 as a parameter. Fig. 3.8a shows the result, being a rapid decrease i efficiency with a growing width of the supports. Moreover, the decrease is less, if the distance r_0 is increased, which means that the supports are fixed nearer to the rim of the main reflector. In this case the "trapezoid" shadow decreases and therefore η_B/η_0 improves.

If the width of the supports is neglected in respect of wavelength, which is possible in some applications, viz. in satellite antennas, the blockage coefficient is entirely depending on the ratio D_s/D. This ratio is mostly 0.1, therefore η_B/η_0 is 0.98 as a maximum. Improvement to 0.99 is possible by using special shaping techniques in double reflector systems [22]. Trentini [119] has used a different method of calculating the blockage coefficient by introducing an average width of the support. The disadvantage of this method lies in the fact that no clear insight is available as to which part of the shadow is formed by spherical waves and which by plane waves. However, his calculations for uniform illumination are as good as correct. For $D = 350\lambda$,

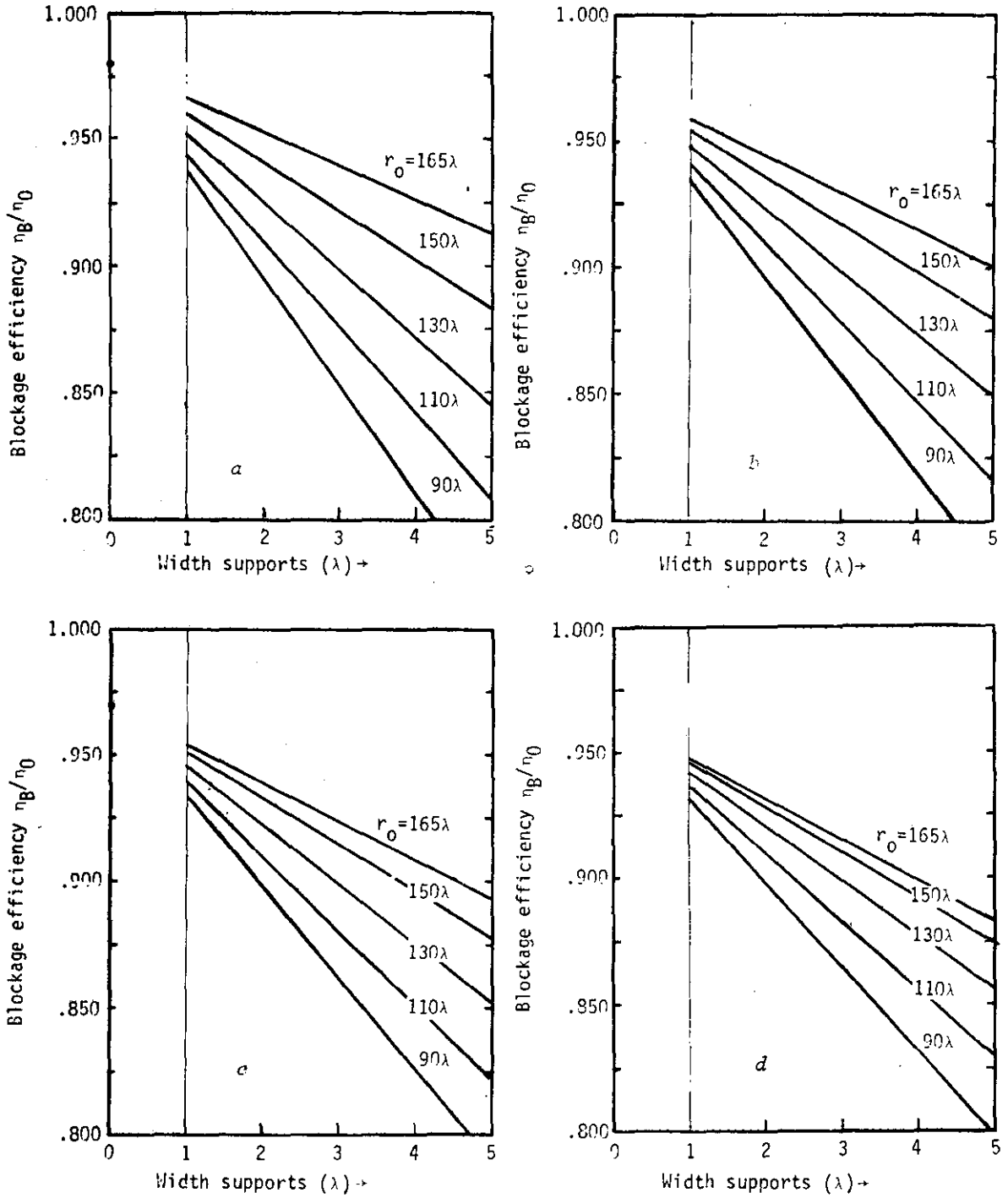

Fig. 3.8
Blockage efficiency as a function of the width of the supports, r_0 *being a parameter.*
$f(r) = 1 - ar^2$ $a = a_1.(2/D)^2$ $\Psi_2 = 75^0$ $D = 330\lambda$ $D_s = 33\lambda$
a) $a_1 = 0.0$ *Uniform illumination* *b)* $a_1 = 0.5$ *edge illumination* -6 dB
c) $a_1 = 0.7$ *edge illumination* -10dB *d)* $a_1 = 0.9$ *edge illumination* -20dB

$D_s = 35\lambda$, $2w = 2\lambda$ and $r_0 = 90\lambda$ his predicted blockage efficiency appears to be 92%, while the exact calculations shown above indicate a result of 89% [Fig. 3.8a].

3.5.3. Tapered illumination

If the illumination of the aperture is tapered toward the edges, the shadows discussed in the previous section will have to be weighted by the aperture illumination function for the purpose of calculating the blockage efficiency. Dealing with such problems, polar coordinates r',ϕ' are mostly used, r' being normalized to unity. Sometimes r is not normalized. The aperture distribution is then $F(r',\phi')$ or $F(r,\phi')$. Sciambi [103, 104] assumes the aperture illumination function to be circularly symmetrical and tapered on a uniform pedestal [Fig. 3.9]. The function may be expressed by

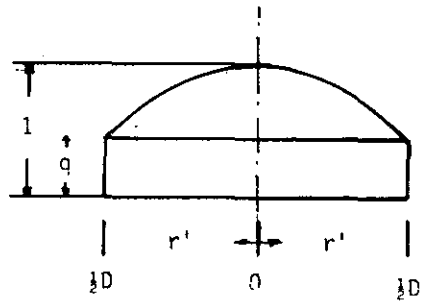

Fig. 3.9
Aperture illumination function
$F(r') = a+(1-a)(1-r'^2)^p$

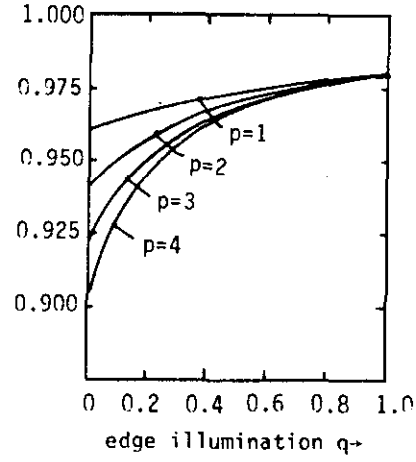

Fig. 3.10
The blockage efficiency as a function of the edge illumination and p *as a parameter using Eq. 3.48 and 3.49*

$$F(r') = q + (1 - q)(1 - r'^2)^p, \quad 0 < q < 1 \quad 0 < r' < 1 \tag{3.48}$$

With this illumination function a great variety of aperture distributions may be realized by varying the parameters q and p. The illumination function is also very similar to illuminations obtained by primary feed patterns of scalar feeds and theoretical $2(n+1)\cos^n\psi$ patterns. Uniform illumination is obtained for q = 1, the aperture being fully tapered for q = 0. Doidge [19] has used this illumination function to calculate the blockage efficiency for the case of a circularly symmetrical obstacle in the centre of the aperture. His final expression contains some inaccuracies and should be

$$\frac{\eta_B}{\eta_0} = \left[1 - \frac{q\Delta^2(p + 1) - (1 - q)(1 - \Delta^2)^{p+1} + 1 - q}{1 + qp}\right]^2 \tag{3.49}$$

Fig. 3.10 shows this revised blockage efficiency as a function of the edge illumination, where Δ, being the ratio D_s/D, equals 0.1.

Several authors, such as Wested [123], use the aperture illumination function as indicated by Eq. 3.3

Wested has introduced very useful information by calculating the blockage effects caused by plane and spherical waves, although the projection of the supports by spherical waves was approximated by a trapezoid. It appears, however, that the variation in the calculated efficiency is less than 1% when either cylindrical or conical spars with opposite orientations are used [123]. Therefore, the shape of the spars seems unimportant with regard to the gain performance, as presumed before.

Gray [43], too, has carried out calculations on the blockage coefficient using an aperture distribution of $1 - r'^2$, $0 < r' < 1$.

This distribution, however, is not very realistic because no variation in the edge illumination is possible. In addition, Gray located the struts at the rim of the main reflector, which is seldom done in practice. Moreover, the work contains some inaccuracies as already observed by Wested [123].

Gillitzer [40] should also be mentioned here, although his approach is somewhat different from the others. Following his method, calculations have been carried out of the blockage effect on antenna gain and sidelobes [Chapter 2].

In the following we calculate as accurately as possible the blockage effects when the illumination is tapered and make use of the results found in the previous sections.

To calculate the tapering effect, in this paper the aperture distribution of Eq. 3.3a has been used as it results in simple mathematics and gives a good insight into the tapering problems [Fig. 3.2].
The contributions to the blockage efficiency, mentioned in Eq. 3.50, are now readily found from the theory in Sec. 3.2. This results in the contribution due to the subreflector, viz.:

$$g_1(0,0) = \pi(\tfrac{1}{2}D_s)^2[1 - \tfrac{1}{2}a(\tfrac{1}{2}D_s)^2] \tag{3.9}$$

The contributions to plane-wave blockage by the struts will be

$$g_2(0,0) = 8w(r_0 - \tfrac{1}{2}D_s) - 8aw[\tfrac{1}{3}r_0^3 - \tfrac{1}{3}(\tfrac{1}{2}D_s)^3] - 8aw^3(\tfrac{1}{3}r_0 - \tfrac{1}{6}D_s) \tag{3.14}$$

The contribution to spherical wave blockage by the struts may be found from Eq. 3.16. However, as it is only an approximation, the contribution by spherical waves discussed in Appendix 3.1 has been used for the 0,0 direction resulting in

$$g_3(0,0) = \frac{8w}{AB}\left[\tfrac{1}{2}\{(\tfrac{1}{2}D)^2 - r_0^2\} - F\tan\alpha(\tfrac{1}{2}D - r_0) + \frac{\tan\alpha}{12F}\{(\tfrac{1}{2}D)^3 - r_0^3\}\right]$$
$$- \frac{8wa}{AB}\left[\tfrac{1}{4}\{(\tfrac{1}{2}D)^4 - r_0^4\} - F\tan\alpha\,\tfrac{1}{3}\{(\tfrac{1}{2}D)^3 - r_0^3\} + \frac{\tan\alpha}{20F}\{(\tfrac{1}{2}D)^5 - r_0^5\}\right] \tag{3.50}$$

Compared with Eq. 3.16 the difference is only a few per cent.
The final blockage efficiency may now be found from Eq. 3.47; $g_1(0,0)$, $g_2(0,0)$ and $g_3(0,0)$ of this equation have been discussed in the previous sections and $g_0(0,0)$ is given by Eq. 3.7, as discussed in Sec. 3.2. The results of a computer program are shown in Fig. 3.8b, c and d, where the blockage efficiency has been calculated as a function of the width $2w$, r_0 and a, while $D/D_s = 0.1$.

3.5.4. Results and conclusions

It appears that the blockage efficiency decreases with increasing taper, although for values of r_0 (110-130λ) and for large values of the width of the struts (4-5λ) not much difference is noticed. For a specific value of $r_0 = 110\lambda$ ($r_0 = 1/3D$) and $2w = 2\lambda$ it hardly matters whether the aperture illumination has been tapered towards the edges or not. This phenomenon is

due to the fact that the blockage by spherical waves, which is the largest, decreases if r_0 becomes large. For one particular case, viz. $D = 330\ \lambda$ $r_0 = 110\lambda$, $D_s = 33\lambda$, and $\psi_0 = 75$ degrees, calculations with a uniformly illuminated aperture have been carried out in such a way that the contributions of each obstacle are clearly presented [Fig. 3.11]. We see that the blockage by spherical waves is the most important of all and that for $2w > 2.25\lambda$ the plane wave blockage by the struts becomes more significant than that by the subreflector. Although Eq. 3.50 contains the parameter F/D ratio of the main reflector and AB and α in that equation depend on the F/D ratio [see Appendix 3.1], calculation shows that the influence of the F/D ratio may be neglected. Figs. 3.12a, b, c show this blockage efficiency as a function of F/D and with edge illuminations of 0 dB, -10 dB and -20 dB. As a typical example, $D = 330\lambda$, $D_s = 33\lambda$ and $2w = 2\lambda$ have been taken with r_0 as parameter.
As will be noticed, the graphs are nearly independent of Ψ_2. This result is not identical with that published by Ruze [101] where the blockage efficiency increases with increasing F/D ratio. No conclusions may be drawn from Figs. 3.11 and 3.12 with regard to the blockage efficiency for $2w < \lambda$, as in that case diffraction effects may not be neglected.
As a practical example we examined the new 28.5-metre antenna of the Dutch ground station at Burum, which was opened officially in September, 1973. This antenna has a prescribed aperture illumination in accordance with techniques discussed in chapter 5. The greater part of the aperture is illuminated uniformly, but at a distance of 1.20 metres from the edge the illumination is tapered linearly until at the edge it is -10 dB. The supports are implanted at $r_0 = 0.2D$ and have an elliptical cross-section of 313 x 121 mm. The predicted blockage efficiency is rather unsatisfactory and not more than 92% at 4 GHz [13].

As a further result of this work it is worth mentioning that the blockage efficiency as indicated by Doidge [19] has been recalculated and improved. A comparison between approximate formulae of blockage by spherical waves with exact formulae shows only little difference. All in all the work presents closed expressions for calculating the blockage efficiency for nearly all practical applications based on geometrical optics.

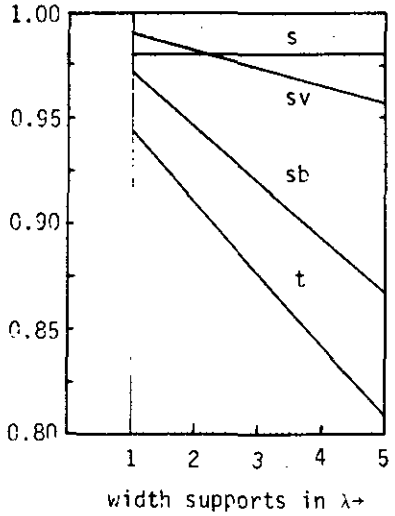

Fig. 3.11
Contribution of the blocking obstacles to the total blockage efficiency
s = *blockage efficiency of subreflector*
sv = *blockage efficiency of supports (plane waves)*
sb = *blockage efficiency of supports (spherical waves)*
t = *total blockage efficiency*
$D = 330\lambda$ $D_s = 33\lambda$ $r_o = 110\lambda$
$\psi_2 = 75^o$ $a_1 = 0$

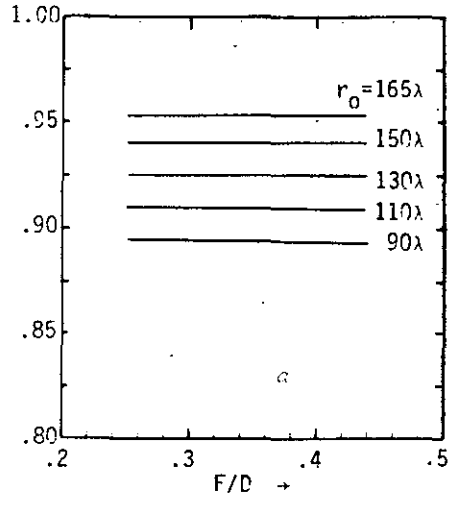

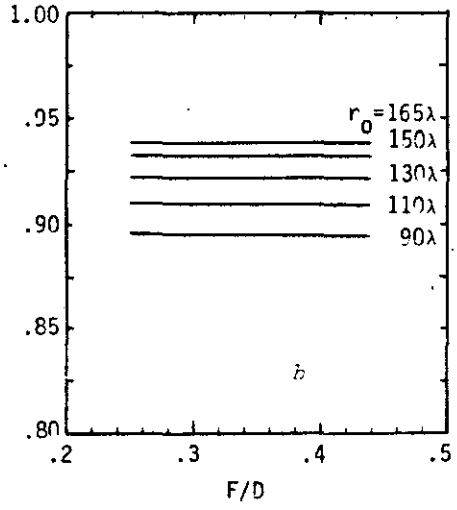

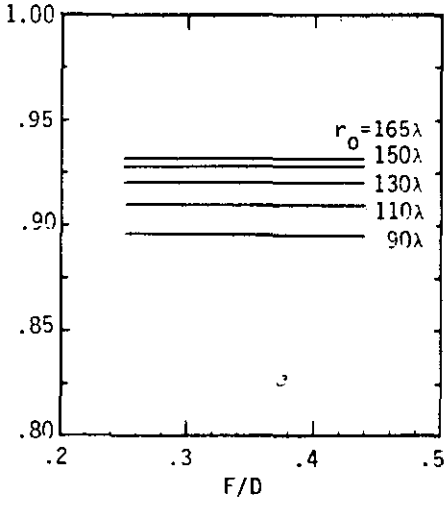

Fig. 3.12
Dependence of the blockage efficiency on the F/D ratio of the main reflector.
$D_s/D = 0.1$ *a) uniform illumination*
$2\bar{w} = 2\lambda$ *b) -10 dB edge illumination*
$D = 330\lambda$ *c) -20 dB edge illumination*

Appendix 3.1. Blockage by spherical waves

The geometry required to calculate the "weighted" blockage of the struts caused by spherical waves is found in Fig. 3.13. Using the law of sines in Δ ABC of this figure we find

$$\frac{AC}{\sin(\alpha + \frac{1}{2}\pi)} = \frac{AB}{\sin(\psi - \alpha)} \tag{1}$$

Further, $x' = AC \sin\psi = (AB \cos\alpha \sin\psi)/[\sin(\psi - \alpha)]$. Using, in addition, Fig. 3.13, the geometry also shows that $x'/r = AC/AC' = w/y$; therefore, $y = wr/x' = [wr \sin(\psi - \alpha)]/(AB \cos\alpha\sin\psi)$.
As in a cassegrain system (Fig. 2.1) $r = 2F \tan\frac{1}{2}\psi_2$, we find that

$$y = \frac{w}{AB} \cdot \frac{\tan\alpha}{4F} r^2 + \frac{wr}{AB} - \frac{wF}{AB} \tan\alpha \tag{2}$$

Therefore, $g_3(0,0) = 4 \int_{r_0}^{\frac{1}{2}D} (1 - ar^2)\, 2ydr$, which results in

$$g_3(0,0) = \frac{8w}{AB} [\tfrac{1}{2}\{(\tfrac{1}{2}D)^2 - r_0^2\} - F(\tfrac{1}{2}D - r_0) \tan\alpha + \frac{\tan\alpha}{12F} \{(\tfrac{1}{2}D)^3 - r_0^3\}]$$

$$- \frac{8wa}{AB} [\tfrac{1}{4}\{(\tfrac{1}{2}D)^4 - r_0^4\} - \tfrac{1}{3}F\{(\tfrac{1}{2}D)^3 - r_0^3\}\tan\alpha + \frac{\tan\alpha}{20F}\{(\tfrac{1}{2}D)^5 - r_0^5\}] \tag{3}$$

For uniform illumination ($\alpha = 0$) Eq. 3 reduces to

$$g_3(0,0) = \frac{8w}{AB} [\tfrac{1}{8}D^2 - \tfrac{1}{2}r_0^2 - (\tfrac{1}{2}D - r_0) F\tan\alpha + \frac{\tan\alpha}{12F} (\tfrac{1}{8}D^3 - r_0^3)] \tag{4}$$

The system constants α and AB may be found from Fig. 3.13 resulting in

$$\tan\alpha = \frac{r_0 - \frac{1}{2}D_s}{2F \cos\Psi_0/(1 + \cos\Psi_0) - \frac{1}{2}D_s/\tan\Psi_2} \tag{5}$$

and as $\tan\alpha = (r_0 - AB)/AR' = \frac{r_0 - AB}{r_0} \tan\Psi_0$, $AB = r_0(1 - \tan\alpha/\tan\Psi_0)$

with $r_0 = 2F \tan\frac{1}{2}\Psi_0$

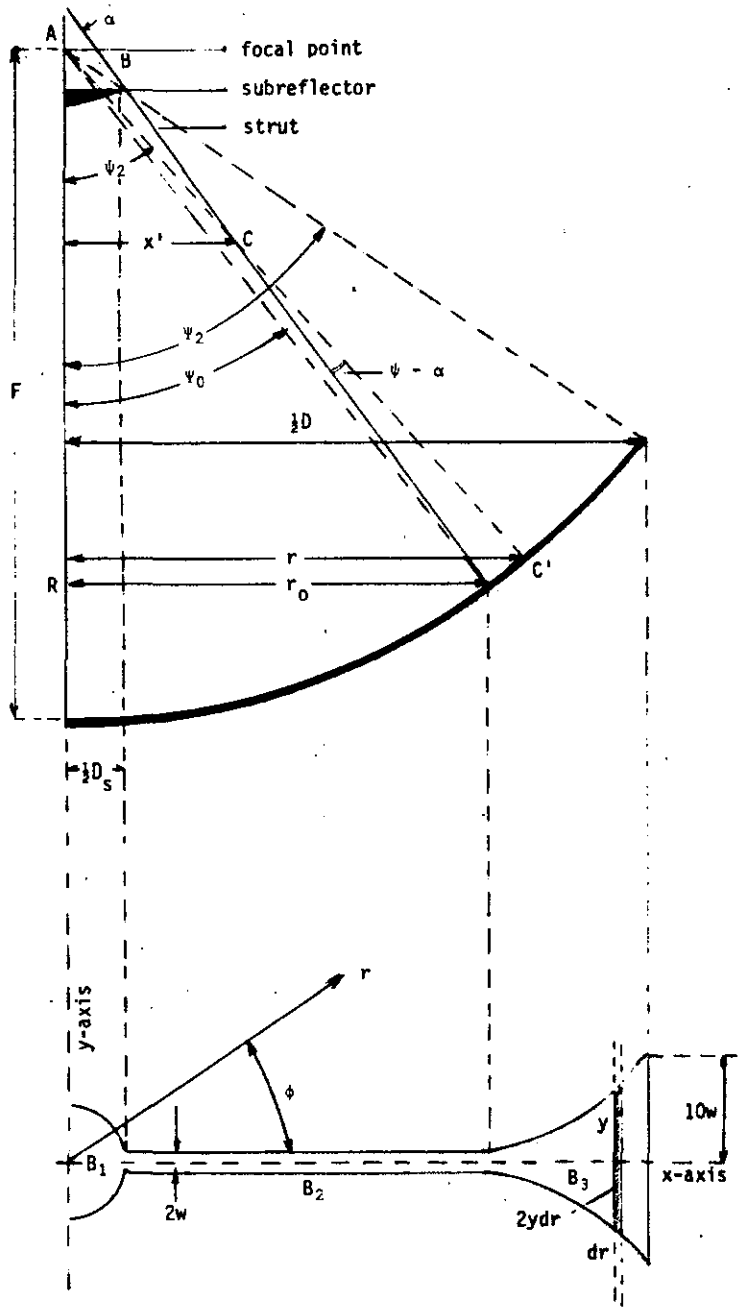

Fig. 3.13
Geometry to determine the contribution to the blockage by spherical waves in cassegrain systems (D_s/D = 0.1)

4. Radiation patterns of reflector antennas

4.1. Introduction

Many investigators have in the past studied problems and published solutions with respect to radiation patterns of reflector antennas. We will concentrate here only on those methods known as asymptotic solutions of Maxwell's equations, such as explained by Kouyoumjian [70]. These solutions may be divided into three classes.

(1) Geometrical optics (G.O.); this theory supposes that propagation of electromagnetic energy takes place along rays. Ordinary laws of optics such as energy conservation, Fermat's principle, Fresnel laws etc. are used to solve a particular scattering problem [4],

(2) Physical optics (P.O.); this theory covers the main part of this chapter.

(3) Geometrical optical theory of diffraction (G.T.D.); this is an extension of the geometrical optics by the introduction of diffracted rays, as G.O. is not valid at the edges or in the shadow of a reflector.

Keller [60] was the first who introduced this theory, later improved by Kouyoumjian [71]. Here, we will not go into details; some comparison with P.O. results will be given later in this chapter.

The physical optics approximation has been used by a great number of scientists such as Afifi [2], Baars [3], Tartakovski [114] and Kinber [62], all calculating the radiation pattern of an illuminated paraboloid. However, not only scattering from paraboloids is important in antenna systems nowadays, since very often also double reflector systems are employed in ground stations for satellite communication. Therefore, the scattered field from main and subreflector should be known. Mostly, the main reflector is a paraboloid, but in gregorian and cassegrainian systems ellipsoids and hyperboloids are used as subreflectors. It is even recommended to calculate the field scattered from a shaped subdish, discussed elsewhere [22]. The work presented here has already partly been performed by Rusch [95] and Ludwig [75], but some disadvantages and errors have been found in their methods as will be discussed below.

It is the purpose of this chapter to obtain a more detailed insight into the radiation properties of reflector antennas such as the paraboloid of revolution. We shall start this chapter by summing up the polarization properties of some feeds such as the electric dipole and the rectangular

open-ended waveguide. These properties will be compared with those of a Huygens source.
In the third section, equations are derived to calculate the radiation pattern of circularly symmetrical reflectors using the physical-optics approximation with feeds of which the polarization vectors are equal to those of a Huygens source. Further, a discussion is devoted to the limitations of physical optics.
Knowing the radiation pattern, gain functions may be calculated and also the relative power that will be radiated in any solid angle. In this way an insight may be obtained into the distribution of power scattered by a reflector antenna under different circumstances.

4.2. Radiation patterns calculated by physical optics

4.2.1. Geometry of the system

We assume that the antenna system is composed of an arbitrary reflector S and a primary source located at the origin of the coordinate system. We further assume that the primary source is equal to a point, in which case the dimmensions of the primary source may be neglected. In Fig. 2.10 a reflector is shown together with three different coordinate systems which we shall use throughout this work. It is a paraboloid reflector, but any other arbitrary circularly symmetrical reflector may replace the paraboloid.
The ρ,ψ,ξ system is a spherical coordinate system describing the reflector and the radiation from the primary source. The R,θ,ϕ system is also a spherical coordinate system used to describe the field in a fieldpoint $P(R,\theta,\phi)$. The x,y,z system is a cartesian coordinate one required to describe the relations between the two other systems and also to define the position of the antenna with respect to the x,y,z system.
In each system we shall define three unit vectors. Each vector indicates the direction in which the particular coordinate increases. We shall indicate these vectors by $\bar{a}$ with an index of the coordinate system to which it belongs, e.g. $\bar{a}_R$, $\bar{a}_\theta$, etc. If any vector belongs to the system (R,θ,ϕ), (ρ,ψ,ξ) or (x,y,z), this will be indicated by an index R, ρ or x, e.g. $(a,b,c)_x$. A detailed description of coordinate transformations from one system into the other is found in Appendix 4.1.

4.2.2. The primary source

As already explained by Silver [108, p.150] the field radiated by a primary source is represented by

$$\bar{E}_i(\rho,\psi,\xi) = [(\mu/\varepsilon)^{\frac{1}{2}} P_T/2\pi]^{\frac{1}{2}} \frac{[G_f(\psi,\xi)]^{\frac{1}{2}}}{\rho} \bar{a}_i(\psi,\xi)\, e^{-jk\rho} , \qquad (4.1)$$

where $G_f(\psi,\xi)$ is the directive gain function of a lossless feed and P_T the total power radiated.
The angles ψ and ξ and the distance ρ are found in Fig. 2.10. The fieldpoint $(\rho,\psi,\xi)_\rho$ situated at the reflector surface is assumed to be located in the far zone of the field radiated by the source. This assumption is correct because generally for the large antennas under discussion the requirement $\rho > 2d^2/\lambda$ is met [108, p.196-199], d being the largest dimension of the feed's aperture. Therefore, the feed may be regarded as a point source. The vector $\bar{a}_i(\psi,\xi)$ is a unit vector defining the polarization of the electric field intensity. The longitudinal component of the unit vector is zero [108, p.150], hence we may write

$$\bar{a}_i(\psi,\xi) = [0,\bar{a}_{i\psi}(\psi,\xi),\bar{a}_{i\xi}(\psi,\xi)]_\rho \qquad (4.2)$$

Very often the feed pattern shows circularly symmetrical properties, therefore we write $G(\psi)$ in stead of $G(\psi,\xi)$.

4.2.2.1. The polarization of the primary source

The polarization vectors used by several authors differ considerably. Pinney [83] describes various arrangements of electric dipole feeds with polarization parallel and perpendicular to the antenna axis. This kind of polarization is also proposed by Korbansky [69]. Others like Yen [126] let the polarization depend on a superposition of a vector in the ψ and one in the ξ plane. The relationship between the amplitudes of the vectors is calculated for horizontal polarization, vertical polarization, linear polarization tilted at a 45^o angle and also for circular polarization. Carberry [5] also uses a combination of two orthogonal polarized vectors.

We shall discuss here the polarization of simple sources, such as the rectangular waveguide and the electric dipole. Other, more advanced feed systems have been treated in detail elsewhere [26,55].

4.2.2.2. The rectangular waveguide

A very popular model used to illuminate a reflector surface is the open waveguide excited by the TE_{10} mode described by Silver [108, p.343], Jones [57], Plonsey [84] and Smith [110]. According to Silver, field components of a rectangular waveguide excited in the TE_{10} mode and the electric field vector oriented along the X-axis are represented by

$$\bar{E}_\psi(\psi,\xi) = C \frac{\cos\xi}{\rho} [1 + \beta_{10}/k \cos\psi] F(\psi,\xi) e^{-jk\rho} \bar{a}_\psi$$

$$\bar{E}_\xi(\psi,\xi) = -C \frac{\sin\xi}{\rho} [\beta_{10}/k + \cos\psi] F(\psi,\xi) e^{-jk\rho} \bar{a}_\xi$$

where

$$F(\psi,\xi) = \frac{\cos[(\pi a/\lambda)\sin\psi\cos\xi]}{[(\pi a/\lambda) \sin\psi\cos\xi]^2 - \frac{1}{4}\pi^2} \cdot \frac{\sin[(\pi b/\lambda) \sin\psi\sin\xi]}{(\pi b/\lambda) \sin\psi\sin\xi} \qquad (4.3)$$

In Eqs. 4.3 it is assumed that the reflection coefficient at the opening of the waveguide is zero. The symbols a and b are waveguide dimensions and C is a coefficient depending on the total amount of power supplied and on the dimensions a and b [108, p.343]. Further, β_{10} stands for the phase constant for the TE_{10} mode, and k the propagation constant, equal to $2\pi/\lambda$. If we compare Eqs. 4.3 with Eqs. 4.1 we may write for the directive gain function:

$$[G_f(\psi,\xi)]^{\frac{1}{2}} \quad :: [\cos^2\xi(1 + \beta_{10}/k \cos\psi)^2 + \sin^2\xi(\cos\psi + \beta_{10}/k)^2]^{\frac{1}{2}} F(\psi,\xi) \qquad (4.4)$$

and for the polarization vector

$$\bar{a}_j = \frac{[0,\cos\xi(1 + \beta_{10}/k \cos\psi),-\sin\xi(\cos\psi + \beta_{10}/k)]}{[\cos^2\xi(1 + \beta_{10}/k \cos\psi)^2 + \sin^2\xi(\cos\psi + \beta_{10}/k)^2]^{\frac{1}{2}}_\rho} \qquad (4.5)$$

If the dimensions of the waveguide are such that $\beta_{10}/k = 1$, the polarisation vector becomes simply:

$$\bar{a}_j(\psi,\xi) = \cos\xi \bar{a}_\psi - \sin\xi \bar{a}_\xi \quad , \qquad (4.6)$$

which is the polarization of a Huygens source [57]. However, in most practical cases it will be difficult to obtain $\beta_{10} = k$, as normally

$$\beta_{10}/k = \lambda/\lambda_{g_{10}}$$

where $\lambda_{g_{10}}$ is the wavelength in the guide. For the TE10 mode

$$\lambda_{g_{10}} = \lambda/[1 - (\lambda/2a)^2]^{\frac{1}{2}}$$

Therefore, $\beta_{10} = k$ only for $\lambda \ll a$.
Nevertheless, this polarization vector is very popular and used by several authors such as Afifi [2], Baars [3], Carter [6] and Tartakovski [114], as it simplifies the complicated mathematical work considerably. This will be shown in the following sections.
Another important advantage of using the polarization vector of Eq. 4.6 lies in the fact that if the reflecting surface is a paraboloid, the current induced at the reflector will show no cross-polarized components. This is proved in Appendix 4.2.

4.2.2.3. The elementary dipole

Using the elementary dipole [108, p.92] located in the focus of a parabolic reflector is still an important way to illuminate reflectors. If such a dipole with length l is directed along the positive X-axis with a current I flowing in that direction, the far zone components of the electric field expressed in ρ,ψ,ξ coordinates are [57]

$$\bar{E} = \frac{jZ_0 I l e^{-jk\rho}}{2\lambda\rho} [-\bar{a}_\psi \cos\xi\cos\psi + \bar{a}_\xi \sin\xi], \qquad (4.7)$$

where $Z_0 = 120\pi$ ohms.
It is readily found that

$$[G_f(\psi,\xi)]^{\frac{1}{2}} :: [\cos^2\psi\cos^2\xi + \sin^2\xi]^{\frac{1}{2}}$$

The polarization follows from

$$\bar{a}_j(\psi,\xi) = (0,-\cos\psi\cos\xi,+\sin\xi)_\rho . [\cos^2\psi\cos^2\xi + \sin^2\xi]^{-\frac{1}{2}} \qquad (4.8)$$

Sletten and Blacksmith [109] have calculated the surface current $\bar{K}$ of a

paraboloid reflector when fed by a linear electrical dipole along the X-axis. It appears that for directions of $\phi \neq 0^0$ and $\phi \neq 90^0$ large components polarized in the y-direction are present. The radiation characteristics of a feed, however, should be such that all the waves are polarized in the same direction after being reflected by the paraboloid surface. Therefore, if the feed is polarized in the X-direction, all field components with polarization perpendicular to the X-direction, also called cross-polarization, are wasted and contribute to minor-lobe radiation. If, however, a short electric dipole and a magnetic dipole of equal intensity are crossly oriented and excited at the reflector focus, the cross component of polarization on the reflector aperture is eliminated [57]. The same combination has been proposed by Tartakovski [114] and also by Kofman [68]. Using a certain combination of E and H fields of the dipoles [68] it appears also possible to obtain current distributions only in one direction on other reflectors such as ellipsoids or hyperboloids.

Reflector antennas illuminated by practical feeds will always show some cross-polarization, decreasing the antenna efficiency. If this effect is neglected, the gain calculated will be too high and the theoretical values of the sidelobes will differ considerably from observed values. The cross-polarization losses are discussed in more detail in Chapter 6.

4.2.3. The reflector

4.2.3.1. General considerations

As Silver [108, p.132] has already explained, the field scattered from a reflector surface is equal to

$$\bar{E}_s(P) = \frac{-j}{4\pi\omega\varepsilon} \int_S [(\bar{K}.\nabla)\nabla + k^2\bar{K}] \frac{e^{-jkr}}{r} dS \qquad (4.9)$$

$$\bar{H}_s(P) = \frac{1}{4\pi} \int_S (\bar{K} \times \nabla) \frac{e^{-jkr}}{r} dS \qquad (4.10)$$

where r is the distance from the field point P to the element of surface dS. If $\bar{K}$ is known in the Eqs. 4.9 and 4.10, the scattered field may be calculated exactly.

The current density $\bar{K}$ may be found in two ways. First, if we use at the reflector the boundary condition $\bar{n} \times \bar{E}_i = -\bar{n} \times \bar{E}_s$ where $\bar{E}_i$ is the initial

field, we find $\bar{K}$ by

$$\bar{n} \times \bar{E}_i = \frac{j}{4\pi\omega\varepsilon} \int_S \bar{n} \times [(\bar{K}.\nabla)\nabla + k^2\bar{K}] \frac{e^{-jkr}}{r} \, dS \qquad (4.11)$$

$\bar{n}$ being the unit vector normal to S at the point of observation and directed outward into the surrounding space.

This integral equation may be solved using numerical techniques [113], but this method is difficult and time consuming and usually not used for reflectors larger than 20 λ [75].

The second method of finding $\bar{K}$ is an approximation. This assumes that on areas illuminated by the source the currents are the same as they would be if the incident field were reflected optically, in other words

$$\bar{K} = 2(\bar{n} \times \bar{H}_i) \qquad (4.12)$$

On shadowed regions the currents are assumed to be zero. This method is known as the physical optics approximation, also known under the name of Vector Kirchhoff Theory or Current Distribution Method.

If this approximation is applied to Eq. 4.9, it becomes:

$$\bar{E}_p = \frac{1}{2\pi j\omega\varepsilon} \int_S [(\bar{n} \times \bar{H}_i).\nabla(\nabla\psi) + k^2(\bar{n} \times \bar{H}_i)\,\psi \, dS \qquad (4.13)$$

If $\bar{\rho}$ is a vector from a given origin (Fig. 4.1) and $\bar{a}_R$ a unit vector from this origin to the field point P at a distance R, it is readily seen that

$$r = R - (\bar{a}_\rho.\bar{a}_R)\,\rho \qquad (4.14)$$

The factor $\psi = \frac{e^{-jkr}}{r}$ may then be approximated by

$$\frac{1}{R} \exp[\{jk\rho(\bar{a}_\rho.\bar{a}_R) - jkR\}] \qquad (4.15)$$

if $R >> \rho$.

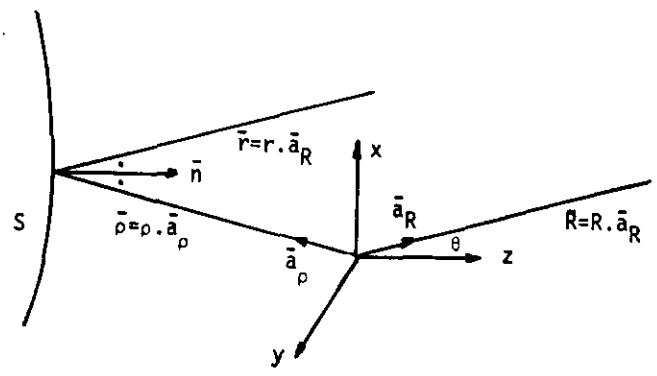

Fig. 4.1
Geometry for Eq. 4.13

Substituting Eq. 4.15 in Eq. 4.13 leads to

$$\bar{E}_p = -\frac{j\omega\mu}{2\pi R}\, e^{-jkR} \int_S [\bar{n} \times \bar{H}_i - \{(\bar{n} \times \bar{H}_i).\bar{a}_R\}\bar{a}_R] e^{jk\rho\, \bar{a}_\rho.\bar{a}_R}\, dS \qquad (4.16)$$

$$\bar{H}_p = (\varepsilon/\mu)^{\frac{1}{2}}\, \bar{a}_R \times \bar{E}_p \qquad (4.17)$$

4.2.3.2. Scattered radiation from the reflector

As explained in the previous section, the current distribution on the surface of the reflector will be expressed by $\bar{K} = 2(\bar{n} \times \bar{H}_i)$. Further

$$\bar{H}_i = (\varepsilon/\mu)^{\frac{1}{2}}(\bar{a}_\rho \times \bar{E}_i) \qquad (4.18)$$

and

$$\bar{E}_i = [(\mu/\varepsilon)^{\frac{1}{2}}\, P_T/2\pi]^{\frac{1}{2}}\, \frac{[G_f(\psi,\xi)]^{\frac{1}{2}}}{\rho}\, \bar{a}_i(\psi,\xi)\, e^{-jk\rho} \qquad (4.1)$$

If we substitute Eqs. 4.1, 4.12 and 4.18 in Eq. 4.16, we obtain for the scattered field in a field point P

$$\bar{E}_p(R,\theta,\phi) = -\frac{j\omega\mu}{2\pi R}\, e^{-jkR}\, [(\varepsilon/\mu)^{\frac{1}{2}}\, P_T/2\pi]^{\frac{1}{2}} \int_S \frac{[G_f(\psi,\xi)]^{\frac{1}{2}}}{\rho}\, e^{-jk(1\, -\, \bar{a}_\rho.\bar{a}_R)\rho}.$$
$$.\{\bar{n} \times (\bar{a}_\rho \times \bar{a}_i)\}\, dS \qquad (4.19)$$

Eq. 4.19 may be used to calculate the scattered radiation from any arbitrary reflector S ; however, in our case we are mainly interested in the investigation of circularly symmetrical truncated surfaces of revolution, which means that S should be independent of the angle ξ. These surfaces may be defined by polar coordinates such as

$$\rho = 2F/(1 + \cos\psi) \qquad (4.20)$$

for a paraboloid of revolution with the origin in the focus (Fig. 2.10). The vector $\bar{n}$ normal to this surface may be expressed in ρ and its derivatives, as well as the surface element dS. Useful relationships from differential geometry may be used [73].

The evaluation of the vector product of Eq. 4.19 is carried out in Appendix 4.3. As the scalar product of

$$(\bar{a}_\rho.\bar{a}_R) = \begin{pmatrix}1\\0\\0\end{pmatrix}_\rho \begin{pmatrix}1\\0\\0\end{pmatrix}_R = \begin{pmatrix}\sin\psi\cos\xi\\ \sin\psi\sin\xi\\ -\cos\psi\end{pmatrix}_x . \begin{pmatrix}\sin\theta\cos\phi\\ \sin\theta\sin\phi\\ \cos\theta\end{pmatrix}_x$$

$$= \sin\psi\cos\xi\sin\theta\cos\phi + \sin\psi\sin\xi\sin\theta\sin\phi - \cos\psi\cos\theta$$

$$= \sin\psi\sin\theta\cos(\xi - \phi) - \cos\psi\cos\theta \quad , \tag{4.21}$$

the exponent $-jk\rho(1-\bar{a}_\rho.\bar{a}_R)$ yields

$$-jk\rho\{1 - \sin\psi\sin\theta\cos(\xi - \phi) + \cos\psi\cos\theta\} \tag{4.22}$$

If we write the results for E_p (Eq. 4.19) in its θ and ϕ directions, the following equations are found

$$\bar{E}_{s\theta} = \left[-\frac{j\omega\mu}{2\pi R} e^{-jkR} \left[(\varepsilon/\mu)^{\frac{1}{2}} P_T/2\pi\right]^{\frac{1}{2}} \int_0^{\Psi}\int_0^{2\pi} \frac{[G_f(\psi,\xi)]^{\frac{1}{2}}}{\rho} e^{-j\alpha}.e^{j\beta\cos(\xi - \phi)}. \right.$$

$$[\rho'\{\cos\theta\cos\xi\sin\psi\cos(\xi - \phi) + \sin\theta\cos\psi\cos\xi\} + \rho\{\cos\theta\cos\psi\cos\xi\cos(\xi - \phi)$$

$$\left. + \cos\theta\sin\xi\sin(\xi - \phi) - \sin\theta\sin\psi\cos\xi\}].\rho\sin\psi d\psi d\xi \right] \bar{a}_\theta \tag{4.23}$$

$$\bar{E}_{s\phi} = \left[-\frac{j\omega\mu}{2\pi R} e^{-jkR} \left[(\varepsilon/\mu)^{\frac{1}{2}} P_T/2\pi\right]^{\frac{1}{2}} \int_0^{\Psi} \frac{[G_f(\psi,\xi)]^{\frac{1}{2}}}{\rho} e^{-j\alpha}[\{\rho'\sin\psi \right.$$

$$- \rho(1 - \cos\psi)\}. \int_0^{2\pi} \cos\xi\sin(\xi - \phi)\, e^{j\beta\cos(\xi - \phi)}\, d\xi \; - \int_0^{2\pi} \rho\sin\phi.$$

$$\left. . e^{j\beta\cos(\xi - \phi)}\, d\xi]\rho\sin\psi d\psi \right] \bar{a}_\phi \tag{4.24}$$

where $\alpha = k\rho(1 + \cos\theta\cos\psi)$, $\beta = k\rho\sin\theta\sin\psi$ and Ψ the subtending angle of the reflector.

4.2.3.3. Evaluation of the integral equations

Generally [1],

$$J_m(z) = \frac{1}{2\pi j^m} \int_0^{2\pi} e^{jz\cos u} \cos mu \, du \tag{4.25}$$

If $m = 0$, $z = \beta$, $u = \xi - \phi$ and $du = d\xi$ then

$$J_0(\beta) = \frac{1}{2\pi} \int_0^{2\pi} e^{j\beta\cos(\xi - \phi)} \, d\xi \tag{4.26}$$

Since [95]

$$-\pi\sin\phi[J_0(\beta) + J_2(\beta)] = \int_0^{2\pi} \cos\xi\sin(\xi - \phi) \, e^{j\beta\cos(\xi - \phi)} \, d\xi \tag{4.27}$$

the double integral in Eq. 4.24 for $E_{s\phi}$ may be written as

$$\bar{E}_{s\phi} = \left[-\frac{j\omega\mu}{2R} e^{-jkR} [(\varepsilon/\mu)^{\frac{1}{2}} P_T/2\pi]^{\frac{1}{2}} \int_0^{\Psi} \frac{[G_f(\psi)]^{\frac{1}{2}}}{\rho} e^{-j\alpha} \sin\phi\sin\psi \right.$$
$$\left. .[\{\rho'\sin\psi + \rho\cos\psi\}\{- J_0(\beta) - J_2(\beta)\} - \rho\{J_0(\beta) - J_2(\beta)\}] \, \rho d\psi \right] \bar{a}_\phi \tag{4.28}$$

It appears also [95] that

$$2\pi j\cos\phi \, J_1(\beta) = \int_0^{2\pi} \cos\xi \, e^{-j\beta\cos(\xi - \phi)} \, d\xi \, , \tag{4.29}$$

$$\pi\cos\phi\left[J_0(\beta) + J_2(\beta)\right] = \int_0^{2\pi} \sin\xi\sin(\xi - \phi) \, e^{j\beta\cos(\xi - \phi)} \, d\xi \, , \tag{4.30}$$

$$\pi\cos\phi\left[J_0(\beta) - J_2(\beta)\right] = \int_0^{2\pi} \cos\xi\cos(\xi - \phi) \, e^{j\beta\cos(\xi - \phi)} \, d\xi \tag{4.31}$$

Similarly as for Eq. 4.24, Eq. 4.23 is now written as

$$\bar{E}_{s\theta} = \left[-\frac{j\omega\mu}{2R} e^{-jkR} \, (\varepsilon/\mu)^{\frac{1}{2}} P_T/2\pi \, ^{\frac{1}{2}} \int_0^{\Psi} \frac{G_f(\psi)^{\frac{1}{2}}}{\rho} e^{-j\alpha} \sin\psi\cos\phi \, . \right.$$
$$. \, [\{J_0(\beta) - J_2(\beta)\}\{\rho'\sin\psi - \rho(1 - \cos\psi)\}\cos\theta + 2\rho\cos\theta \, J_0(\beta)$$
$$\left. + 2j\sin\theta \, J_1(\beta)\{\rho'\cos\psi - \rho\sin\psi\}]\sin\psi \, d\psi \right] \bar{a}_\theta \tag{4.32}$$

4.2.3.4. Calculation of the total electric field

As explained by Silver [108, p.150], the total electric field is made up of a superposition of the direct incident field and the scattered field of the reflector.
The incident field is generally represented by

$$\bar{E}_i = [(\mu/\epsilon)^{\frac{1}{2}} P_T/2\pi]^{\frac{1}{2}} \frac{[G_f(\theta,\phi)]^{\frac{1}{2}}}{R} \bar{a}_i(\theta,\phi)\, e^{-jkR} \tag{4.1}$$

and the scattered field by Eqs. 4.28 and 4.32. The total field at the field-point $P(R,\theta,\phi)$ is then

$$\bar{E}_\theta = \bar{E}_{i\theta} + \bar{E}_{s\theta} \text{ and } \bar{E}_\phi = \bar{E}_{i\phi} + \bar{E}_{s\phi} \tag{4.33}$$

where the polarization vector of Eq. 4.1 should be expressed in (R,θ,ϕ) coordinates, viz.

$$\bar{a}_i(\theta,\phi) = -\cos\phi\, \bar{a}_\theta - \sin\phi\, \bar{a}_\phi \tag{4.34}$$

The components of the scattered field are now split into a real and an imaginary part in order to solve Eqs. 4.33. Therefore, we first write

$$E_{\phi tot} = -\frac{j}{2}\frac{e^{-jkR}}{R}[(\mu/\epsilon)^{\frac{1}{2}} P_T/2\pi]^{\frac{1}{2}}\left[\int_0^{\Psi} k \frac{[G_f(\psi)]^{\frac{1}{2}}}{\rho} \cos\alpha\sin\phi\sin\psi.\zeta.\rho d\psi\right.$$
$$\left. - j\left(\int_0^{\Psi} k \frac{[G_f(\psi)]^{\frac{1}{2}}}{\rho} \sin\alpha\sin\phi\sin\psi\ \zeta\ \rho d\psi + 2\sqrt{G_f(\theta)}\sin\phi\right)\right]\bar{a}_\phi\ , \tag{4.35}$$

where

$$\zeta = \{\rho'\sin\psi + \rho\cos\psi\}\{-J_0(\beta) - J_2(\beta)\} - \rho\{J_0(\beta) - J_2(\beta)\} \tag{4.36}$$

$$\bar{E}_{\theta tot} = -\frac{j}{2}\frac{e^{-jkR}}{R}[(\mu/\epsilon)^{\frac{1}{2}} P_T/2\pi]^{\frac{1}{2}}\left[\int_0^{\Psi} k \frac{[G_f(\psi)]^{\frac{1}{2}}}{\rho} \cos\alpha\cos\phi\sin\psi\ (\gamma + j\delta)\rho d\psi\right.$$

$$- j\left(\int_0^{\Psi} k\,\frac{[G_f(\psi)]^{\frac{1}{2}}}{\rho}\,\sin\alpha\cos\phi\sin\psi\;(\gamma + j\delta)\rho d\psi + 2\sqrt{G_f(\theta)}\,\cos\phi\right]\bar{a}_\theta \tag{4.37}$$

where

$$\gamma = \{J_0(\beta) - J_2(\beta)\}\{\rho'\sin\psi - \rho(1 - \cos\psi)\}\cos\theta + 2\rho\cos\theta\, J_0(\beta) \tag{4.38}$$

$$\delta = 2\sin\theta(\rho'\cos\psi - \rho\sin\psi)\, J_1'(\beta) \tag{4.39}$$

By choosing the polarization of the incident field in accordance with Eq. 4.34, the electric field in the plane $\phi = 0$, (E-plane) depends only on E_θ, while in the H-plane, where $\phi = 90^0$, only an electric field E_ϕ has to be taken into consideration.

4.2.3.5. The gain function of the composite system

As explained by Silver [108, p.151], the gain function of an antenna system may generally be represented by

$$G(\theta,\phi) = 2\pi(\varepsilon/\mu)^{\frac{1}{2}}\,[|E_\theta|^2 + |E_\phi|^2]R^2/P_T \tag{4.40}$$

For the purpose of easier handling in a computer program we shall write the real and imaginary parts of $\bar{E}_\phi$ and $\bar{E}_\theta$ as follows:

$$(\text{Re } E_\phi) = -\tfrac{1}{2}\,\frac{e^{-jkR}}{R}\,[(\mu/\varepsilon)^{\frac{1}{2}}\,P_T/2\pi]^{\frac{1}{2}}\,\sin\phi\left[\int_0^{\Psi} k\,\frac{[G_f(\psi)]^{\frac{1}{2}}}{\rho}\,\sin\alpha\sin\psi\;\zeta\;\rho d\psi + 2[G_f(\theta)]^{\frac{1}{2}}\right]$$

$$= \text{constant}.\sin\phi\; T_\phi \tag{4.41a}$$

$$(\text{Im } E_\phi) = -\tfrac{1}{2}\,\frac{e^{-jkR}}{R}\,[(\mu/\varepsilon)^{\frac{1}{2}}\,P_T/2\pi]^{\frac{1}{2}}\,\sin\phi\int_0^{\Psi} k\,\frac{[G_f(\psi)]^{\frac{1}{2}}}{\rho}\,\cos\alpha\sin\psi\;\zeta\;\rho d\psi$$

$$= \text{constant}.\sin\phi\; R_\phi \tag{4.41b}$$

$$(\text{Re } E_\theta) = +\tfrac{1}{2}\,\frac{e^{-jkR}}{R}\,[(\mu/\varepsilon)^{\frac{1}{2}}\,P_T/2\pi]^{\frac{1}{2}}\,\cos\phi\left[\int_0^{\Psi} k\,\frac{[G_f(\psi)]^{\frac{1}{2}}}{\rho}\,\sin\psi(\delta\cos\alpha - \gamma\sin\alpha)\rho d\psi - 2[G_f(\theta)]^{\frac{1}{2}}\right]$$

$$= \text{constant}.\cos\phi\; T_\theta \tag{4.42a}$$

$$(\text{Im } E_\theta) = -\tfrac{1}{2}\,\frac{e^{-jkR}}{R}\,[(\mu/\varepsilon)^{\frac{1}{2}}\,P_T/2\pi]^{\frac{1}{2}}\,\cos\phi\int_0^{\Psi} k\,\frac{[G_f(\psi)]^{\frac{1}{2}}}{\rho}\,\sin\psi(\gamma\cos\alpha + \delta\sin\alpha)\rho d\psi$$

$$= \text{constant}\,\cos\phi\; R_\theta \tag{4.42b}$$

Substituting Eqs. 4.41 and 4.42 in Eq. 4.40 leads to

$$G(\theta,\phi) = \tfrac{1}{4}[\sin^2\phi(R_\phi^{\,2} + T_\phi^{\,2}) + \cos^2\phi(R_\theta^{\,2} + T_\theta^{\,2})] \ , \tag{4.43}$$

thus for the E-plane ($\phi = 0^u$) $G(\theta,\phi) = \tfrac{1}{4}(R_\theta^{\,2} + T_\theta^{\,2})$ and for the H-plane ($\phi = 90^0$) $G(\theta,\phi) = \tfrac{1}{4}(R_\phi^{\,2} + T_\phi^{\,2})$

4.2.4. Discussion of some special cases

Eqs. 4.41 and 4.42 found in the previous section can easily be checked if the reflector is a paraboloid with a uniformly illuminated aperture. In this case the directive gain found in the main direction ($\theta = 0$, $\phi = 0$) will be

$$G_{max} = (\pi D/\lambda)^2 \tag{4.44}$$

where D is the diameter of the paraboloid. The relationship between diameter, focal length, and angular aperture Ψ is found from (see also Fig. 2.10)

$$D = 4F \tan\tfrac{1}{2}\Psi \tag{2.4}$$

The gain function of a feed which produces uniform illumination in the aperture of a paraboloid is [108, p.433]

$$G_f(\psi,\xi) = \cot^2\tfrac{1}{2}\Psi/\cos^4\tfrac{1}{2}\psi \tag{3.10}$$

If $\theta = 0$, then $\alpha = 4\pi F/\lambda$, $\beta = 0$, $\gamma = 2\rho$ and $\delta = 0$.
Using these results and Eq. 3.10, we find for Eq. 4.42a

$$R_\theta = k \cot\tfrac{1}{2}\Psi \; 4F\cos\alpha \int_0^{\Psi} \frac{\sin\psi}{\cos^2\tfrac{1}{2}\psi(1 + \cos\psi)} \, d\psi \ , \text{ or}$$

$$R_\theta = k \cot\tfrac{1}{2}\Psi \; 4F\cos\alpha \tan^2\tfrac{1}{2}\Psi = 4kF\cos\alpha \tan\tfrac{1}{2}\Psi \tag{4.45}$$

In a similar way we find that

$$T_\theta = 4kF\sin\alpha \tan\tfrac{1}{2}\Psi \tag{4.46}$$

Substituting these results in Eq. 4.43 we obtain

$$G(0,0) = \tfrac{1}{4}k^2(4F\tan\tfrac{1}{2}\Psi)^2 \tag{4.47}$$

which is equal to Eq. 4.44 if Eq. 2.4 is used. Equal results are obtained if the H-plane is considered. Of much interest is the back radiation of the antenna for $\theta = \pi$. In that case we find

$$\alpha = \frac{4\pi F}{\lambda}\,\frac{1 - \cos\psi}{1 + \cos\psi}\,,\ \beta = 0\,,\ \gamma = -2\rho \text{ and } \delta = 0 \quad .$$

After some calculating [App. 4.4] and assuming uniform illumination over the aperture, we find

$$R_\theta = 2\cot\tfrac{1}{2}\Psi \sin\left(\frac{4\pi F}{\lambda}\cdot\frac{1 - \cos\Psi}{1 + \cos\Psi}\right) \tag{4.48}$$

and

$$T_\theta = 2\cot\tfrac{1}{2}\Psi \cos\left(\frac{4\pi F}{\lambda}\cdot\frac{1 - \cos\Psi}{1 + \cos\Psi}\right) \tag{4.49}$$

If we substitute the values of R_θ and T_θ in the equation for the gain (Eq. 4.43) we find

$$G(\pi) = \cot^2\tfrac{1}{2}\Psi$$

Comparing this value with G(0) we find a relationship for uniform illumination

$$G(0)/G(\pi) = (\pi D/\lambda\ \tan\tfrac{1}{2}\Psi)^2 \tag{4.50}$$

which relation is equal to that found by Kritikos [72] along totally different ways. Apparently the back-radiation found for $\theta = \pi$ is equal to the radiation of the feed for that same direction without any scattered contribution of the reflector. This effect has been noticed before and is known as the Poisson spot[127].

4.3. Some limitations of physical optics

4.3.1. Introduction

The physical optics approximation has been investigated and employed by a great number of scientists. Their comments differ considerably. Some of them are not in favour of the method at all, but others recommend it.
It is agreed that the results obtained with the physical optics approximation become better if the dimensions of the system with respect to the wavelength become larger [38, 106].
This may be explained by the fact that the current distribution on the surface of the reflector is calculated by geometrical optical methods. As is well known, the results of geometrical optics are only reliable if the dimensions of the scatterer are much larger than the wavelength. Sometimes the remark is made that physical optics gives incorrect results, but these conclusions are in several cases drawn from reflectors with small dimensions of the order of 10 λ or less [54, 93].
Siegel [106] explains further that not only should the reflector be large with respect to the wavelength, but incorrect answers can also be expected if the body has a radius of curvature which is small with respect to the wavelength [3].
Several authors [74, 102] notice that satisfactory results are only obtained in the region about the specular direction and that the physical optics approximation is unreliable in the shadow region because the currents on the back of the reflector are neglected.
This current distribution shows discontinuity at the edge of the reflector. It is assumed that in the shadow region the current is zero, independent of the edge illumination. In reality, such truncated current distribution is not to be expected, so that the physical optics current distribution at the edge is wrong.
Kinber, Tandit and Tartakovski [62, 63, 112, 115] have proposed corrections in the P.O. current distribution as explained by Afifi and Van Hoof [2, 51]. Afifi has found that these correction currents are of minor importance.
Later, Kinber and Tseytlin [65] introduced other corrections of the P.O. current distribution for the calculation of phase centres of parabolic reflectors. The new correction is the difference between the P.O. current distribution and the current distribution of Sommerfeld at the edge

of a half plane. Calculated radiation patterns are not reported.
Oshiro and Mitzner [81] proposed to use the P.O. current distribution at the specular region and the current distribution which is obtained by solving the integral equation (Eq. 4.11) at the shadow region. However, P.O. should not be judged by whether it yields the correct currents but by whether the final computed scattered fields are correct. Examples are known of badly approximated currents, but the radiation patterns coincide very well with practice. Well known is the fact that the field scattered from a half infinite cone is very reliable if calculated by means of P.O., but the G.O. current distribution is not correct at all at the cone's vertex [94, p.48]. This phenomenon may be explained by the fact that the error in the current distribution has oscillatory behaviour over the surface and its integrated contribution to the scattered field is small [75].
Probably the difference between the P.O. current distribution and the true currents serves to built up the near field. In this near field there is a phase difference between the electric and magnetic field. The wave impedance has a capacitive or inductive character and in the near field the energy is stored. In the far field E and H are in phase and the wave impedance is real. As the radiation patterns are calculated for the far field, we do not notice anything of the energy stored in the near field. Therefore, we neither notice anything of the error in the G.O. current distribution.
In general, the P.O. approximation does not meet the reciprocity theorem [70]; this means that for a given angle of incidence and the corresponding scattering angle two separate expressions are obtained for the far zone amplitude, whereas there should be only a single expression. In the direction of specular reflections, however, physical optics does satisfy reciprocity and it is assumed that in the neighbourhood of this direction it provides satisfactory approximation. This seems reasonable from the physical viewpoint; in the specular direction the more accurate currents from the central region of the reflector are in phase, making a large contribution to the far zone, which suppresses the failure to approximate the edge currents [70].
As Kouyoumjian [70] explains further, P.O. does give reasonable approximation of the specular backscatter if ka ($k = 2\pi/\lambda$) is larger than 8, where $2a$ is the diameter of a circular plate or the side of a square plate. The main beam and sidelobe maxima are predicted satisfactorily within 20 degrees of normal incidence for $ka > 8.5$. Outside this angular range the

agreement seems poor. However, no explanation is given to what extent. It may be explained that if the sidelobe level is very low, e.g. -60 dB and P.O. indicates -70 dB, the error has very little influence on the calculation of the noise temperature, so that P.O. may be applied with success. Carter [6] is one of the few authors who also considered the edge illumination. He comments that the field on the shadow side of the reflector is assumed to vanish, which is a consequence of using the approximations of the geometrical optics method of calculating the field over the reflector. Normally, there will be small currents at the edge and on the shadow side of the reflector which will contribute to the diffraction field, especially in the shadow region. However, if the edge of the reflector is very near a deep null of the primary feed pattern, these currents will be negligibly small. Rusch [98] has programmed the Kouyoumjian version of the G.T.D. scattered field for a hyperboloid (D = 25λ) illuminated by a spherical wave, and has compared this with results of the Keller version of G.T.D. with G.O. and with P.O. In general, the P.O. and Kouyoumjian G.T.D. curves agree closely in magnitude both in the illuminated and shadowed regions. In particular the agreement between the P.O. and Kouyoumjian G.T.D. results in the vicinity of the reflection boundary are emphasized. (Fig. 4.2)

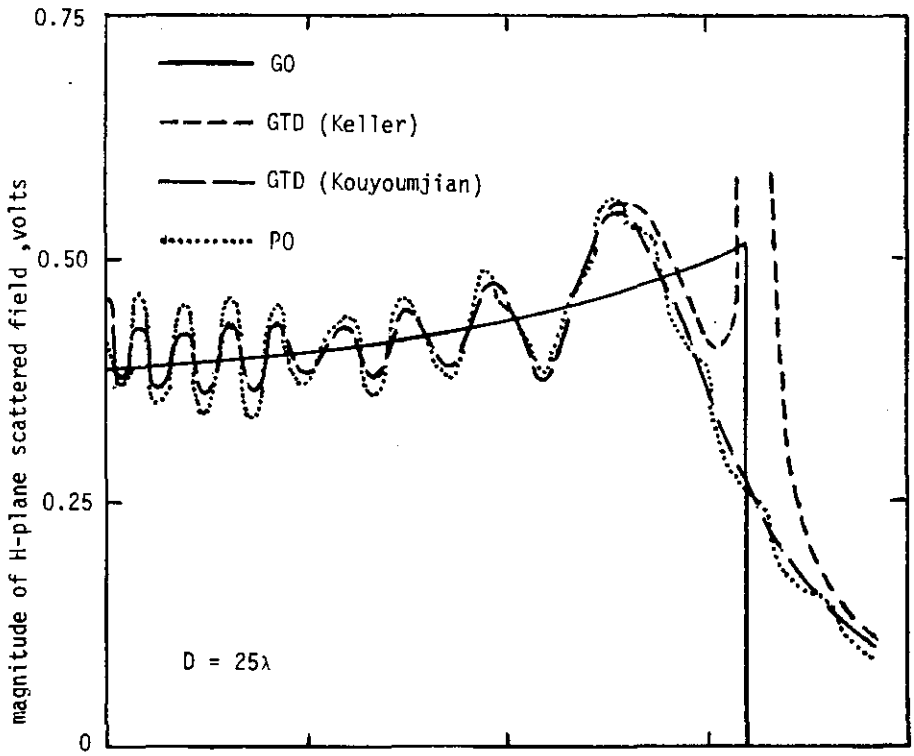

Fig. 4.2 Scattered radiation from a hyperboloid

In the following we shall investigate the various comments. We shall especially study the influence of the feed pattern on the total field of reflector and feed. We shall also investigate the influence of the diameter and the edge illumination. We shall use the definition of the gain pattern $G(\theta,\phi)$, which should yield 4π, integrating this pattern over the entire sphere.

4.3.2. Some errors in calculating radiation patterns of reflector antennas using physical optics approximation

4.3.2.1. Mathematical models of antenna feeds

It is useful in computer programs to approximate the patterns of antenna feeds by mathematical expressions simplifying the computing work. For this purpose we shall discuss the three different mathematical feeds as used by several authors [22, 30, 82, 96, 108]:

(a) the feed pattern giving constant fieldstrength within a solid angle at equal distances from the origin as suggested by Rusch [96]. Outside this region the pattern is zero (Fig. 4.3a). The illumination is discontinuous; it does not give uniform illumination over the aperture of a paraboloid;

(b) the feed pattern that produces uniform illumination over the aperture of a paraboloid antenna as explained before [108, p.433]. This pattern is also truncated at $\psi = \Psi$ (Fig. 4.3b) and is circularly symmetrical as well;

(c) the tapered cosine pattern that belongs to the class of feed patterns defined by $G_f(\psi) = 2(n+1)\cos^n\psi$ (Eq. 2.31).

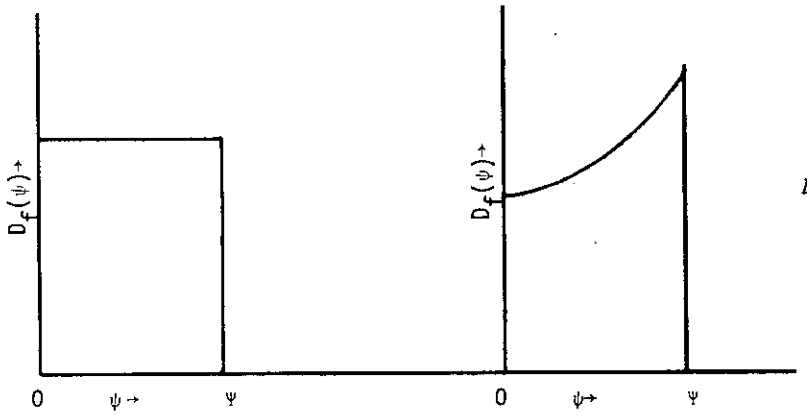

Fig. 4.3 a) Constant feed pattern
b) Uniform feed pattern

This last pattern, which was already mentioned by Silver [108, p.425], is circularly symmetrical and is now very popular. It has been used by several investigators for analysis of reflector antennas [22,30,82]. For $\psi \rightarrow 90^0$ the gain function approaches gradually to zero and there is no back radiation. A further advantage of this feed pattern lies in the fact that by a combination of different values for ψ and n all possible tapers at the edges of reflectors may be realized.

All antenna patterns have to meet the equation

$$\int_{4\pi} G(\psi,\xi)\, d\Omega = 4\pi \tag{4.51}$$

where $G(\psi,\xi)$ represents the antenna pattern and $d\Omega$ the element of solid angle.

4.3.2.2. Errors due to truncated feed patterns

The discontinuity of an electromagnetic field can only be supported by surface currents and charges. If there are no currents along the interface between 2 media the tangential fieldstrength has to be continuous; consequently, the truncated fields at the discontinuity do not satisfy Maxwell's equations and should not be used as a primary source to calculate scattered radiation from a reflector system.

If they are used [96], errors in the results are to be expected. The errors may be evaluated using the Kirchhoff integration [108, p.149] by calculating first the field scattered by the reflector and adding the feed pattern to it to obtain the total field at a distance R. If the electric field has components in the θ and ϕ directions, the gain factor of the composite system may be represented by

$$G(\theta,\phi) = 2\pi(\varepsilon/\mu)^{\frac{1}{2}} \frac{[|E_\theta|^2 + |E_\phi|^2]R^2}{P_T}, \tag{4.40}$$

P_T being the total power radiated by the feed. This composite gain factor has also to meet Eq. 4.51.

When the feed pattern has a polarization vector of $(0, \cos\xi, -\sin\xi)$ in ρ,ψ,ξ coordinates, it can be proved that in the $\phi = 0$ plane the electric field only depends on E_θ while in the $\phi = 90^0$ plane only an electric field E_ϕ has to be considered [95].
It now appears that if a truncated theoretical feed pattern is used, Eq.4.51 does not yield 4π but more.
These phenomena may be illustrated by some examples as shown below in table 4.1. Here, a paraboloid reflector has been illuminated by a truncated feed pattern giving uniform illumination over the aperture with the diameter and angular apertures as parameters.
After $G(\theta,\phi)$ of Eq. 4.40 was known, we calculated Eq. 4.51 by using Eq. 4.43.

Table 4.1

Ψ	D/λ	aperture illumination	$\int_\Omega G(\theta,\phi)\, d\Omega$
60	15	uniform	4.62π
90	15	"	4.57π
60	30	"	4.46π
90	30	"	4.42π
60	50	"	4.37π
90	50	"	4.34π
60	75	"	4.33π
90	75	"	4.31π
60	100	"	4.29π
90	100	"	4.27π

As is shown, some of the results contain errors of more than 10% in this power distribution, which are far too large to make accurate calculations. The errors become smaller as the diameter of the reflector becomes larger. If, on the other hand, we illuminate paraboloid reflectors with "smooth" gain functions, such as the tapered cosine pattern, it appears that the results are more reliable (Table 4.2)

Table 4.2

Ψ	D/λ	n	relative edge illumination dB	$\int_{\Omega} G(\theta,\phi)d\Omega$
50^0	50	2	- 5.6	3,99 π
		4	- 9.4	4.00 π
		6	-13.2	4.00 π
60^0	50	2	- 8.5	4.00 π
		4	-14.5	4.00 π
		6	-20.5	4.00 π

Fig. 4.4. shows a typical example of a calculated radiation pattern of a parabolic reflector with a diameter of 15 λ and an angular aperture of $\Psi = 60^0$. The reflector is illuminated by a truncated feed pattern, giving uniform illumination over the aperture. The first sidelobes are identical with those obtained by the scalar aperture method [108, p.192].
Far sidelobes cannot be checked in this way since the scalar aperture method gives only reliable results for the first two or three sidelobes. Back radiation is also correct; this may be shown by using a relationship found by Kritikos [72] between the gain in forward and backward direction, viz.

$$\frac{G(0)}{G(\pi)} = (\pi D/\lambda \tan\tfrac{1}{2}\Psi)^2 \qquad (4.50)$$

From the above the conclusion may be drawn that the radiation pattern contains too much power in the far sidelobes and that, therefore, the level of the far sidelobes is too high. A theoretical truncated feed pattern should therefore not be used as a primary source to calculate radiation patterns of reflector antennas. When the antenna noise temperature is calculated, the results are wrong, indicating too high a temperature.

No difficulties in the power conservation are to be expected, if the tapered cosine or other patterns are used which do not show a sudden truncation of the fieldstrength at the edge of the reflector.

It will be clear that the use of Eq.4.51 is a very powerful tool to judge whether a calculated antenna pattern is correct or not and that this additional verification deserves more attention in the literature.

Commenting on a letter which was recently published, Van Hoof [33,51] disagrees with the conclusion that truncation is the main reason of poor power conservation of the total radiation pattern, if a truncated feed is used. He states that the currents on the surface of the reflector are not derived from rigorous solutions and that this limits the accuracy of the calculation, especially in the shadow region. He refers to the corrections of the current distribution as investigated by Russian authors mentioned before [62, 63, 112, 115], and recommends to check the power conservation after the corrections have been introduced.
Summarizing, Van Hoof states that the main reason for poor power conservation using uniform illumination should be looked for in the fact that in this case the edge of the reflector is illuminated high, and that the error will decrease if the illumination towards the edge is tapered.
The remarks made by Van Hoof have led to some calculations of radiation patterns of paraboloids excited by a number of mathematical models of antenna feeds.
The results with a feed pattern producing uniform illumination over the aperture of the paraboloid have been discussed before [33]. We extended the calculations with a feed producing constant fieldstrength within the solid angle subtended by the main reflector [Fig.4.3a] and with tapered

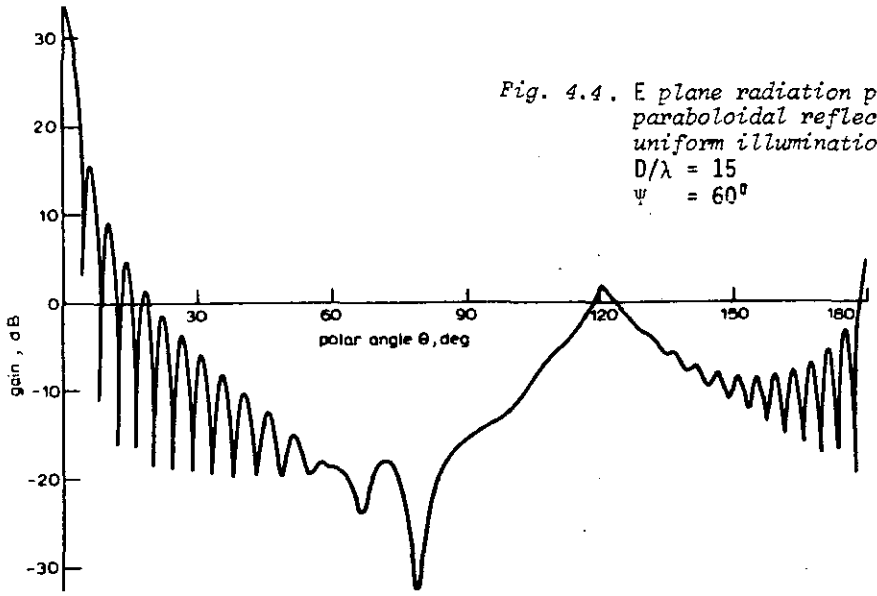

Fig. 4.4. E plane radiation pattern from paraboloidal reflector under uniform illumination
$D/\lambda = 15$
$\psi = 60^0$

cosine patterns. However, the tapered cosine patterns have been truncated at the angular aperture Ψ of the main reflector. The cosine patterns are then defined by

$$G_f(\psi) = \text{Constant}.\cos^n\psi \quad \text{for} \quad 0 < \psi < \Psi$$

$$G_f(\psi) = 0 \qquad\qquad \psi > \Psi$$

As

$$\int_{4\pi} G(\psi,\xi)\, d\Omega = 4\pi \quad ,$$

it is readily found that

$$\text{Constant} = \frac{2(n+1)}{1 - \cos^{n+1}\Psi}$$

By taking different values for n, the edge illumination of the main reflector may be modified. The results are shown in table 4.3.

Table 4.3

diameter main reflector 50 λ	Ψ	edge illumination	$\int_\Omega G d\Omega$
1. uniform illumination over aperture	60^0	0 dB	4.30 π
2. constant fieldstrength pattern	60^0	-2.5 dB	4.26 π
3. cosine pattern n=2	60^0	-8.5 dB	4.16 π
4. cosine pattern n=4	60^0	-14.5 dB	4.06 π

The results with non-truncated primary cosine patterns have been mentioned before [33].

A second experiment has been carried out with truncated patterns producing uniform illumination over the aperture, not truncated at $\psi = \Psi$, however, but at larger angles [Table 4.4].

The results from these experiments enable us te draw some conclusions. It appears that the edge illumination plays a role in the correctness of the power distribution if the truncation angle of the feed pattern coincides with the subtending angle of the paraboloid. The lower the edge illumination

the better the results. However, differences still exist between truncated cosine patterns and non-truncated cosine patterns. The latter has a correct power distribution for $n = 2$ and $n = 4$, while the truncated pattern shows errors. Therefore, it appears that not only the edge illumination and thus the current distribution near the edge plays a role in the final results but also the location of the feed pattern truncation.

Table 4.4

D/λ	Ψ reflector	Ψ feed	$\int_{\Omega} G(\theta,\phi)d\Omega$
50	60^0	60^0	$4.30\ \pi$
50	60^0	70^0	$4.00\ \pi$
50	60^0	80^0	$4.00\ \pi$

4.3.3. The influence of the reflector diameter

It is often said that the results obtained with the physical optics approximation become better if the dimensions of the reflector with respect to the wavelength become larger [38, 106]. To investigate this problem we have used Eq. 4.51 again after calculating the pattern of a paraboloid illuminated by a cosine feed defined by

$$G_f(\psi) = 6\cos^2\psi \quad , \quad 0 < \psi < \tfrac{1}{2}\pi$$

$$G_f(\psi) = 0 \quad , \quad \psi > \tfrac{1}{2}\pi$$

The paraboloid has a subtending angle of $\Psi = 60^0$ and the results are found in table 4.5 below. By using this primary feed pattern the edge illumination remains constant at -8.5 dB.

A similar experiment has been carried out with a hyperboloid; the subtending angle was 20^0 and $\Psi_2 = 80^0$, the eccentricity 1.53 and $G_f(\psi) = 90 \cdot \cos^{44}\psi$. The results are found in table 4.6. The edge illumination of the subreflector in this experiment was about -12 dB.

Table 4.5 Paraboloid illuminated by cosine feed (n=2)

D/λ	$\int_{\Omega} G(\theta,\phi)d\Omega$
5	3.961 π
10	3.979 π
15	3.983 π
25	3.986 π
50	3.996 π
100	4.000 π

Table 4.6 Hyperboloid illuminated by cosine feed (n=44)

D/λ	$\int_{\Omega} G(\theta,\phi)d\Omega$
15	4.074 π
25	4.023 π
50	4.005 π
75	4.001 π
100	4.000 π

As will be noticed, the results become indeed better if the diameter increases. At a diameter of 50 λ, the deviations from the theoretical value of 4π are of the order of 0.1%, which is in accordance with Kouyoumjian's statement [70] that for $D/\lambda > 25\ \lambda$ the results with the physical optics approximation are reliable.

4.3.4. The influence of the edge illumination

As Carter [6] has mentioned before, the errors caused by the currents near the edge of the reflector may be negligibly small if the illumination towards the edge is tapered. For this reason we investigated Eq. 4.51 for a number of paraboloids with a variable edge illumination. This variation may be obtained by varying the exponent n in Eq. 2.31. The results are found in table 4.7.

Table 4.7

D/λ	ψ	n	edge illumination (dB)	$\int_{\Omega} G(\theta,\phi)d\Omega$
50	60^0	1	-5.5	3.994 π
50	60^0	2	-8.5	3.996 π
50	60^0	3	-11.5	3.999 π
50	60^0	4	-14.5	4.000 π
50	60^0	5	-17.5	4.004 π
50	60^0	6	-20.5	4.002 π
50	50^0	1	-3.6	3.993 π
50	50^0	2	-5.6	3.994 π
50	50^0	3	-7.5	3.996 π
50	50^0	4	-9.4	3.997 π
50	50^0	5	-11.3	3.999 π
50	50^0	6	-13.2	4.001 π
50	50^0	7	-15.2	4.001 π
50	50^0	8	-17.1	4.001 π

It will be seen that the power pattern adds up very accurately even if uniform illumination is approached. The largest differences noticed so far are of the order of 0.2%.

4.3.5. Conclusions

By integrating the antenna pattern $G(\theta,\phi)$ over the entire sphere, a method is presented to make certain whether a calculated or observed pattern of a reflector antenna is correct or not. If this integration does not yield 4π, the pattern is incorrect. If the pattern yields 4π all parts contributing to the integration add up correctly. This does not prove that low far sidelobes have been calculated correctly, as such sidelobes practically do not contribute to the integral within the accuracy of computation.
It is expected [99] that G.T.D. will not yield 4π as this method shows errors in the main direction.
There remain a number of unsolved problems. The behaviour of P.O. when the main reflector is uniformly illuminated or overilluminated [30] has not been investigated. Further, the behaviour of the pattern when truncated

feeds are employed has not yet been explained satisfactorily.
So far, no methods are known to calculate the influence of struts on the far sidelobes.
Therefore, comparison of a calculated pattern with an observed pattern gives no answer to the question whether the pattern has been calculated correctly, since a measured pattern always contains the influence of the struts.
All in all, P.O. is a reliable method of calculating the radiation pattern of reflector antennas with a diameter of more than approx. 25 λ.

Appendix 4.1

Coordinate transformations

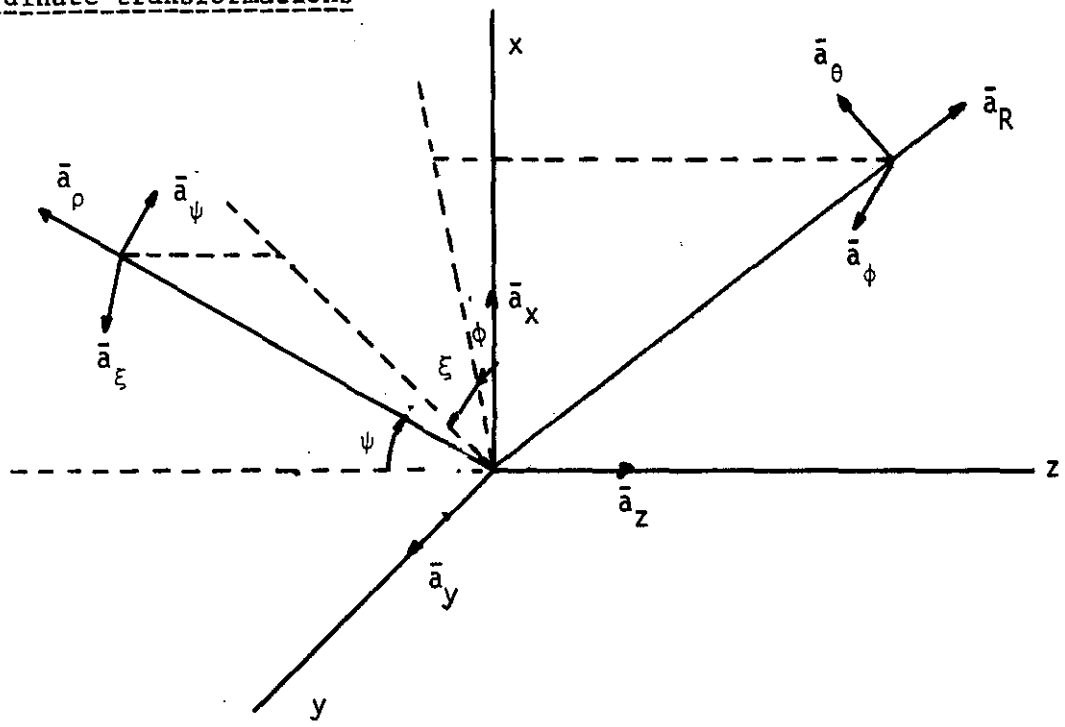

Fig. 1 Unit vectors in different coordinate systems

$(x,y,z) \rightleftarrows (\rho,\psi,\xi)$

$$\begin{aligned}
\bar{a}_x &= \bar{a}_\rho \sin\psi\cos\xi + \bar{a}_\psi \cos\psi\cos\xi - \bar{a}_\xi \sin\xi \\
\bar{a}_y &= \bar{a}_\rho \sin\psi\sin\xi + \bar{a}_\psi \cos\psi\sin\xi + \bar{a}_\xi \cos\xi \\
\bar{a}_z &= -\bar{a}_\rho \cos\psi + \bar{a}_\psi \sin\psi
\end{aligned}$$

$$\begin{aligned}
\bar{a}_\rho &= \bar{a}_x \sin\psi\cos\xi + \bar{a}_y \sin\psi\sin\xi - \bar{a}_z \cos\psi \\
\bar{a}_\psi &= \bar{a}_x \cos\psi\cos\xi + \bar{a}_y \cos\psi\sin\xi + \bar{a}_z \sin\psi \\
\bar{a}_\xi &= -\bar{a}_x \sin\xi + \bar{a}_y \cos\xi
\end{aligned}$$

$(x,y,z) \rightleftarrows (R,\theta,\phi)$

$$\begin{aligned}
\bar{a}_x &= \bar{a}_R \sin\theta\cos\phi + \bar{a}_\theta \cos\theta\cos\phi - \bar{a}_\phi \sin\phi \\
\bar{a}_y &= \bar{a}_R \sin\theta\sin\phi + \bar{a}_\theta \cos\theta\sin\phi + \bar{a}_\phi \cos\phi \\
\bar{a}_z &= \bar{a}_R \cos\theta - \bar{a}_\theta \sin\theta
\end{aligned}$$

$$\begin{aligned}
\bar{a}_R &= \bar{a}_x \sin\theta\cos\phi + \bar{a}_y \sin\theta\sin\phi + \bar{a}_z \cos\theta \\
\bar{a}_\theta &= \bar{a}_x \cos\theta\cos\phi + \bar{a}_y \cos\theta\sin\phi - \bar{a}_z \sin\theta \\
\bar{a}_\phi &= -\bar{a}_x \sin\phi + \bar{a}_y \cos\phi
\end{aligned}$$

Appendix 4.2 Calculations of current distribution on paraboloid surface

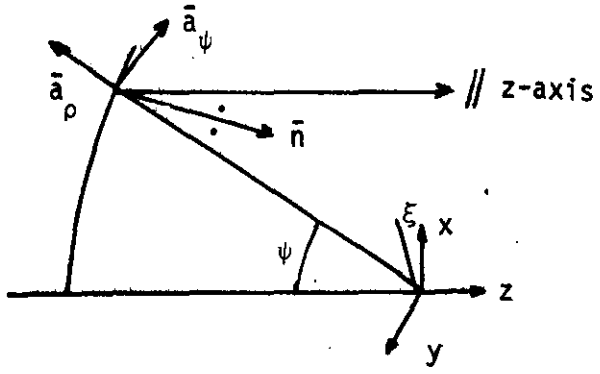

Fig. 1
Normal and unit vectors at a paraboloid reflector

We shall consider a paraboloid illuminated by feed systems with a polarization vector

$$\bar{a}_i(\psi,\xi) = \cos\xi\ \bar{a}_\psi - \sin\xi\ \bar{a}_\xi$$

For a paraboloid

$$\bar{n} = -\cos\tfrac{1}{2}\psi\ \bar{a}_\rho + \sin\tfrac{1}{2}\psi\ \bar{a}_\psi\ ,$$

therefore, the current distribution will be

$$\bar{K} = 2(\bar{n} \times \bar{H}_i) = 2(\varepsilon/\mu)^{\frac{1}{2}}\ \bar{n} \times (\bar{a}_\rho \times \bar{a}_i).\ E_i$$

or

$$\bar{K} = 2(\varepsilon/\mu)^{\frac{1}{2}}\ [\cos\tfrac{1}{2}\psi,\ 0\ ,\ \cos\xi\sin\tfrac{1}{2}\psi]_x.E_i$$

Thus, the y component of the current distribution disappears entirely.

Appendix 4.3 Evaluation of the vector product $\bar{n} \times (\bar{a}_\rho \times \bar{a}_i)$

Generally, the equation $r = r(u,v)$ represents a surface and the unit vector to this surface may be written as [73, p. 70 - 74].

$$\bar{n} = \frac{\frac{\delta \bar{r}}{\delta u} \times \frac{\delta \bar{r}}{\delta v}}{\left| \frac{\delta \bar{r}}{\delta u} \times \frac{\delta \bar{r}}{\delta v} \right|} \tag{1}$$

The differential surface element dS of the surface is

$$dS = \left| \frac{\delta \bar{r}}{\delta u} \times \frac{\delta \bar{r}}{\delta v} \right| \, dudv \tag{2}$$

If $u = \psi$ and $v = \xi$, the surface written in cartesian coordinates is

$$\bar{r} = \rho \sin\psi \cos\xi \, \bar{x} + \rho \sin\psi \sin\xi \bar{y} - \rho \cos\psi \, \bar{z} \tag{3}$$

After some calculation it is found that

$$\bar{n} = \frac{-\rho \bar{a}_\rho + \rho' \bar{a}_\psi}{\sqrt{\rho^2 + \rho'^2}} \tag{4}$$

and

$$dS = \rho \sqrt{\rho^2 + \rho'^2} \, \sin\psi d\psi d\xi \tag{5}$$

ρ' being the first derivative to ψ. Let further the unit vector $\bar{a}_i$ be

$$\bar{a}_i(\psi,\xi) = \cos\xi \, \bar{a}_\psi - \sin\xi \, \bar{a}_\xi \tag{4.6}$$

then the vector product $\bar{a}_\rho \times \bar{a}_i$ yields

$$\bar{a}_\rho \times \bar{a}_i = \begin{pmatrix} 1 \\ 0 \\ 0 \end{pmatrix}_\rho \times \begin{pmatrix} 0 \\ \cos\xi \\ -\sin\xi \end{pmatrix}_\rho = \begin{pmatrix} 0 \\ \sin\xi \\ \cos\xi \end{pmatrix}_\rho \tag{6}$$

and

$$\bar{n} \times (\bar{a}_\rho \times \bar{a}_i) = \frac{1}{\sqrt{\rho^2 + \rho'^2}} \begin{pmatrix} -\rho \\ \rho' \\ 0 \end{pmatrix} \times \begin{pmatrix} 0 \\ \sin\xi \\ \cos\xi \end{pmatrix} \tag{7}$$

$$= \frac{1}{\sqrt{\rho^2 + \rho'^2}} \begin{pmatrix} \rho' \cos\xi \\ \rho \cos\xi \\ -\rho \sin\xi \end{pmatrix}_\rho$$

The result is still expressed in ρ,ψ,ξ coordinates and will have to be transformed into R,θ,ϕ coordinates (Appendix 4.1). Leaving out the term $1/\sqrt{(\rho^2 + \rho'^2)}$ Eq.7 becomes

$$\begin{bmatrix} \rho'\cos\xi(\bar{x}\sin\psi\cos\xi + \bar{y}\sin\psi\sin\xi - \bar{z}\cos\psi) \\ \rho\cos\xi(\bar{x}\cos\psi\cos\xi + \bar{y}\cos\psi\sin\xi + \bar{z}\sin\psi) \\ -\rho\sin\xi(-\bar{x}\sin\xi + \bar{y}\cos\xi) \end{bmatrix}_x \tag{8}$$

or

$$\begin{bmatrix} \bar{x}(\rho'\sin\psi\cos^2\xi + \rho\cos\psi\cos^2\xi + \rho\sin^2\xi) \\ \bar{y}(\rho'\sin\psi\sin\xi\cos\xi + \rho\cos\psi\sin\xi\cos\xi - \rho\sin\xi\cos\xi) \\ \bar{z}(-\rho'\cos\psi\cos\xi + \rho\sin\psi\cos\xi) \end{bmatrix} x \tag{9}$$

and in R,θ,ϕ coordinates

$$\begin{bmatrix} 0 \\ \cos\theta\cos\phi(\rho'\sin\psi\cos^2\xi + \rho\cos\psi\cos^2\xi + \rho\sin^2\xi) + \cos\theta\sin\phi(\rho'\sin\psi\sin\xi\cos\xi \\ + \rho\cos\psi\sin\xi\cos\xi - \rho\sin\xi\cos\xi) - \sin\theta(-\rho'\cos\psi\cos\xi + \rho\sin\psi\cos\xi) \\ -\sin\phi(\rho'\sin\psi\cos^2\xi + \rho\cos\psi\cos^2\xi + \rho\sin^2\xi) + \cos\phi(\rho'\sin\psi\sin\xi\cos\xi + \\ \cos\psi\sin\xi\cos\xi - \rho\sin\xi\cos\xi) \end{bmatrix}$$

resulting in a θ component of

$$\bar{n} \times (\bar{a}_\rho \times \bar{a}_i)_\theta = \rho'[\cos\theta\cos\xi\sin\psi\cos(\xi - \phi) + \sin\theta\cos\psi\cos\xi] + \rho[\cos\theta\cos\psi\cos\xi\cos(\xi - \phi) + \cos\theta\sin\xi\sin(\xi - \phi) - \sin\theta\sin\psi\cos\xi] \tag{10}$$

and in a ϕ component of

$$\bar{n} \times (\bar{a}_\rho \times \bar{a}_i)_\phi = \rho'[-\sin\phi\sin\psi\cos^2\xi + \cos\phi\sin\psi\sin\xi\cos\xi] + \rho[-\sin\phi\cos\psi\cos^2\xi - \sin\phi\sin^2\xi + \cos\phi\cos\psi\sin\xi\cos\xi - \cos\phi\sin\xi\cos\xi] \tag{11}$$

Eq. 11 may be modified into

$$\rho'\sin\psi\cos\xi\sin(\xi - \phi) - \rho\cos\xi\cos\psi\sin(\xi - \phi) - \rho\sin\xi\cos(\xi - \phi)$$

or

$$[\rho'\sin\psi - \rho(1 - \cos\psi)]\cos\xi\sin(\xi - \phi) - \rho\sin\phi \tag{12}$$

Appendix 4.4 Calculation of back radiation of a paraboloid

In the case of back radiation $\theta = \pi$, then,

$$\alpha = \frac{4\pi F}{\lambda}\,\frac{1 - \cos\psi}{1 + \cos\psi}\,,\ \beta = 0\,,\ \gamma = -2\rho\,,\ \delta = 0\,,\ J_0(\beta) = 1 \text{ and } J_2(\beta) = 0$$

Then the expressions for R_θ and T_θ (Eqs. 4.42) become for uniform illumination of the paraboloid

$$R_\theta = k\int_0^{\Psi} \frac{\cot\frac{1}{2}\Psi\,\sec^2\frac{1}{2}\psi}{\lambda}\,\sin\psi 2\rho\cos\alpha\ \rho d\psi \tag{1}$$

or as

$$\rho = 2F/(1 + \cos\psi)$$

$$R_\theta = k\cot\tfrac{1}{2}\Psi\int_0^{\Psi} \frac{2}{1 + \cos\psi}\,\sin\psi\ \frac{4F}{1 + \cos\psi}\,\cos\alpha\, d\psi \tag{2}$$

or

$$R_\theta = k\cot\tfrac{1}{2}\Psi\int_0^{\Psi} \frac{8F\sin\psi}{(1 + \cos\psi)^2}\,\cos\left(\frac{4\pi F}{\lambda}\,\frac{1 - \cos\psi}{1 + \cos\psi}\right) d\psi \tag{3}$$

Since

$$\alpha = \frac{4\pi F}{\lambda}\,\frac{1 - \cos\psi}{1 + \cos\psi}\,,\ \text{then } d\alpha = \frac{8\pi F}{\lambda}\,\frac{\sin\psi}{(1 + \cos\psi)^2}\ d\psi$$

Eq. 3 then simply becomes

$$R_\theta = 2\cot\tfrac{1}{2}\Psi\int_0^{x_1} \cos\alpha\, d\alpha\,,\ \alpha_1 \text{ being } \frac{4\pi F}{\lambda}\,\frac{1 - \cos\Psi}{1 + \cos\Psi}\,,$$

or
$$R_\theta = 2\cot\tfrac{1}{2}\Psi\,\sin\left(\frac{4\pi F}{\lambda}\,\frac{1 - \cos\Psi}{1 + \cos\Psi}\right). \tag{4}$$

In a similar way we find for T_θ

$$T_\theta = 2\cot\tfrac{1}{2}\Psi\int_0^{\alpha_1} \sin\alpha\, d\alpha - 2[G_f(\theta)]^{\frac{1}{2}} \tag{5}$$

For $\theta = \pi$, $G_f(\theta) = \cot^2\frac{1}{2}\Psi$ thus

$$T_\theta = 2\cot\tfrac{1}{2}\Psi\left(1 - \cos\left\{\frac{4\pi F}{\lambda}\,\frac{1 - \cos\Psi}{1 + \cos\Psi}\right\}\right) - 2\cot\tfrac{1}{2}\Psi \tag{6}$$

5. SHAPED DOUBLE REFLECTOR SYSTEMS

5.1. Introduction

A disadvantage of the cassegrain system is the decrease in antenna efficiency by blocking and diffraction introduced by the subreflector and supports as explained before. A further limitation of the classical cassegrain antennas lies in the fact that the aperture illumination is mostly so selected that the antenna gain reaches a maximum. By doing this, the aperture illumination is fixed and no means of controlling the efficiency and sidelobes are available. The possibility of obtaining a specified pattern, was,however,already reported by Silver [108, p. 474], who shaped the reflector surface.

Kinber [64] discusses the possibility of forming an a priori distribution of amplitude and phase in the aperture of an antenna with the aid of two reflectors. He shows that a solution exists in the two-dimensional case but not necessarily in the three-dimensional case.

Morgan [80] also indicates the possibilities of deviating from the standard hyperboloid and paraboloid of cassegrain systems to improve the reflected wavefront and to prevent power from being reradiated into the feed.

Publications of Jet Propulsion Lab. [86,88] give the impression that their solution, providing the subreflector with a flange to decrease spillover losses, is not found ideal. Apparently other solutions proposing more radical modifications of the reflector surfaces offer more possibilities.

The problem of obtaining a dual antenna with a specified amplitude and phase distribution in the aperture can be tackled in two ways:

(a) An arbitrary primary feed with a known radiation pattern illuminates a subreflector. The surfaces of main and subreflector must now meet certain requirements in order that the required aperture field may be obtained.

(b) An arbitrary main reflector, mostly a paraboloid, is available and an arbitrary aperture field is required. The feed must now possess a dictated radiation pattern and the subreflector needs modification. This paper only deals with possibility (a), as feeds with prescribed radiation patterns and large bandwidths [88] are very difficult to realize or not at all. Pioneering work as to possibility (a) has been carried out by Galindo [39].

In this paper Galindo's method of calculating the reflector surfaces is mainly applied. Calculations proposed by Green [44] and Williams [124] are also followed. It is noticed that nowadays the work of Galindo [39] and Williams [124] is being translated into commercial applications and it is expected that this subject will continue to be developed in the years to come.

However, research on these systems is still going on in order to obtain even more improvements. Clarricoats et al. [9] have proposed a spherical reflector system consisting of two small shaped reflectors. In this way the efficiency of the spherical reflector may be improved considerably. Clarricoats [10] also studied the problem with respect to existing systems, where it is not possible to shape the main reflector. This is usually the case for large apertures such as radiotelescopes and antennas for satellite communication ground stations.

This chapter discusses in general the equations required to design a dual reflector system; it also discusses a solution. Further, a solution is proposed in which the blockage efficiency is increased to an absolute maximum and attention is paid to the antenna pattern scattered by shaped and non-shaped subreflectors.

The high overall efficiency, however, is only obtained for one particular feed pattern. If the feed pattern differs from the original for which the system has been calculated, the aperture efficiency decreases [89].This may happen for an antenna system whose feed pattern varies with frequency. It is the purpose of this chapter to investigate aperture efficiency, sub-reflector blockage efficiency, and spillover efficiency of cassegrain antenna systems which do not use a hyperboloid reflector and contain an approximate feed system, so that an estimate of the efficiency of the system may be obtained.

The radiation pattern will also be calculated to investigate the location and amplitude of the near sidelobes .

5.2. The design of a circularly symmetrical antenna system

5.2.1. The system's geometry

The design of a two-reflector system utilizes optical principles such as:
(1) Snell's Law applied to each reflector.

(2) Conservation of energy flow in any solid angle bounded by ray trajectories [108, p.112].

(3) The surfaces of constant phase are normal to the ray trajectories even after a number of reflections (Theorem of Malus) [3, p.131].

The application of these laws leads to a number of equations of constraint for the system.

Snell's law applied to the subreflector [Fig. 5.1] leads to the equation:

$$\frac{dy_1}{dx_1} = \tan\tfrac{1}{2}(\psi_1 - \psi_2) \tag{5.1}$$

where

$$\tan\psi_2 = \frac{x_2 - x_1}{\alpha + \beta - y_1 + y_2} \tag{5.2}$$

Snell's law applied to the main reflector leads to the equation

$$\frac{dy_2}{dx_2} = -\tan\tfrac{1}{2}\psi_2 \tag{5.3}$$

If we assume that the antenna system is circularly symmetrical, the relative power radiated by the primary feed within the increment $d\psi_1$ of

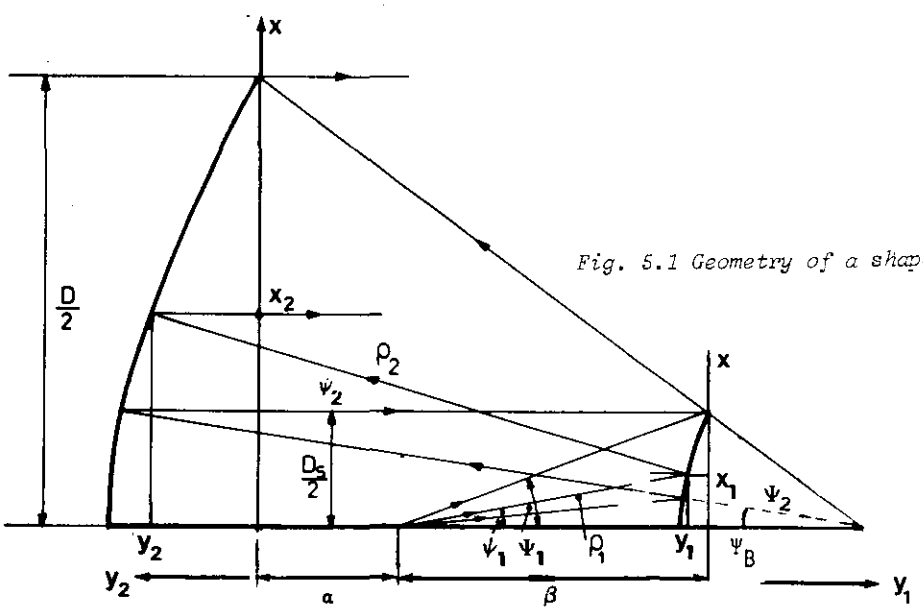

Fig. 5.1 Geometry of a shaped double reflector system

the pattern $G_1(\psi_1)$ is equal to $2\pi G_1(\psi_1) \sin\psi_1 \, d\psi_1$, where $G_1(\psi_1)$ is the gain function of the primary feed. The total power from $\psi_1 = 0$ to any angle Ψ_1 will be

$$\int_0^{\Psi_1} 2\pi G_1(\psi_1) \sin\psi_1 \, d\psi_1$$

According to the principle of energy conservation the power within $d\psi_1$ should be equal to the power radiated by the corresponding increment of the aperture, viz., $2\pi H(r)\, rdr$, where $H(r)$ is the illumination function of the aperture. The total relative power within the region from zero to x_2 is

$$\int_0^{x_2} 2\pi H(r)\, r dr$$

If both expressions are normalized by the total radiated power, we obtain

$$\frac{\int_0^{x_2} H(r)\, r dr}{\int_0^{\frac{1}{2}D} H(r)\, r dr} = \frac{\int_0^{\psi_1} G_1(\psi_1) \sin\psi_1 \, d\psi_1}{\int_0^{\Psi_1} G_1(\psi_1) \sin\psi_1 \, d\psi_1} \qquad (5.4)$$

If uniform illumination has to be produced in the aperture, Eq. 5.4 will be simplified since the function $H(r)$ must be a constant.
If in the aperture constant phase of all rays is required, the pathlength of each ray is simply

$$\rho_1 + \rho_2 + y_2 = K \, , \qquad (5.5a)$$

where all rays are coming from one common point.
Sometimes the phasefront is not spherical. By adding a term $\lambda(\psi)$ to Eq. 5.5a, the aperture phase becomes

$$\rho_1 + \rho_2 + y_2 + \lambda(\psi_1) = K \qquad (5.5b)$$

where K is a constant if the aperture has uniform phase.
With the geometry of Fig. 5.1 we write Eq. 5.5b:

$$K = (\beta - y_1)/(\cos\psi_1) + y_2 + [(x_2 - x_1)^2 + (\alpha + \beta + y_2 - y_1)^2]^{\frac{1}{2}} + \lambda(\psi_1) \tag{5.6}$$

where α and β are functions of ψ_1 and $\alpha + \beta$ is a given constant. The intersection of the primary rays with the y_1 axis determines α and β [39].
Directly from Fig. 5.1 is found

$$\tan\psi_1 = x_1/(\beta - y_1) \tag{5.7}$$

The boundary conditions are also found in Fig. 5.1, viz,

$$\tan\Psi_1 = D_s/2\beta(\Psi_1) \tag{5.8}$$

$$\tan\Psi_2 = (D - D_s)/2[\alpha(\Psi_1) + \beta(\Psi_1)] \tag{5.9}$$

$$K = \frac{\beta(\Psi_1)}{\cos\Psi_1} + \frac{\alpha(\Psi_1) + \beta(\Psi_1)}{\cos\Psi_2} + \lambda(\Psi_1) \tag{5.10}$$

After choosing Ψ_1, Ψ_2, the ratio D_s/D, $H(r)$, $G_1(\psi_1)$, and $\lambda(\psi_1)$, the whole system is determined.
If the antenna is illuminated by a point source $\lambda(\psi_1) = 0$, α and β are readily found from equations 5.8, 5.9 and 5.10 and are constants.
Using six equations out of Eqs.5.1 - 5.7, the six unknowns (ψ_1, ψ_2, x_1, x_2, y_1 and y_2) can be evaluated, and a solution of the modified system is found [20].
Introducing the term $\lambda(\psi_1)$, the values $\alpha(\psi_1)$ and $\beta(\psi_1)$ are no longer constants. The wavefront is not spherical and the rays have no common point of origin. The sum $\alpha+\beta$ is now found from Eq. 5.9 and K from Eq. 5.10. As soon as $\lambda(\psi_1)$ is known, α, β and the remaining six unknowns may be found using all equations 5.1 to 5.7.
By substitution, the 7 equations are reduced to two differential equations with the three unknowns ψ_1, y_1, and y_2.
With ψ_1 as the independant variable, the equations are solved by means of a computer [20,39].

5.2.2. Possible solution of the optimum blockage efficiency

It has been proved in Sec. 3.4.2 that theoretically the relative blockage efficiency in case of uniform illumination becomes

$$\left(\frac{\eta_B}{\eta_0}\right) = 1 - \frac{B}{A} \tag{3.46}$$

When looking carefully to the blocked parts of a dual shaped antenna system with blocking obstacles (in the zero-field concept), it is easily shown that, if the antenna is used for receiving only, power of the incoming plane waves is intercepted by the obstacles. The power intercepted by these obstacles is always wasted and can never be delivered to the feed of a shaped reflector system in the proper way.
We will therefore distinguish between the blocked parts of the aperture, where B_{plane} and B_{sph} represent shadows in the aperture of plane waves and shadows of (nearly) spherical waves, respectively. By proper shaping no parts of the aperture will now be blocked by spherical waves any longer. In that case both main reflector and subreflector will have to be provided with grooves and ripples (as shown in a example for the subreflector in Fig. 5.2) to utilize the power blocked by the subreflector supports.
The optimum blockage efficiency obtainable in the case of uniform illumination, assuming the zero field concept, is therefore

$$\left(\frac{\eta_B}{\eta_0}\right)_{max} = \left|1 - \frac{B_{plane}}{A}\right| \tag{3.47}$$

Mathematical expressions to calculate the surface shape of main reflector and subreflector are still subjects for further study. To utilize the power blocked by the subreflector itself, this could have a cone-shaped protuberance in the middle, which can be calculated very simply. For this purpose it is sufficient to replace the lower integration limit of the aperture integrals in Eq. 5.4 by $\frac{1}{2} D_s$ instead of zero.
Therefore,

$$\frac{\int_{\frac{1}{2}D_s}^{x_2} H(r)\, r\,dr}{\int_{\frac{1}{2}D_s}^{\frac{1}{2}D} H(r)\, r\,dr} = \frac{\int_{0}^{\psi_1} G_1(\psi_1)\, \sin\psi_1\, d\psi_1}{\int_{0}^{\Psi_1} G_1(\psi_1)\, \sin\psi_1\, d\psi_1} \tag{5.11}$$

Using theoretical cosine feed patterns (Eq. 2.31) Eq. 5.11 is written as

$$\frac{4x_2^2 - D_s^2}{D^2 - D_s^2} = \frac{1 - \cos^{n+1}\psi_1}{1 - \cos^{n+1}\Psi_1} \tag{5.12}$$

The results of a computer program are shown in Fig. 5.3, where the coordinates of the reflector system have been calculated for uniform illumination. The function $G_1(\psi_1) = 122\ \cos^{60}\psi_1$ served as primary feed pattern. The diameter of the subreflector is 0.1D. The angle Ψ_2 would correspond with an F/D ratio of 0.33 if the cassegrain system had been classical. It will be clear that when the mainreflector has been shaped, no focus can be defined.

Apart from showing the shaped contours of main and subreflector, Fig. 5.3 also presents a true paraboloid with an F/D ratio of 0.33. By causing the edges of the two main reflectors to coincide, the differences are clearly demonstrated. Computer calculations indicate that the maximum deviation of the shaped paraboloid from the true paraboloid is about 0.01D. However, it is also possible to compare the shaped paraboloid with what is popularly known as a best-fit paraboloid, also called regression paraboloid, which can be found by the method of least squares. The maximum difference between true and shaped paraboloid now reduces to about 0.0005D.

Using a subreflector as discussed above, the increase in blocking efficiency obtainable is not very important, but the decrease in noise temperature may be noticeable [22].

It may be noticed that the subreflector is slightly cone-shaped around the symmetry axis. However, if Eq. 5.4 is used in stead of Eq. 5.11 the subreflector does not show a cone, the tangent at the subreflector vertex is perpendicular to the symmetry axis and no improvement of subreflector blockage efficiency is obtained.

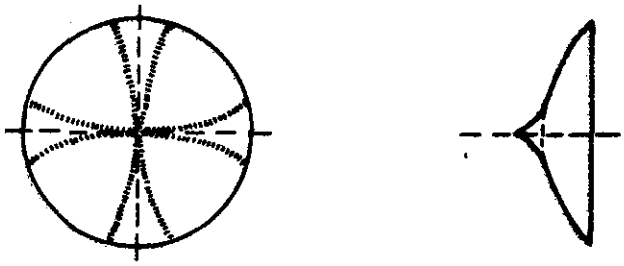

Fig. 5.2 Front view and cross-section of a shaped subreflector

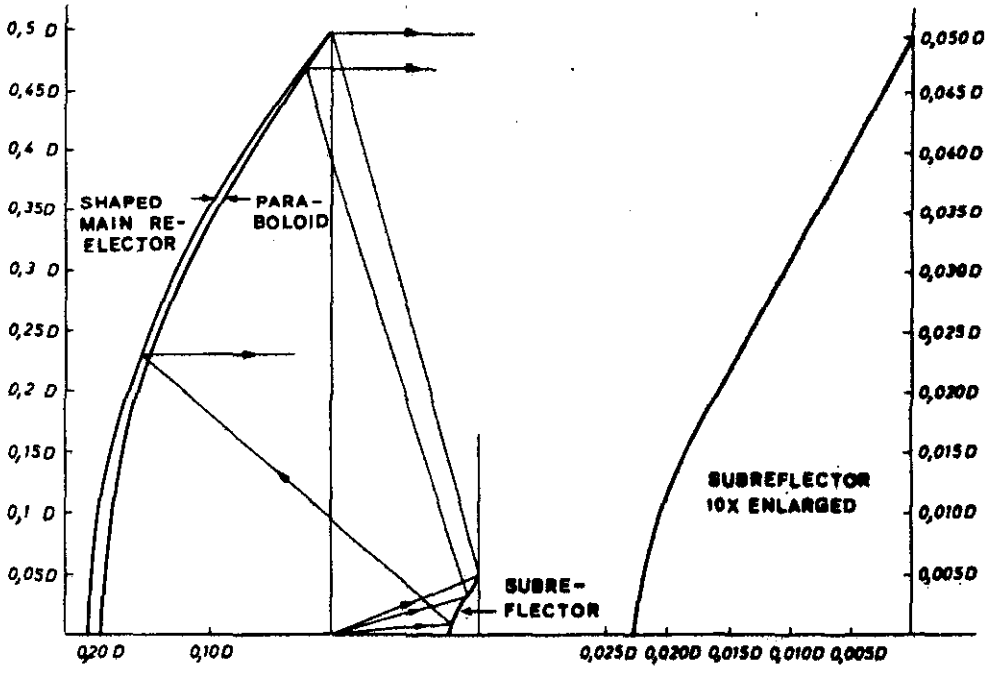

Fig. 5.3 The shaped reflector system

5.2.3. The radiation patterns of shaped subreflectors

In Chapter 4 much attention has been paid to the physical optics approximation to determine the gain function of reflectors. We will consider here not only subreflectors with a hyperboloid contour but also shaped subreflectors with and without a "cone" (Fig. 5.2). To make comparison possible, the shaped reflectors have been so calculated that uniform illumination over the aperture of the main reflector is achieved.
Referring to Fig. 5.1, the system investigated has the following properties: $\Psi_1 = 20^u$, $\Psi_2 = 80^0$ and $D_s/D = 0.2$. The feed pattern is that of a cosine function as described in Chapter 2 with $n = 44$ [Eq. 2.31]. Although the ratio $D_s/D = 0.2$ is somewhat unrealistic, we have chosen this ratio to enable us to demonstrate the differences clearly. The diameter of the subreflector varies between 15λ and 100λ.

Some of the radiation patterns are given in Fig. 5.4a to e. We only show the E plane pattern as the H plane pattern is very similar.
As explained in Chapter 4, it is recommended to verify the results by means of calculating Eq. 4.51, which should yield 4π.
The results are found in Table 5.1, together with those of a corresponding hyperboloid.

Table 5.1 Power conservation $\int_{4\pi} G(\theta\psi)d\Omega$

D/λ	n	with cone	without cone	hyperboloid
15	44	4.08π	4.08π	4.07π
25	44	4.03π	4.03π	4.02π
50	44	4.00π	4.01π	4.00π
80	44	4.00π	3.99π	4.00π
100	44	4.00π	4.00π	4.00π

As may be noticed, the value of the integral is very close to 4π for all subreflectors except if D/λ is smaller than 25.
As we have explained before, the shaped subreflector forms part of a double reflector system with uniform illumination. Silver [108, p. 433] already

pointed out that uniform illumination over the aperture of a paraboloid may be obtained by means of a source with a gain function according to Eq. 3.10 (Fig. 4.3b).

As the main reflector of shaped double reflector systems differs only little from a true paraboloid, it may be expected that the field reflected by the subreflector is very similar to Eq. 5.13. Fig. 5.4.d shows this similarity very clearly.

We also notice that for shaped subreflectors having a cone, the illumination of the aperture of the main reflector is not zero in the region blocked by the subreflector. This phenomenon is noticed especially for $D/\lambda = 15$; for larger values of D/λ it is shown that the illumination of the blocked parts decreases rapidly. The blockage angle Ψ_B of the subreflectors under investigation is 19° (Fig. 5.1). In Table 5.2 the power blocked by the 3 subreflectors under discussion is given for various values of D_s/λ.

Table 5.2 Power blocked by subreflectors in %

		shaped subreflector	
D/λ	hyperboloid	with cone	without cone
15	10.6	1.3	3.2
25	10.5	0.8	3.2
50	10.6	0.4	3.1
80	10.5	0.2	3.1
100	10.5	0.1	3.1

It appears that only for subreflectors with a cone the blocked power decreases with increasing diameter. It is not surprising that the hyperboloid has the largest blockage losses. As follows from the radiation pattern, the intensity of the field scattered from the subreflector is largest in the area where blockage takes place. This means also that the edge of the main reflector is more tapered than when a shaped subreflector is used. Using a shaped subreflector, the illumination of the main reflector aperture reaches a maximum very near the main reflector edge, after which the illumination decreases rapidly. The slope of the decrease becomes sharper if the diameter of the subreflector increases. This phenomenon is in agreement with geometrical optical laws.

Table 5.3 shows the difference between the angle Θ_{max}, where the radiation pattern of the subreflector reaches its maximum, and the main reflector subtending angle Ψ_2. The difference between these two angles becomes smaller with increasing diameter.

Table 5.3 $\Psi_2 - \Theta_{max}$ in degrees

shaped subreflector

D/λ	with cone	without cone
15	7.5	8
25	5.5	5.5
50	3	3.5
80	2.5	2.5
100	2	2

The radiation pattern of a shaped subreflector shows edge illumination at the main reflector much higher than that of a hyperboloid. This means also that in the latter case the spillover along the main reflector edge is much lower. Table 5.4 shows this phenomenon.

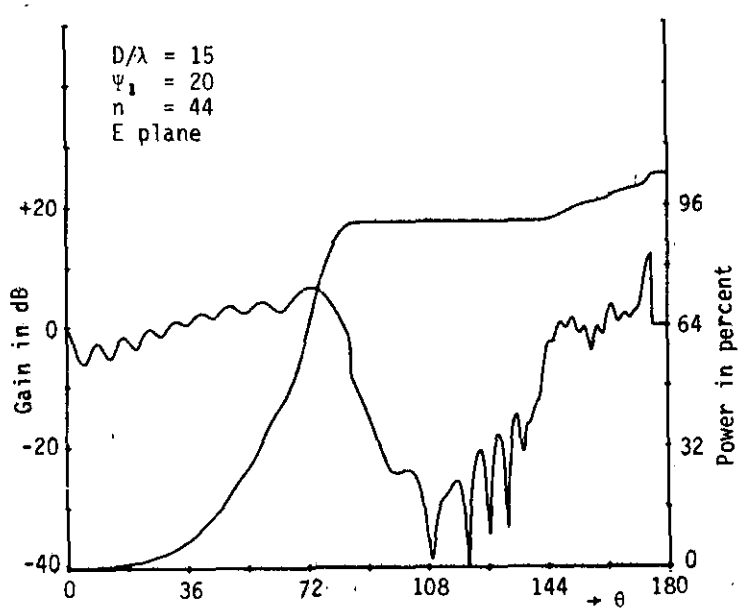

Fig. 5.4a Radiation pattern shaped subdish with cone

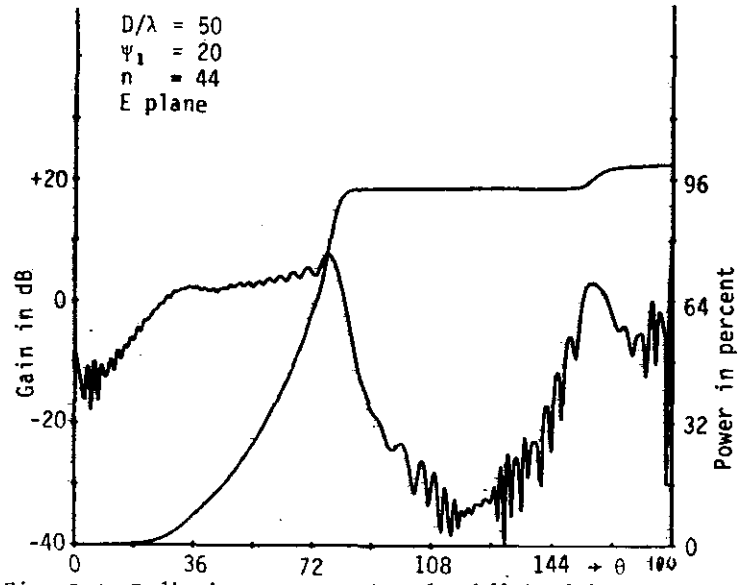

Fig. 5.4c Radiation pattern shaped subdish with cone

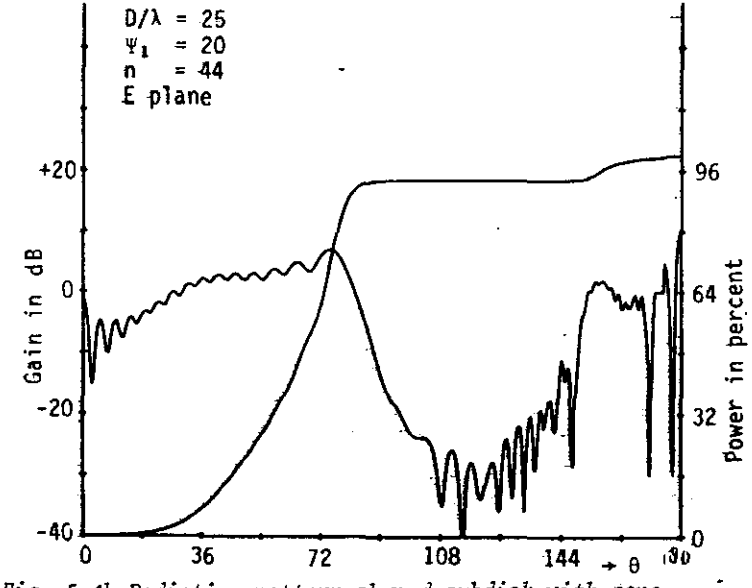

Fig. 5.4b Radiation pattern shaped subdish with cone

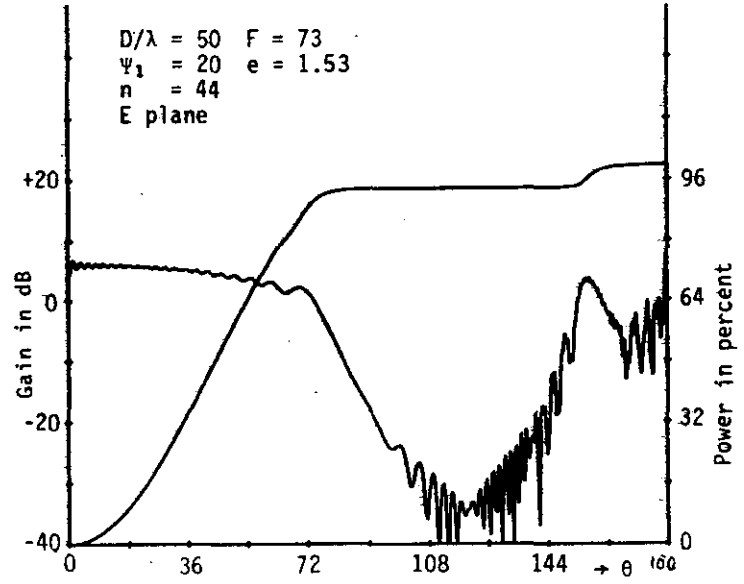

Fig. 5.4e Radiation pattern hyperboloidal subdish

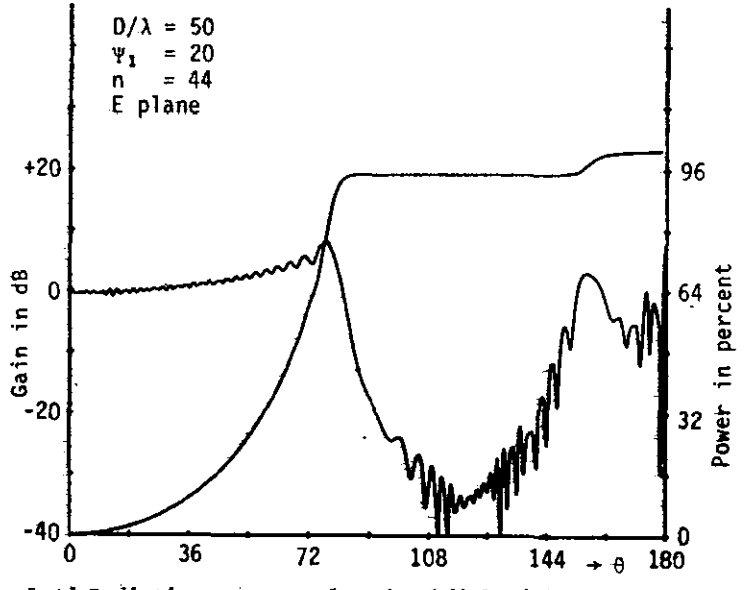

Fig. 5.4d Radiation pattern shaped subdish without cone

Table 5.4 Power transmitted from $0 < \theta < \Psi_2 = 80^0$ in %

D/λ	hyperboloid	shaped subreflector with cone	shaped subreflector without cone
15	92.3	86.5	86.8
25	92.8	88.1	88.4
50	93.1	89.6	89.9
80	93.3	90.3	90.6
100	93.4	90.6	90.9

We notice that only at increasing diameter at the main reflector spillover losses in shaped double reflector systems decrease, although the level of classical cassegrain systems is not reached, even not at $D_s = 100\lambda$.
It is also useful to consider the power captured by the main reflector minus the power blocked. This difference largely determines the efficiency.(Table 5.5)

Table 5.5 Useful power in %

D/λ	hyperboloid	shaped subreflector with cone	shaped subreflector without cone
15	81.7	85.2	83.6
25	82.3	87.2	85.2
50	82.5	89.2	86.8
80	82.8	90.1	87.5
100	82.9	90.5	87.8

Here the shaped subreflectors with cone also show the best figures.
If we study the radiation pattern in more detail, we notice that within the solid angle from 0^0 - 75^0 small oscillations are present and that for all reflectors the reflection is nearly in accordance with geometrical optical laws just as Rusch [96] has found for hyperboloid reflectors. From about 75^0 - 90^0 the field intensity decreases rapidly. The power available in the solid angle from 0^0 to 90^0 is found in Table 5.6, the spillover in this solid angle being shown in brackets.

Table 5.6 Power present in solid angle 0^o - 90^o and spillover

D/λ	hyperboloid	shaped reflector with cone	shaped reflector without cone
15	93.2 (0.9)	91.7 (5.2)	92.8 (6.0)
25	93.5 (0.7)	93.4 (5.2)	93.4 (5.0)
50	93.7 (0.6)	93.7 (4.1)	93.7 (3.8)
80	93.8 (0.5)	93.8 (3.5)	93.8 (3.2)
100	93.8 (0.4)	93.8 (3.2)	93.8 (2.9)

The solid angle from 90^o - 180^o shows heavy oscillations and also a large sidelobe caused by the spillover of the subreflector. It appears that at increasing diameter the total amount of power within the solid angle from 0^o - 90^o is almost the same.

Up till now we have only discussed the results of two reflector systems with uniform illumination over the aperture of the main reflector. We noticed that the large increase in the aperture illumination is partly spoiled by high spillover losses (Table 5.4).

Some calculations have been carried out with shaped reflector systems having an edge illumination over the main reflector of -10dB. The other parameters in the system remain the same. The results of this investigation are found in Table 5.7.

Table 5.7 Power distribution of shaped reflector systems
($D/\lambda = 50$, $n = 44$, $\Psi_1 = 20^o$, $\Psi_2 = 80^o$, $D_s/D = 0.2$)
edge illumination main reflector - 10 dB

	with cone	without cone
Blocked power	0.5	7.4
Power up to 80^o	93.0	93.1
Useful power	92.5	85.7
Power up to 90^o	93.7	93.7
Spillover up to 90^o	0.7	0.6

Compared with Table 5.5, the figures of a shaped reflector with cone are much better; those of a shaped subreflector without cone decrease as relatively more energy is concentrated in the blocked central part of the aperture of the main reflector. The spillover decreases considerably.

5.2.4. Conclusions

By modifying the reflector surfaces, great advantages can be obtained over classical cassegrain antenna systems. The power captured by the subreflector is reflected by the subreflector in such a way that together with the shaped main reflector a uniform illuminated aperture may be obtained; apparently the surplus of power in the middle of the aperture is spread towards the edge of the main reflector. Moreover, in this way, spillover efficiency and illumination efficiency can be optimized independently of each other.

Secondly, the edge of the subreflector may be illuminated much lower than in classical cassegrain systems. It is possible to illuminate the edge of the subreflector at values as low as -20 dB. By studying Fig. 5.5, where the subreflector spillover efficiency η_s is shown as a function of the edge illumination, it is readily seen that a spillover efficiency of about 98% can now be realized. The product of subreflector spillover efficiency and aperture efficiency of classical cassegrain antennas is about 74%. [20].

The increase in antenna efficiency by shaping the reflectors can therefore be considerable. The antenna gain can be increased by about 1 dB. This means that a modified cassegrain antenna with a main reflector diameter of 27 metres will have the same gain as a classical cassegrain system with a main reflector of 30 metres diameter.

The low spillover losses have a favourable influence on the antenna noise temperature: consequently, this will be lower. A further advantage of low subreflector edge illumination is the large decrease in diffraction losses. Computations carried out recently [21] show this clearly.

A disadvantage is the fact that by illuminating the aperture uniformly, diffraction effects at the edge of the main reflector have to be taken into account (Chapter 4). In classical systems this contribution can be neglected as the illumination is tapered towards the edge. It is possible, however, to abandon the overall uniform illumination and leave a one-metre ring along the main reflector edge under-illuminated, as demonstrated in the

later Raisting Antennas [92], and the Dutch antenna at Burum. This possibility was predicted before [20]. The aperture efficiency will decrease, but on the other hand the contribution to noise temperature by this part of the scattered power also becomes less. Optimizing this problem is a subject of further study.

In an antenna system designed for satellite communication valuable advantages can further be obtained by causing the main reflector to intercept properly the power blocked by subreflector and supports. This results in

- higher antenna efficiency
- decrease in noise temperature.

Further theoretical and experimental study will be required to calculate the effects of the grooves and ripples and to see whether this solution offers practical possibilities.

Nowadays most antennas for satellite communication ground stations are constructed on the principles discussed above. A fine example is the antenna at Fucino [Fig. 5.6], [25].

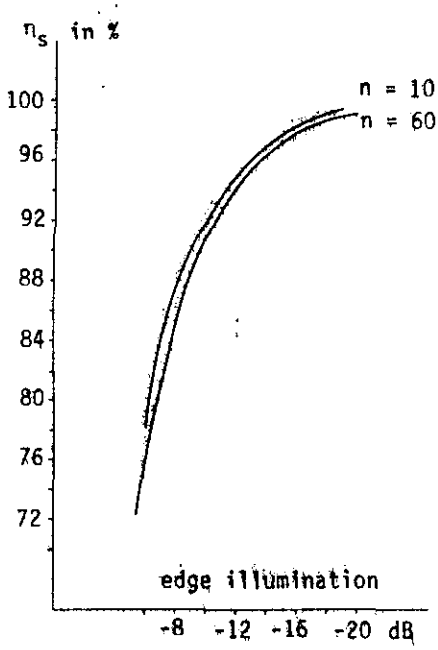

Fig. 5.5
The spillover efficiency η_s as a function of the edge illumination of the subreflector.
Gain functions feed
$G(\psi_1) = 122 \cos^{60}\psi_1$ *and*
$G(\psi_1) = 22 \cos^{10}\psi_1$

Fig. 5.6 The Fucino ground station.

5.3. Mismatched shaped cassegrain antenna systems

5.3.1. Aperture and spillover efficiency

Let

$$G_1(\psi_1) = 2(n + 1)\cos^n\psi_1 \ , \qquad 0 < \psi_1 < \tfrac{1}{2}\pi \tag{5.14}$$

be the circularly symmetrical directive gain pattern of the feed in a shaped cassegrain system (Fig. 5.1), designed to produce uniform aperture illumination and let

$$G_2(\psi_1) = 2(m + 1)\cos^m\psi_1 \qquad 0 < \psi_1 < \tfrac{1}{2}\pi \tag{5.15}$$

be the directive gain pattern of a different feed.
The general expression for the aperture efficiency of a shaped cassegrain system designed for G_1 but illuminated by G_2 is given by [89]:

$$\eta_A = \frac{\left| \int_0^{\Psi_1} [G_1(\psi_1)]^{\frac{1}{2}}[G_2(\psi_1)]^{\frac{1}{2}} \sin\psi_1 \, d\psi_1 \right|^2}{\int_0^{\Psi_1} G_1(\psi_1) \sin\psi_1 \, d\psi_1 \int_0^{\Psi_1} G_2(\psi_1)\sin\psi_1 \, d\psi_1} \tag{5.16}$$

where Ψ_1 is the subtended angle of the subreflector. It can easily be proved that this expression also applies to subreflectors with cone-shaped protuberances [22].
For this purpose we will use the principle of the power conservation flow along the ray trajectories as discussed in Sec. 5.2.1, viz.:

$$2\pi \, G_1(\psi_1) \sin\psi_1 \, d\psi_1 = 2\pi \, H_1(r) \, r dr \tag{5.17}$$

If we take the aperture distribution to be uniform, $H_1(r)$ will have to be constant. Integrating Eq. 5.17, this constant C is readily found:

$$C = \frac{8}{D^2 - D_s^2} \int_0^{\Psi_1} G_1(\psi_1) \sin\psi_1 \, d\psi_1 \tag{5.18}$$

Substituting C for $H_1(r)$ in Eq. 5.17 leads to

$$\frac{C}{G_1(\psi_1)} = \frac{\sin\psi_1}{r} \cdot \frac{d\psi_1}{dr} \tag{5.19}$$

If now the feed pattern changes from $G_1(\psi_1)$ into $G_2(\psi_1)$ we find from Eq. 5.17 in a similar way

$$\frac{H_2(r)}{G_2(\psi_1)} = \frac{\sin\psi_1}{r} \frac{d\psi_1}{dr} \tag{5.20}$$

Combining the equations 5.19 and 5.20, we obtain

$$H_2(r) = C.G_2(\psi_1)/G_1(\psi_1) \tag{5.21}$$

where $H_2(r)$ is the new aperture distribution corresponding with the feed pattern $G_2(\psi_1)$. The aperture efficiency [108, p.177] is then found from the relation

$$\eta_A = \frac{2\pi}{A} \frac{\left| \int_{\frac{1}{2}D_s}^{\frac{1}{2}D} [H_2(r)]^{\frac{1}{2}} \, r\,dr \right|^2}{\int_{\frac{1}{2}D_s}^{\frac{1}{2}D} H_2(r)\, r\,dr} \tag{5.22}$$

A being the illuminated part of the aperture, which is equal to $\frac{1}{4}\pi(D^2-D_s^2)$ not considering the contribution of the struts.
The aperture is further defined by $\frac{1}{2}D_s < r < \frac{1}{2}D$; if the aperture illumination is uniform, $\eta_A = 1$. By means of Eqs. 5.19, 5.20 and 5.21 we find for the aperture efficiency

$$\eta_A = \frac{2\pi}{AC^2} \frac{\left| \int_0^{\psi_1} [G_1(\psi_1).G_2(\psi_1)]^{\frac{1}{2}} \sin\psi_1 \, d\psi_1 \right|^2}{\int_0^{\psi_1} G_2(\psi_1) \sin\psi_1 \, d\psi_1} \tag{5.23}$$

Substituting in Eq. 5.23 $\frac{1}{4}\pi[D^2-D_s^2]$ for A and Eq. 5.18 for C, we finally obtain Eq. 5.16. If we substitute Eqs. 5.14 and 5.15 in Eq. 5.16 and solve the integrals, we obtain

$$\eta_A = \frac{4(m+1)(n+1)}{(n+m+2)^2} \cdot \frac{[1-(\cos\Psi_1)^{\frac{1}{2}(n+m+2)}]^2}{[1-(\cos\Psi_1)^{n+1}][1-(\cos\Psi_1)^{m+1}]} \tag{5.24}$$

It is easily shown that for $n = m$, $\eta_A = 1$.

The spillover efficiency is readily found from the expression

$$\eta_S = \tfrac{1}{2}\int_0^{\Psi_1} G_2(\psi_1)\,\sin\psi_1\,d\psi_1\ , \tag{5.25}$$

which leads to

$$\eta_S = 1 - \cos^{m+1}\Psi_1 \tag{5.26}$$

The simple relations found in Eqs. 5.24 and 5.26 now offer the possibility of investigating the aperture efficiency, spillover efficiency and their product as a function of n, m and Ψ_1. It appears that in shaped double reflector systems no other parameters are of importance in calculating the aperture and spillover efficiency.

A typical example is found in Fig. 5.7, which shows the results of a

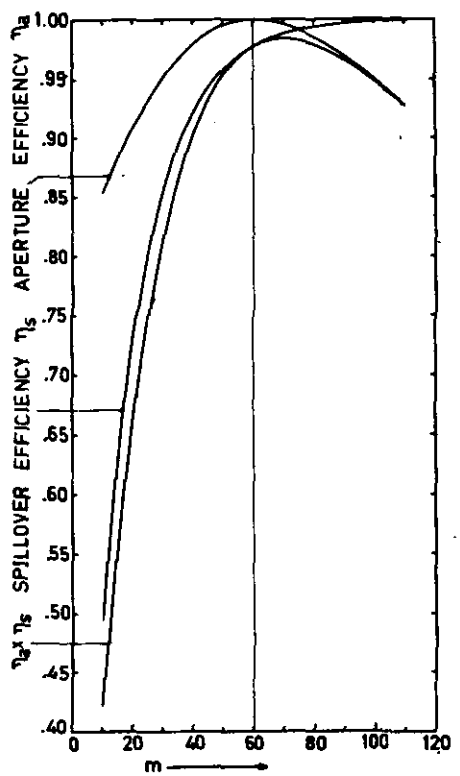

Fig. 5.7
Aperture and spillover efficiency as a function of m; edge illumination = -16dB, $\Psi_1 = 20°$, $\Psi_2 = 60°$, n = 60

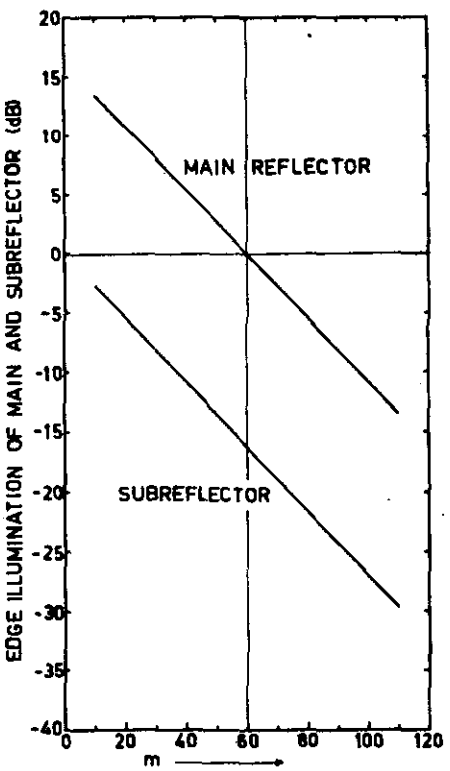

Fig. 5.9
The edge illumination of main- and subreflector as a function of m; $\Psi_1 = 20°$, $\Psi_2 = 60°$, n = 60

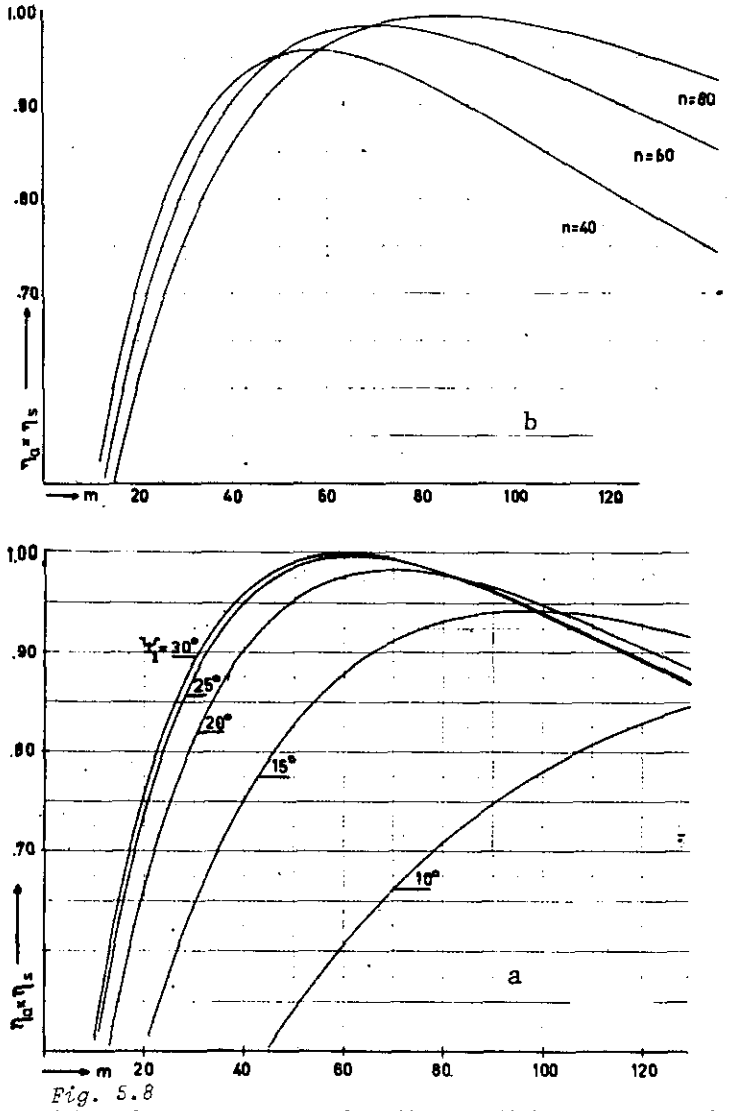

Fig. 5.8
(a) Product of aperture and spillover efficiency as a function of m, Ψ *being a parameter. (b) Product of aperture and spillover efficiency as a function of* m, *edge illumination being a parameter;* n = 40, 60, *and* 80, *respectively;* $\Psi_1 = 20^0$.

shaped double-reflector system with uniform aperture illumination and $n = 60$. The subtending angles of main reflector and subreflector are 60° and 20° respectively. The edge illumination of the subreflector is then about -16 dB. The spillover efficiency reaches 100 percent because at increasing m the directive gain pattern of the feed becomes narrower and narrower so that more and more power is intercepted by the subreflector and transported to the main reflector.

The aperture efficiency decreases more rapidly for $m < n$ than in the case of $m > n$. The result is that the product of aperture and spillover efficiency no longer has its maximum at $m = 60$, but at $m \approx 70$. Furthermore it appears that for $m > 70$ the overall efficiency decreases only gradually. This phenomenon is also noticed for different edge illuminations of the subreflector, and for different values of Ψ_1 (see Fig. 5.8a where the maximum of the product of Eqs. 5.24 and 5.26 has been plotted for different values of Ψ_1 and m, with $n = 60$). For larger values of Ψ_1 $\eta_S \times \eta_A$ approaches 1. This is due to the fact that the spillover efficiency is almost 1. Fig. 5.8b shows the total efficiency for antennas with $\Psi_1 = 20^\circ$ ($\Psi_2 = 60^\circ$), shaped so that the edge illumination is approximately 10, 15 and 20 dB respectively.

5.3.2. Aperture illumination

It has previously been pointed out [89] that the illumination over the aperture is given by

$$H(r) = C.G_2(\psi_1)/(G_1(\psi_1) \tag{5.21}$$

where C is a constant.

Using the gain functions for Eqs. 5.14 and 5.15, Eq. 5.21 becomes

$$H(r) = C.(m + 1)/(n + 1) \cos^{m-n} \psi_1 \tag{5.27}$$

The edge illumination of main reflector and subreflector will differ considerably for different values of m. The edge illumination at the main reflector follows from Eq. 5.27 and that of the subreflector from $\cos^m \psi_1$. In the case of the subreflector the small difference in space loss for $\psi_1 = 0$ and $\psi_1 = \Psi_1$ has been neglected. Fig. 5.9 shows this edge illumination

as a function of m, where n = 60 gives uniform aperture illumination. It is also possible to calculate the illumination over the aperture for the case where $m \neq n$. For that purpose $H(r)$ has to be calculated which may be done by means of Eq. 5.27, given the relationship between ψ_1 and r. This relationship can be expressed only numerically , as it must be calculated from the nine equations determining a shaped cassegrain system [20]. For the same example discussed before, $D/D_s = 0.1$, $\psi_1 = 20^0$, $\psi_2 = 60^0$, etc., the results are shown in Fig. 5.10

It is worth mentioning that for the case of $m < n$, the aperture illumination shows higher edge illumination than the centre of the aperture, while for $m > n$ the aperture illumination becomes more normal and is tapered towards the edges.

5.3.3. The radiation pattern near the axis

This pattern may be found from scalar aperture theory [108, Ch. 6], where the pattern of a circular aperture (Fig. 5.11) becomes

$$g(\theta,\phi) = \int\int F(r,\phi')\, e^{jkr \sin\theta \cos(\phi - \phi')}\, r\,dr\,d\phi' \qquad (5.28)$$

The illumination function $F(r,\phi')$ is equivalent to $|H(r)|^{\frac{1}{2}}$. As previously explained [22], we let the aperture illumination be zero for $0 < r < \frac{1}{2}D_s$ for purposes of obtaining maximum blockage efficiency. Then

$$g(\theta,\phi) = \int_{\frac{1}{2}D_s}^{\frac{1}{2}D} [H(r)]^{\frac{1}{2}}\, r\,dr \int_0^{2\pi} e^{jkr \sin\theta \cos(\phi - \phi')}\, d\phi' \ , \qquad (5.29)$$

or, carrying out the integration over ϕ',

$$g(\theta) = 2\pi \int_{\frac{1}{2}D_s}^{\frac{1}{2}D} [H(r)]^{\frac{1}{2}}\, J_0(kr \sin\theta)\, r\,dr \qquad (5.30)$$

where $J_0(kr\sin\theta)$ is the Bessel function of zeroth order. Again, knowing the aperture illumination function $|H(r)|^{\frac{1}{2}}$ numerically, the radiation pattern near the main lobe may be calculated. The computed results are shown in Fig. 5.12 .

Compared with uniform illumination ($n = 60$), it appears that for values $m < n$ the system has very high sidelobes; if, for instance, $m = 20$, which results in an illumination that is about 14 dB higher at the edges than in

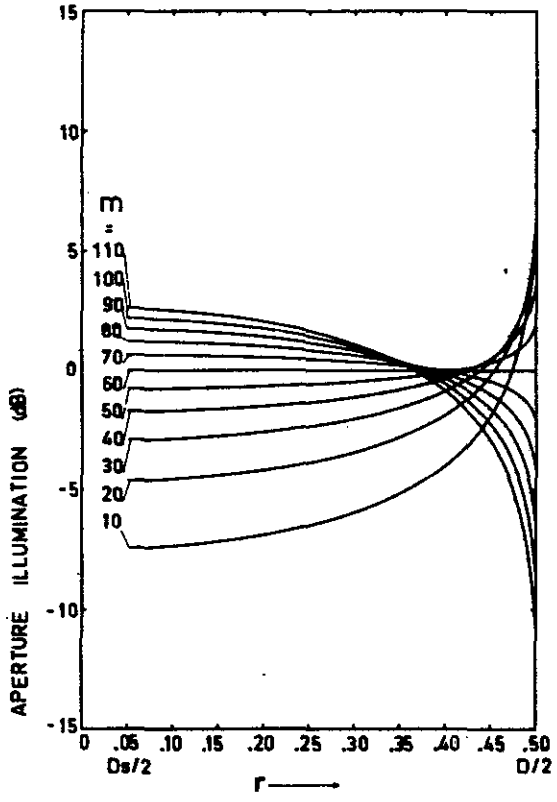

Fig. 5.10
The illumination of the aperture of the main reflector as a function of r, m *being a parameter.* $\Psi_1 = 20^0$, $\Psi_2 = 60^0$, n = 60.

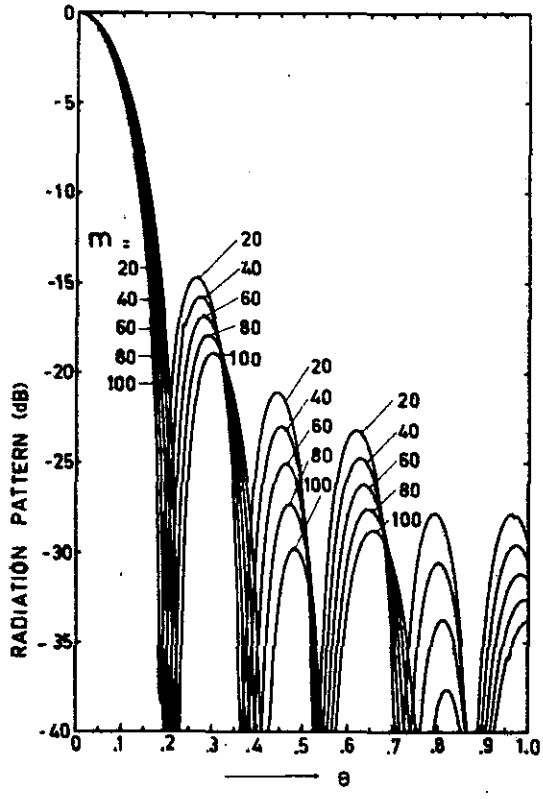

Fig. 5.12
Relative directive gain pattern of a dual shaped antenna system as a function of θ; $\Psi_1 = 20^0$, $\Psi_2 = 60^0$, n = 60, $D/D_s = 0.1$ *and* $D/\lambda = 330$

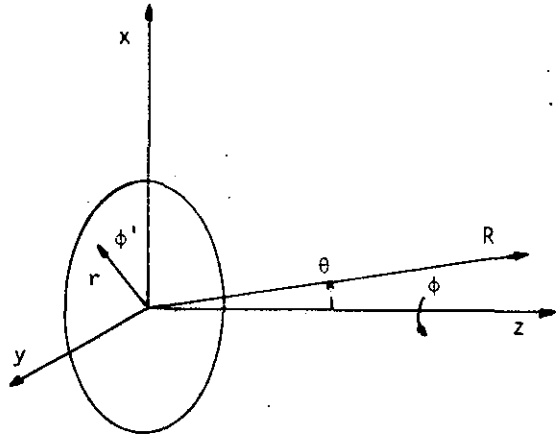

Fig. 5.11 System coordinates

the centre, the first sidelobe increases to about -14.5 dB, while -17.6 dB is normal for uniform illumination. For values of $m > n$, we obtain the more normal situation, where the aperture is tapered towards the edges.

5.3.4. Subreflector blockage efficiency

The antenna system has been shaped in accordance with the relations presented in a previous paper [22]. This means that if the aperture is illuminated uniformly,

$$\frac{\eta_B}{\eta_0} = 1 - \frac{B}{A} \tag{3.46}$$

where A is the surface of the unblocked aperture, B that of the blocking obstacles and η_0 the efficiency of an unblocked aperture.
Blockage caused by the subreflector supports has been neglected for the moment, but the subreflector has been taken into account, resulting in a cone-shaped protuberance. Since in the calculations in this paper $D_s = 0.1\ D$, $\eta_B/\eta_0 = 0.99$ will be the absolute maximum.
To obtain an impression of the overall efficiency, the result of Fig. 5.8 should be multiplied by this factor. It may be shown from Fig. 5.12 that the radiation patterns are not a result of a radiating unblocked aperture, but from a circular aperture blocked in the middle by a circular obstacle. This results in an irregular distribution of the second, third and further sidelobes, e.g. for $m = 100$ the third sidelobe is higher than the second.

5.3.5. Conclusions

The examples presented here prove that the product of spillover efficiency and aperture efficiency of shaped double reflector systems has a certain maximum value. This value is not found with feed patterns for which the antenna system has uniform illumination, but is found with those having a beamwidth somewhat smaller than that for which the shaped antenna system was designed. Various computer experiments have been carried out, for different edge illuminations of the subreflector and for different subreflector subtending angles, all showing similar phenomena.
Further results show that the overall efficiency rapidly decreases for antenna systems having a feed with a much wider beamwidth than that for

which the system was designed. The theory developed is of great importance to those antenna systems equipped with a feed system having a frequency dependent radiation pattern. It appears that the best results are obtained if the antenna system is designed and shaped for the lowest frequency to be used by the system.

Great care has to be taken when a feed is employed having a wider beamwidth than the feed for which the antenna system has been shaped. The edges of the aperture are in this case over-illuminated, resulting in near-in side-lobes, which are even higher than those of a uniformly illuminated aperture.

6. OFFSET ANTENNAS

6.1. Introduction

As explained in the previous chapters, the front-fed paraboloid antenna and the various types of symmetrical double reflector antennas, such as the cassegrain antenna, suffer from aperture blockage caused by subreflector, feed and supports. Depending upon the geometry of these components within the antenna system and the radiation patterns of the primary feed, a considerable amount of transmitted power may get lost by scattering against the obstacles. However, it is possible to construct so-called offset reflector antennas by locating the feed or subreflector outside the ray trajectories coming from the aperture of the main reflector. Therefore, there is no blockage at all. If the paraboloid antenna is front-fed and if we want such an antenna to become offset, the symmetry axis of feed and paraboloid must no longer coincide but form an angle known as the offset angle Ψ_0. The reflector is now formed by a surface which is found by intersection of the paraboloid and a cone with top angle Ψ. The latter then becomes the subtended angle of the paraboloid (Fig. 6.1).
It is also possible to construct an offset cassegrain antenna known as the open cassegrain antenna (Fig. 6.2). The constructions used nowadays [67] locate the feed mostly at the surface of the main reflector on the symmetry axis of the hyperboloid subreflector. The symmetry axis of hyperboloid and paraboloid do not coincide.
It is the purpose of this chapter to discuss some of the properties of these antennas. We shall first look into the geometry and calculate further the gain factor.
Finally, the cross-polarization properties will be investigated in detail.

6.2. The geometry of offset antennas

Describing the geometrical properties of offset antennas, the paper of Cook, Elam and Zucker [12] is of great importance and a short review of this paper is certainly required here. The use of two sets of rectangular co-ordinates is very practical. The first set, x_p, y_p and z_p, with the origin at the paraboloid focus and z_p lying along the axis of revolution, is shown in Fig. 6.3. The coordinates x_s, y_s and z_s in Fig. 6.4 have the

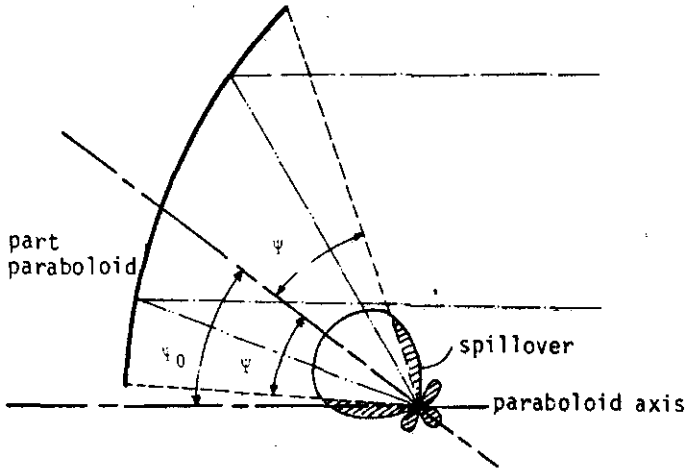

Fig. 6.1 The offset paraboloid reflector

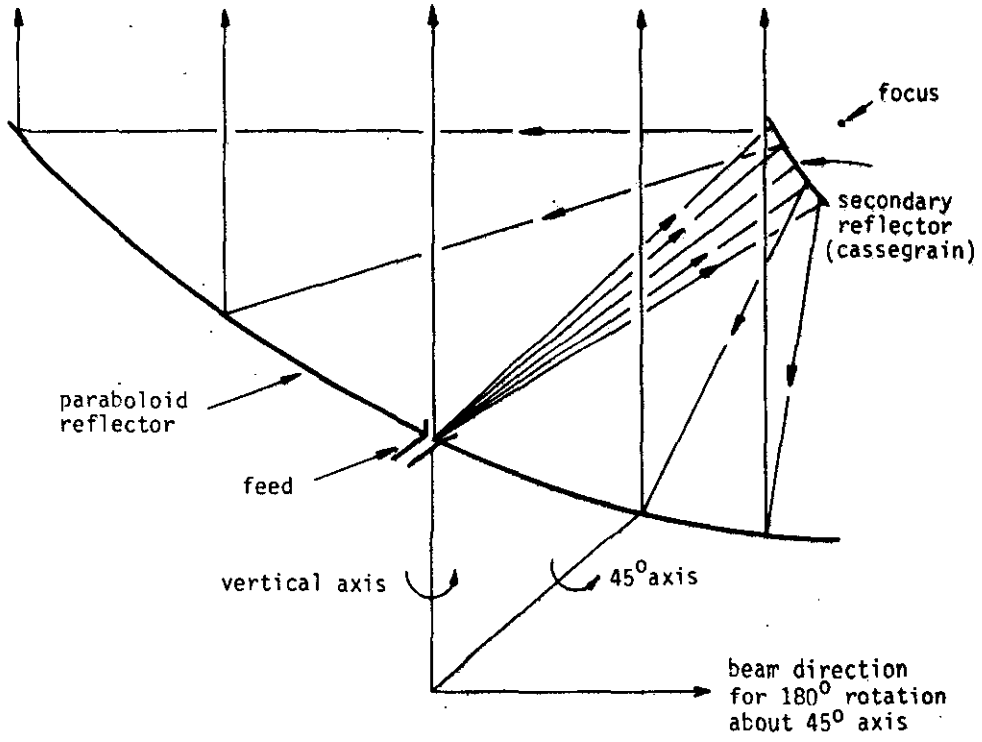

Fig. 6.2 Offset cassegrain

same origin but rotated so that z_s coincides with the symmetry axis of the hyperboloid. It is indicated that the equation of the paraboloid is

$$\rho = \frac{2F}{1 + \cos\psi_2 \cos\Psi_0 - \sin\psi_2 \sin\Psi_0 \cos\xi} \tag{6.1}$$

As Cook et al. [12] explain, the curves of intersection of the paraboloid surface with cones $\psi = \Psi_2$ are ellipses and lie in planes perpendicular to the x_p, z_p plane. The projections of these intersections on to the aperture plane (x_p, y_p) are circles and given by

$$(x_p - \frac{2F \sin\Psi_0}{\cos\Psi_2 + \cos\Psi_0})^2 + y_p^2 = 4F^2 \, (\frac{\sin\Psi_2}{\cos\Psi_2 + \cos\Psi_0})^2 \tag{6.2}$$

It also appears that the intersection of cones having a constant value of ψ_s, i.e. 10^0, 20^0, 30^0 and 40^0, with a plane perpendicular to the z_s-axis are all concentric circles around the z_s-axis. The intersections of these cones with the paraboloid are ellipses. Projecting these ellipses on to the aperture x_p - y_p plane yields circles again; however, these circles are no longer concentric (Fig. 6.5) since radius and centre point are functions of Ψ_0 and Ψ_s.

The projection on the x_p, y_p plane of the intersections of the planes defined by the z_s-axis and the line in the x_s - y_s plane, making a constant angle $\xi = \xi_c$ with the x_s-axis is a circle (Fig. 6.5). It may be proved [18] that these circles are given by

$$(x_p + 2F\cot\Psi_0)^2 + (y_p - \frac{2F \cot\xi_c}{\sin\Psi_0})^2 = \frac{4F^2}{\sin^2\Psi_0 \sin^2\xi_c} \tag{6.3}$$

In the following we shall concentrate on open cassegrain antennas having the phase centre on the surface of the paraboloid. If the diameter of the aperture is D, it follows from Eq. 6.2 that

$$D = \frac{4F\sin\Psi_2}{\cos\Psi_2 + \cos\Psi_0} \tag{6.4}$$

It can be proved [18] that the diameter of the hyperboloid subreflector under no-blockage conditions is represented by

$$D_s = \frac{4F \sin\Psi_2 \sin(\Psi_0 - \Psi_2)}{[1 + \cos(\Psi_0 - \Psi_2)] \sin(\Psi_0 + \Psi_2)} \tag{6.5}$$

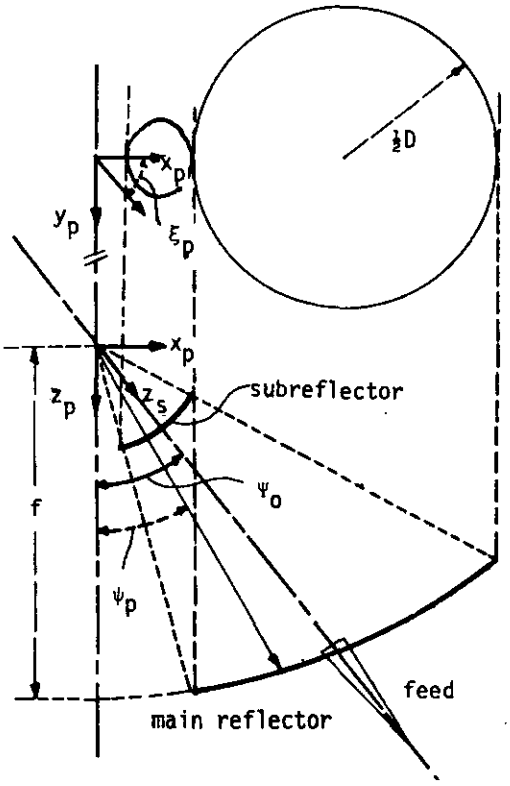

Fig. 6.3 Open cassegrain antenna; primary coordinates

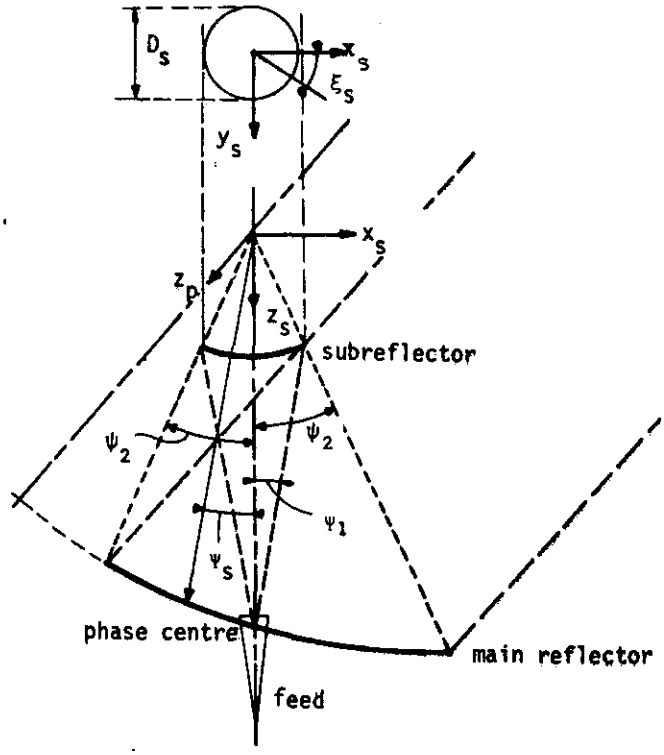

Fig. 6.4 Open cassegrain antenna; secondary coordinates

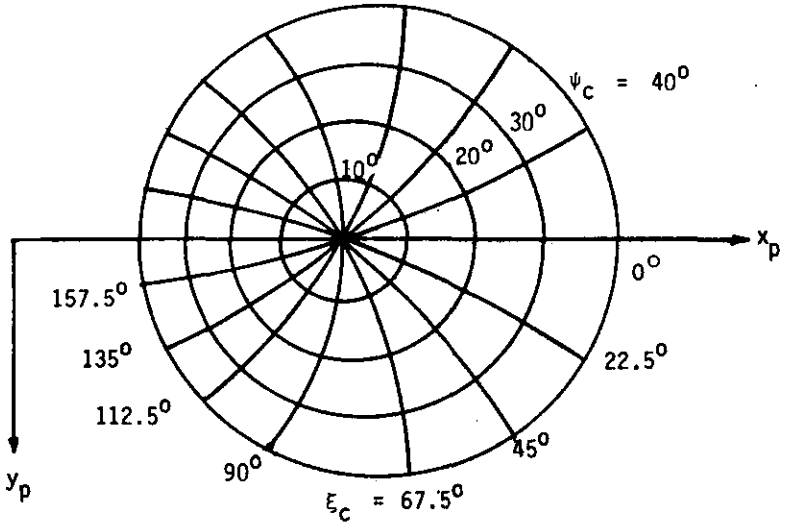

Fig. 6.5 Projected circles on the aperture for Ψ_c = 47.5°

or by

$$D_s = \frac{2F\,(e^2 - 1)\,\sin\Psi_2}{(1 + \cos\Psi_0)(e^2\cos\Psi_2 + e)} \tag{6.6}$$

The relationship Eq. 2.9 between ψ_1 and ψ_2 as discussed in Chapter 2 may also be used here. The equations 6.4, 6.5, 6.6 and 2.9 describe the geometry of the open cassegrain antenna entirely. There are 7 parameters. We shall take the offset angle Ψ_0, the diameter D and the subtending angle of the hyperboloid Ψ_1, as independent variables. The entire system is then defined.

6.3. The gain factor of open cassegrain antennas

The gain factor of the conventional circular paraboloid reflector and the influence of the primary pattern width and angular aperture on the gain factor have been derived by Silver [108, p.413].
Pagones [82] has derived the gain factor of the offset reflector and has also taken into consideration the effects of pattern width and angular aperture. This chapter deals with similar calculations carried out for the open cassegrain antenna. For this purpose we shall have to make use of some of the equations mentioned already in Chapter 2, viz. Eqs. 2.9 and 2.11.
We shall use tapered cosine patterns as indicated by Eq. 2.31.
Combining the equations 2.9, 2.11 and 2.31 results in

$$G_2(\psi_2) = 2(n+1)\,\cos^n[2\arctan\{(e-1)/(e+1)\,\tan\tfrac{1}{2}\psi_2\}] \times \frac{\sin^2[2\arctan\{(e-1)/(e+1)\,\tan\tfrac{1}{2}\psi_2\}]}{\sin^2\psi_2} \tag{6.7}$$

Following the methods carried out by Pagones [82], it is now readily found that the gain factor of an open cassegrain antenna may be represented by

$$g = 2(n+1)\left[\frac{\cos\Psi_0 + \cos\Psi_2}{\sin\Psi_2}\right]\left|\int_0^{\Psi_2} \cos^{\frac{1}{2}n}\left[2 \arctan\left\{\frac{e-1}{e+1}\tan\tfrac{1}{2}\psi_2\right\}\right]\right.$$
$$\left. \times \frac{\sin\left[2 \arctan\left\{\frac{e-1}{e+1}\tan\tfrac{1}{2}\psi_2\right\}\right]}{\cos\Psi_2 + \cos\psi_2}\, d\psi_2 \right|^2 \qquad (6.8)$$

Mention has been made in Sec. 6.2. of four equations defining the entire antenna geometry. These equations contain 7 variables, viz.:

(1) D = diameter of the aperture of the main reflector

(2) F = focal distance of the paraboloid main reflector

(3) Ψ_0 = offset angle of the antenna

(4) Ψ_2 = Subtending angle of the main reflector measured from the paraboloid's focus

(5) D_s = maximum diameter of the subreflector giving no blockage

(6) e = eccentricity of the hyperboloid subreflector

(7) Ψ_1 = subtending angle of the subreflector, measured from the hyperboloid's focus which is located on the surface of the main reflector.

As we have only 4 equations and 7 unknowns, 3 unknowns have to be chosen. Therefore, we take D fixed and Ψ_0 as a parameter, while Ψ_1 is a variable. It is this last angle which is responsible for the amount of spillover originated by the primary feed.

The results are found in Table 6.1 below.

It appears that for various values of the subtending angle Ψ_1 a maximum is found. It is also noticed that this maximum is mostly of the order of 80% and has a tendency to decrease for higher values of the offset angle Ψ_0. This value of 80% is practically the same as found by Silver [108, p.413] for symmetrical paraboloids and by Pagones [82] for offset paraboloids. Fig. 6.6, finally, shows the gain factor as a function of the primary source with the subtending angle Ψ_1, as a parameter for $\Psi_0 = 50^0$ being a typical value for the offset angle.

If diffraction effects of the subreflector have to be taken into account, the values found in Fig. 6.6 will decrease in accordance with Sec. 2.4.2.

Table 6.1

Ψ_0	Ψ_1	Ψ_2	gainfactor g	n
			g	
30	6	18.42		n > 250
	8	14.41	0.813	n > 250
40	6	28.97		n > 250
	8	25.06	0.810	n > 250
	10	21.06	0.810	162
	12	16.96	0.811	112
50	6	39.85		n > 250
	8	36.12	0.792	n > 250
	10	32.30	0.796	162
	12	28.30	0.800	112
	14	24.18	0.804	82
	16	19.94	0.807	62
60	6	51.14		n > 250
	8	47.77	0.750	n > 250
	10	44.22	0.760	160
	12	40.49	0.770	112
	14	36.55	0.778	82
	16	32.42	0.786	62
	18	28.11	0.794	48
	20	23.65	0.800	40
70	6	63.01		n > 250
	8	60.26	0.654	246
	10	57.23	0.672	156
	12	53.98	0.690	108
	14	50.45	0.708	80
	16	46.62	0.725	62
	18	42.53	0.742	48

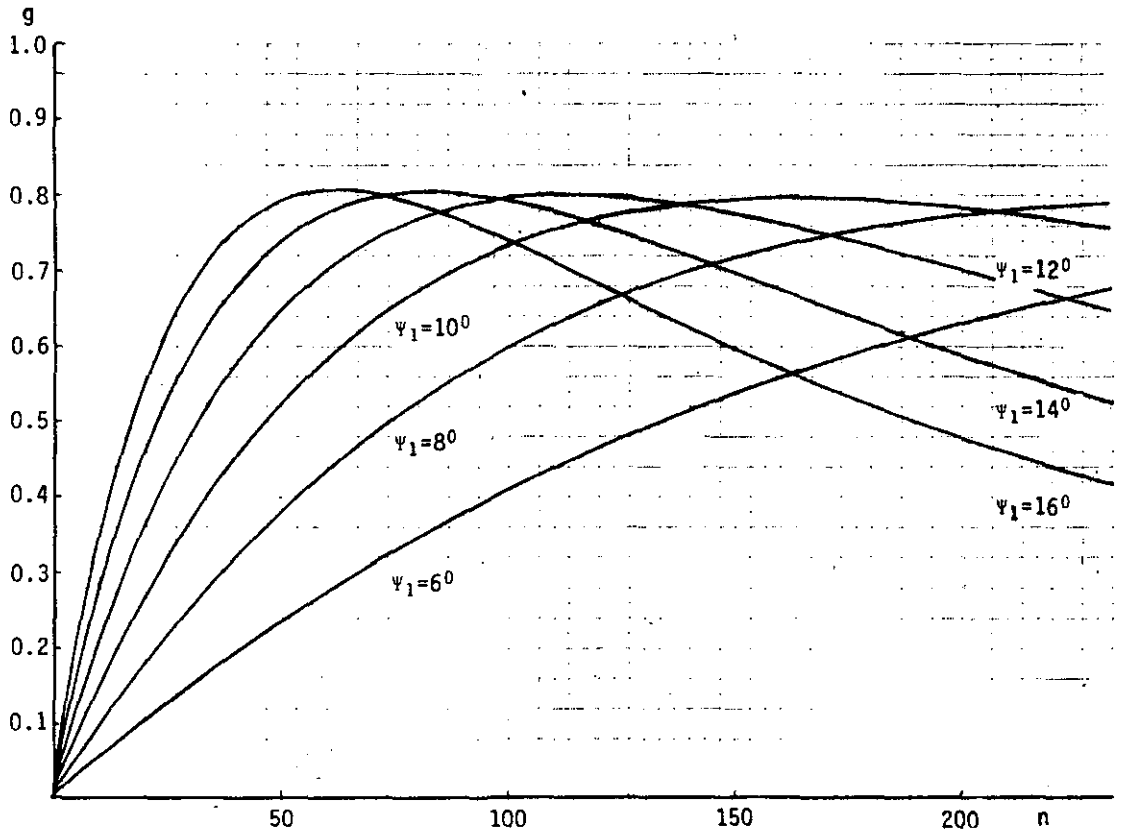

Fig. 6.6 Gain factor of open cassegrain antenna; $\Psi_0 = 50^0$, Ψ_1 *is a parameter; gain function of primary source is* $G(\psi_1) = 2(n+1)\cos^n\psi_1$

6.4 Cross polarization properties

6.4.1. Introduction

It has been known for several years that, if a paraboloid reflector antenna is fed by a linearly polarized electrical dipole, the antenna system will radiate not only energy in the main polarization, but also a fair amount in an unwanted polarization, mostly called cross polarization or depolarization.
Condon [11] was one of the first to give a detailed analysis of this phenomenon. It appears that cross-polarized lobes, also called Condon lobes, are formed, having a maximum in planes at 45° to the principle plane.
Silver [108, p.423] also mentions this cross-polarization, mainly as an abstract of Condon's work.
Cutler [15] gives a physical explanation as to the relation between aperture electric field lines and the polarization of the dipole feed, and explaines the very unfavourable situation which occurs if the focus of the paraboloid falls between the aperture and apex of the paraboloid.
This work has been continued by Jones [57], who investigated the radiation characteristics of paraboloid reflector antennas excited in their foci by a short electrical dipole feed, a short magnetic dipole feed, and a plane wave source, being a combination of an electric and a magnetic dipole. If this dipole pair is represented by dipole fields of equal intensity, commonly known as Huygens source, it has been proved that the cross-polarized component of the aperture illumination could be made to disappear [57].
Kofman [68] has extended this work by considering other conical sections of revolutions as well as the paraboloid. The cross-polarized pattern of the reflector excited by any arbitrary feed system may be calculated, using the methods of Afifi [2], while Potter [85] has found an analytical expression for the polarization loss or polarization efficiency.
It is the latter expression which will also be reviewed in this paper.
Potter [87] has also found a similar expression for cassegrain antennas which will be included in the present study.
Watson and Ghobrial [122] have investigated the cross-polarization isolation at off-axis incidence for classical cassegrain antennas and front-fed paraboloidal reflectors. It is shown that the cassegrain antenna is

much superior to the equivalent front-fed antenna.
Not much is known so far about offset paraboloids and open cassegrain [12] antennas. Hanfling [45] has shown a stereographic mapping method which contains the aperture field lines of an offset antenna, excited by several field sources, but without further details, while Graham [41,42] describes the polarization of offset antennas and states that an offset cassegrain antenna can be designed to have low cross-polarization losses, which was experimentally found out by letting the axis of main- and subreflector differ only a few degrees. No calculations have been mentioned.
Since plans now exist of frequency re-use above 10 GHz by polarization diversity, the interest in cross-polarization problems has recently increased considerably.
Ludwig [76] has published a paper on the definition of cross-polarization, and Kinber and Tischenko [66] calculated the current distribution of various reflector antennas with different illumination. Unfortunately no numerical results are shown.

Chu and Turrin [8] have discussed the beamshift of offset antennas with circular polarization and have calculated the level of cross-polarization sidelobes. The poor polarization performance of the open cassegrain antenna has been predicted.

It is the purpose of the present paper to obtain a more detailed insight into the cross-polarization losses of offset antennas. For this purpose we shall compare the front-fed paraboloid, the true cassegrain antenna, the offset front-fed paraboloid, and the open cassegrain antenna. In all the cases we shall use a short electrical linearly polarized dipole and a Huygens source as a primary radiator. We will first compare the aperture electric fields, define afterwards the polarization efficiency and calculate this for different configuratons. Finally, we show a practical example.

6.4.2. Aperture fields of reflector antennas illuminated by an electric dipole

Let us consider a short electric dipole of length l [108, p.92], lying along the X axis of a cartesian coordinate system (Fig. 6.7), with a current I flowing in the direction of the positive X-axis.

Expressed in ρ,ψ,ξ coordinates, the far zone components of the complex electric field are

$$\bar{E} = E_\psi \bar{a}_\psi + E_\xi \bar{a}_\xi \qquad \text{or}$$

$$\bar{E} = \frac{j\eta I l e^{-jk\rho}}{2\lambda\rho}(-\bar{a}_\psi \cos\psi\cos\xi + \bar{a}_\xi \sin\xi), \tag{6.9}$$

where $\eta = 120\ \pi$ Ohms, $\bar{a}_\psi$ and $\bar{a}_\xi$ are unit vectors along the ψ and ξ axes, respectively, and k the wave number.

In x,y,z coordinates Eq. 6.9 becomes

$$\bar{E} = -E_0[\bar{a}_x(\cos^2\psi\cos^2\xi + \sin^2\xi) - \tfrac{1}{2}\bar{a}_y \sin^2\psi \sin 2\xi + \tfrac{1}{2}\bar{a}_z \sin 2\psi\cos\xi], \tag{6.10}$$

where $E_0 = j\eta I l e^{-jk\rho}/2\lambda\rho$.

If the dipole is oriented along the positive y-axis, it is readily seen that the electric field becomes

$$\bar{E} = (-\bar{a}_\psi \cos\psi\sin\xi - \bar{a}_\xi \cos\xi) \tag{6.11}$$

or

$$\bar{E} = -E_0[-\tfrac{1}{2}\bar{a}_x \sin^2\psi\sin 2\xi + \bar{a}_y(\cos^2\psi\sin^2\xi + \cos^2\xi) + \tfrac{1}{2}\bar{a}_z \sin 2\psi\sin\xi]. \tag{6.12}$$

These fields will induce surface currents in any arbitrary reflector using geometrical optical techniques.

Using the method employed before by Jones [57] the aperture field may now be found by calculating the surface-current density of the reflector $\bar{K} = 2(\bar{n} \times \bar{H}_i)$, $\bar{H}_i$ being the incident field and $\bar{n}$ the unit vector normal to the surface at the point of incidence and projecting $\bar{K}$ on the aperture.

A simpler way to find the aperture field may be followed by investigating what happens with the fields $E_\psi \bar{a}_\psi$ and $E_\xi \bar{a}_\xi$ at the point of incidence. From Fig. 6.8 it is readily seen that the vector $E_\xi \bar{a}_\xi$ is perpendicular to the plane comprising the z-axis, radius ρ from focus to the surface of the reflector, the reflected ray, and the vector $\bar{n}$ at the point of incidence (plane FGH). After reflection this vector remains perpendicular to the surface, but its direction reverses. Therefore,

$$\bar{E}^r_\xi = -E_\xi \bar{a}_\xi \tag{6.13}$$

the index r indicating reflection.

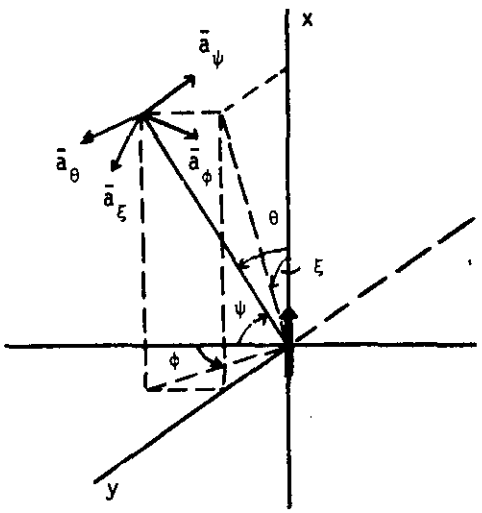

Fig. 6.7 Electric dipole oriented along the positive x-axis of a cartesian coordinate system

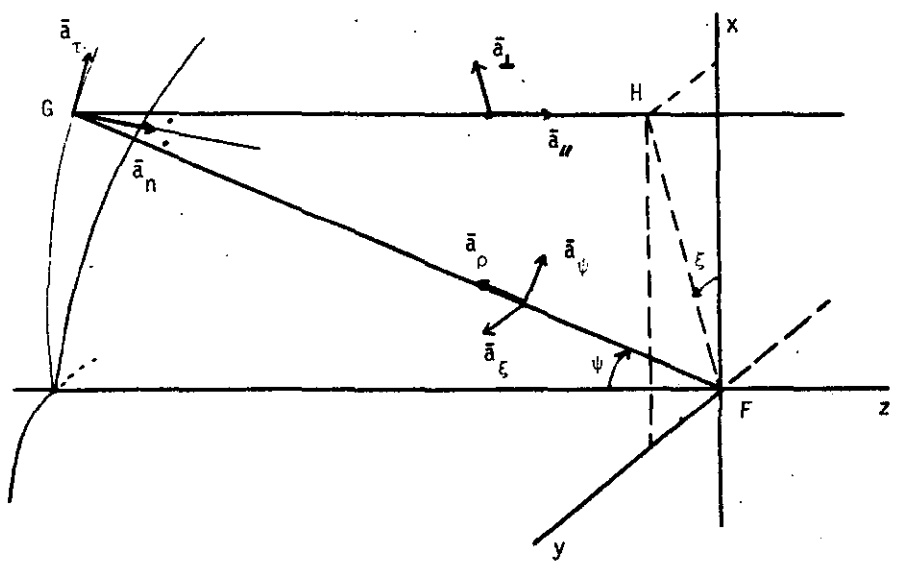

Fig. 6.8 Geometry of the parabolic reflector with incident and reflected rays end vectors

The vector $E_\psi \bar{a}_\psi$ lies in plane FGH and is perpendicular to the radius. To find out what happens with $E_\psi \bar{a}_\psi$ we will use Fig. 6.8 and define the indices n and τ as the directions normal and tangential to the paraboloid surface at the point of incidence. We now resolve E_ψ in $E_{\psi,n}$ and $E_{\psi,\tau}$ resulting in

$$E_{\psi,n} = E_\psi \sin\tfrac{1}{2}\psi$$
$$E_{\psi,\tau} = E_\psi \cos\tfrac{1}{2}\psi \tag{6.14}$$

After reflection, $E_{\psi,n}$ is continuous and $E_{\psi,\tau}$ reverses its sign. Therefore,

$$E^r_{\psi,n} = E_\psi \sin\tfrac{1}{2}\psi$$
$$E^r_{\psi,\tau} = -E_\psi \cos\tfrac{1}{2}\psi \tag{6.15}$$

By means of vectors $\bar{a}_\perp$ and $\bar{a}_{/\!/}$ [Fig. 6.8] and by resolving $E_{\psi,n}$ and $E_{\psi,\tau}$ along these vectors it is readily found, using Eqs. 6.15 that

$$E^r_\perp = -E^r_{\psi,n} \sin\tfrac{1}{2}\psi + E^r_{\psi,\tau} \cos\tfrac{1}{2}\psi = -E_\psi, \tag{6.16}$$
$$E^r_{/\!/} = E^r_{\psi,n} \cos\tfrac{1}{2}\psi + E^r_{\psi,\tau} \sin\tfrac{1}{2}\psi = 0. \tag{6.17}$$

The unit vector $\bar{a}_\perp$ may be written

$$\bar{a}_\perp = \bar{x}\cos\xi + \bar{y}\sin\xi \tag{6.18}$$

If we use an electric dipole oriented along the positive x-axis, the reflected field $\bar{E}^r_\psi$ follows from Eqs. 6.9, 6.16 and 6.18 resulting in

$$\bar{E}^r_\psi = E_0 \cos\psi\cos\xi\ (\cos\xi, \sin\xi, 0), \tag{6.19}$$

and Eq. 6.13 becomes

$$\bar{E}^r_\xi = -E_0 \sin\xi\ \bar{a}_\xi$$

By means of Eqs. 6.9, 6.13 and 6.19 the aperture field E_A yields

$$\bar{E}_A = E^r(x,y,z) = E_0\cos\psi\cos\xi(\cos\xi,\sin\xi,0) - E_0\sin\xi(-\sin\xi,\cos\xi,0)$$

or

$$\bar{E}_A = E_0[\{1 - \cos^2\xi(1 - \cos\psi)\}\bar{x} - \tfrac{1}{2}\sin 2\xi(1 - \cos\psi)\bar{y}] \qquad (6.20)$$

where

$$E_0 = \frac{jn\,Ile^{-jk(F + z_0)}}{2\lambda\rho}$$

Using the same technique as described above, we readily find the aperture field, if the dipole is oriented along the positive y- or z-axis [34].
The offset paraboloid is illustrated in Fig. 6.9. If the electric dipole is located in the focus of the paraboloid oriented along the positive x'-axis of a x',y',z' coordinate system, the aperture field appears to be

$$\bar{E}_A = [E_0\cos\Psi_0\{1 - \cos^2\xi(1 - \cos\psi)\} + E_0\sin\Psi_0\sin\psi\cos\xi]\bar{x}$$

$$+ [E_0\cos\Psi_0\{-\tfrac{1}{2}\sin 2\xi(1 - \cos\psi)\} + E_0\sin\Psi_0\sin\psi\sin\xi]\bar{y} \qquad (6.21)$$

The results in case that the dipole is oriented along the y' or z' axis are found elsewhere [34].
The same technique as used for the front-fed paraboloid may be employed to calculate the fields in the aperture of a cassegrain antenna. However, there are some fundamental differences because the dipole field is reflected twice before it arrives at the main reflector aperture. Therefore the components $\bar{E}_\xi$ and $\bar{E}_\psi$ are to be known after this double reflection in order to calculate this aperture field. If the electric dipole is located in focus F_1 and oriented along the positive x-axis [Fig. 6.10], the aperture field is

$$\bar{E}_A = -E_0'[\{1 - \cos^2\xi(1 - \cos\psi_1)\}\bar{x} - \tfrac{1}{2}\sin 2\xi(1 - \cos\psi_1)\bar{y}] \qquad (6.22)$$

In Eq. 6.22 $E_0' = jn\,Ile^{-jkr_a} / 2\lambda\rho'$

where ρ' is the distance between the primary focus and the surface of the main reflector. It is readily found that $r_a = f/e + F + Z_0$ and $\rho' = 2F/(1 + \cos\psi) + f/e$, where f is the distance between the two hyperboloid foci, e the hyperboloid eccentricity and Z_0 the depth of the paraboloid. If the dipole is oriented along the positive y or z-axis similar equations may be found [34].

The calculation of the aperture field of an open cassegrain antenna is much more complicated than the previous ones. The geometry is presented in Fig. 6.11. In general, the planes KGH (with the z-axis) and F_1KG (with the z' axis) will not coincide. Therefore, the ray from the primary focus F_1 to the subreflector and the ray reflected from the paraboloid (GH) will generally not be located in the same plane. The calculation of the aperture field leads to long algebraic equations. The reader is referred to a report recently issued [34] where a detailed description of these equations is given [121].

6.4.3. The aperture fields of reflector antennas illuminated by a Huygens source

A combination of an electric dipole and a magnetic dipole of equal intensity and crossly oriented is often called a Huygens source [57]. If this source is located in the focus of a paraboloid antenna in such a way that the electric dipole orients along the positive x-axis and the magnetic dipole along the positive y-axis, the aperture fields are readily found by superposition of the aperture fields caused by illumination with electric and magnetic dipole. The reader is referred to a report [34] recently issued for the aperture fields of reflector antennas fed by a magnetic dipole.

In accordance with Jones [57], we find

$$\bar{E}_A = E_0(1 + \cos\psi)\bar{x} \tag{6.23}$$

In the same way if the electric dipole is oriented along the +y axis and the magnetic dipole along the -x axis

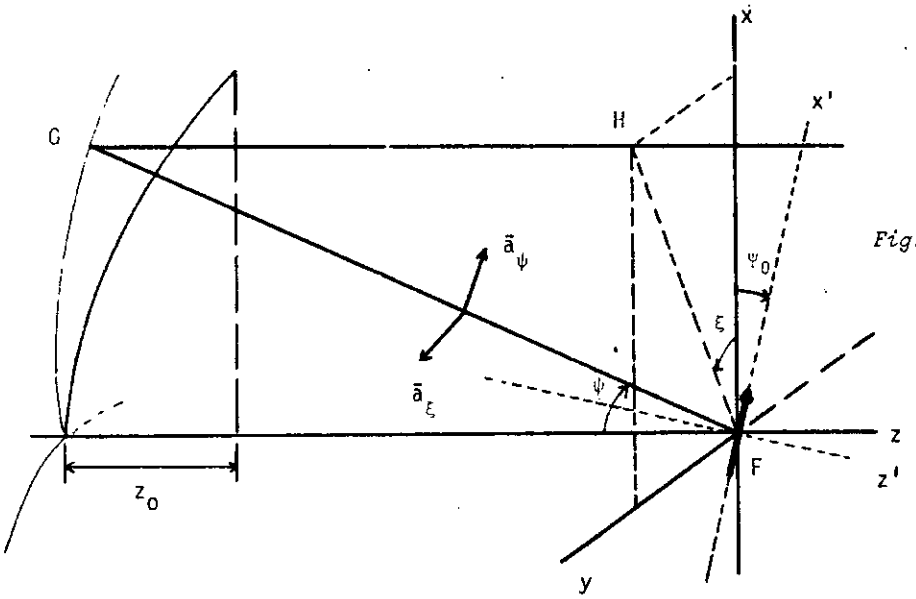

Fig. 6.9 Geometry of the offset paraboloidal reflector

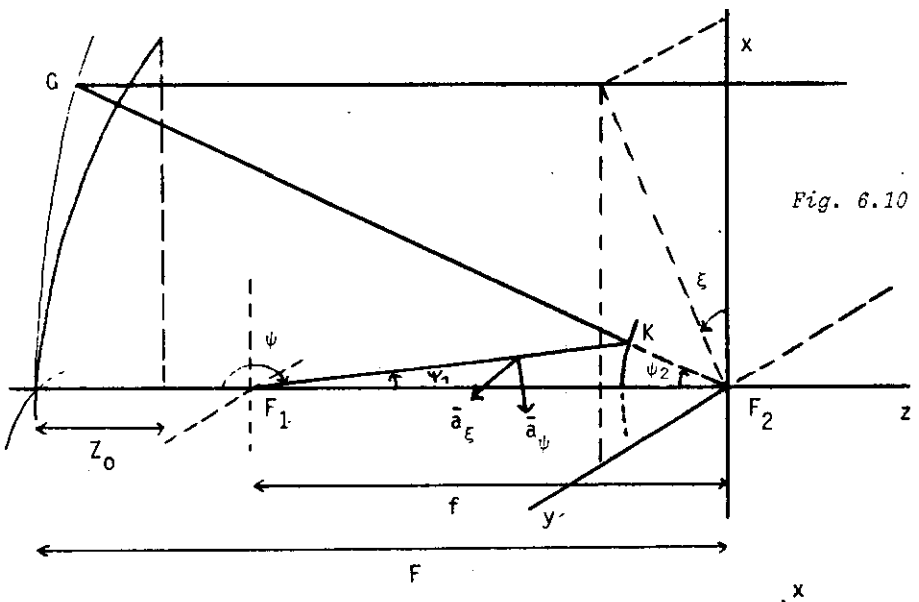

Fig. 6.10 Geometry of the classical cassegrain antenna

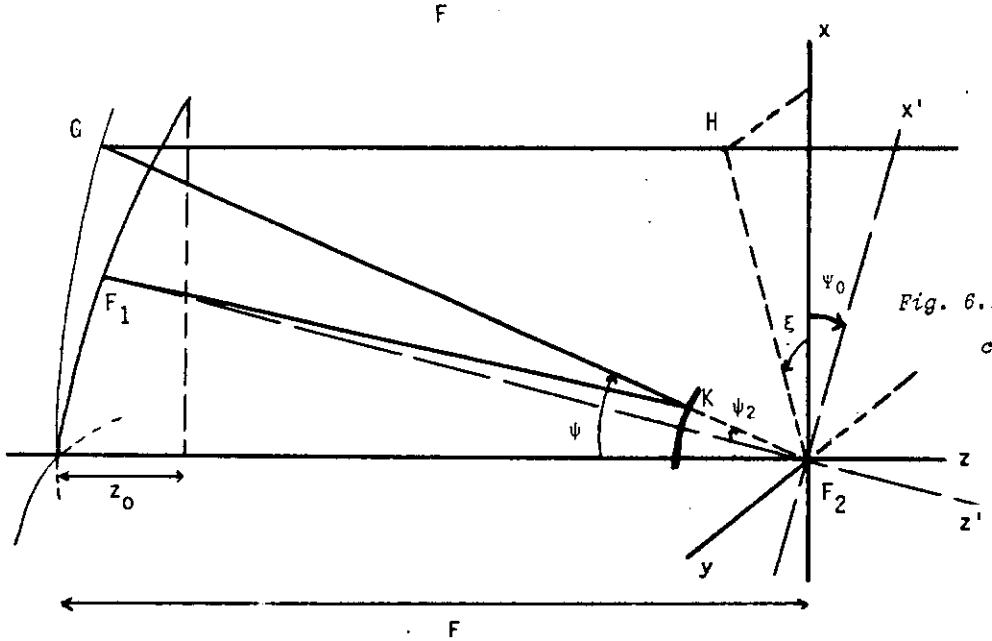

Fig. 6.11 Geometry of the open cassegrain antenna

$$\bar{E}_A = E_0(1 + \cos\psi)\bar{y} \tag{6.24}$$

It appears that in both cases the cross-polarization component disappears. A classical cassegrain antenna shows similar results and the cross-polarization component disappears as well.
The aperture field of an offset antenna illuminated by a Huygens source may be found by combining the aperture fields originated by an electric dipole oriented along the positive x'-axis and a magnetic dipole oriented along the positive y'-axis, or by an electric dipole oriented along the positive y'-axis and the magnetic dipole along the negative x'-axis. As will be noticed, the cross-polarization component does not disappear.
If we try to find the aperture fields of an open cassegrain antenna, it appears also that no simplification takes place. Therefore, it is of little value to rewrite here the equations found before. As will be noticed, the cross-polarization component in the aperture does not disappear either.

6.4.4. The polarization efficiency

In accordance with Potter [85], the polarization efficiency of an antenna is defined by the ratio of the antenna gain if the cross polarized energy were zero everywhere, to the antenna gain including the effects of cross-polarization. Thus

$$\eta_p = \frac{\left| \int_0^{2\pi} \int_0^{\Psi} E_{mp}(\psi,\xi)\, \rho^2 \sin\psi \, d\psi d\xi \right|^2}{\int_0^{2\pi} \int_0^{\Psi} \left[E^2_{mp}(\psi,\xi) + E^2_{cp}(\psi,\xi)\right]^{\frac{1}{2}} \rho^2 \sin\psi d\psi d\xi \Big|^2} \tag{6.25}$$

where $E_{mp}(\psi,\xi)$ represents the electric field in the aperture with principal polarization and $E_{cp}(\psi,\xi)$ that of the cross polarization. By means of Eq. 6.25 and the equations of the electric field in the aperture found in the previous paragraphs it is now possible to calculate the polarization efficiency.
In the case that a front-fed paraboloid is investigated, the distance ρ between paraboloid and focus is $\rho = 2F/(1+\cos\psi)$, and because all the fields involved are proportional to $\exp[-jk(F+z_0)]/\rho$, Eq. 6.25 may be replaced by

$$\eta_p = \frac{\left| \int_0^{2\pi} \int_0^{\Psi} E_{mp}(\psi,\xi)/E_0 \tan\tfrac{1}{2}\psi \, d\psi d\xi \right|^2}{\left| \int_0^{2\pi} \int_0^{\Psi} [\{E_{mp}(\psi,\xi)/E_0\}^2 + \{E_{cp}(\psi,\xi)/E_0\}^2]^{\frac{1}{2}} \tan\tfrac{1}{2}\psi \, d\psi d\xi \right|^2} \tag{6.26}$$

If the paraboloid is illuminated by an electric dipole oriented along the +X-axis, the aperture fields to be used are

$$E_{mp} = E_0[1 - \cos^2\xi(1 - \cos\psi)] \tag{6.27}$$

$$E_{cp} = -\tfrac{1}{2}E_0 \sin 2\xi(1 - \cos\psi) \tag{6.28}$$

where

$$E_0 = \frac{j\eta I l e^{-jk(F + z_0)}}{2\lambda\rho}$$

It is possible to simplify Eq. 6.26 by substituting Eq. 6.27 and Eq. 6.28, but this does not increase the insight into the problem. An approximation of this equation as carried out by Potter [85], has the drawback that it gives only reliable results for very shallow paraboloid reflectors with subtending angles of less than 60 degrees. The results of Eq. 6.26, computed without any approximation, applied to front-fed paraboloid reflector antennas are presented in Fig. 6.12.

In the case of a classical cassegrain antenna (Fig. 6.10), the integration is carried out over the angles ξ and ψ_2. We can now replace Eq. 6.26 by

$$\eta_p = \frac{\left| \int_0^{2\pi} \int_0^{\Psi_2} E_{mp}(\xi,\psi_2)/E_0 \tan\tfrac{1}{2}\psi_2 \, d\xi d\psi_2 \right|^2}{\left| \int_0^{2\pi} \int_0^{\Psi_2} [(E_{mp}(\xi,\psi_2)/E_0)^2 + (E_{cp}(\xi,\psi_2)/E_0)^2]^{\frac{1}{2}} \tan\tfrac{1}{2}\psi_2 \, d\xi d\psi_2 \right|^2} \tag{6.29}$$

If the subreflector is illuminated by an electric dipole, oriented along the positive X-axis, the aperture fields to be used are

$$E_{mp}/E_0' = -1 + \cos^2\xi[1 - \cos \; 2\arctan\{(e - 1)/(e + 1) \tan\tfrac{1}{2}\psi_2\}] \tag{6.30}$$

$$E_{cp}/E_0' = \tfrac{1}{2}\sin 2\xi[1 - \cos \; 2\arctan\{(e - 1)/(e + 1) \tan\tfrac{1}{2}\psi_2\}] \tag{6.31}$$

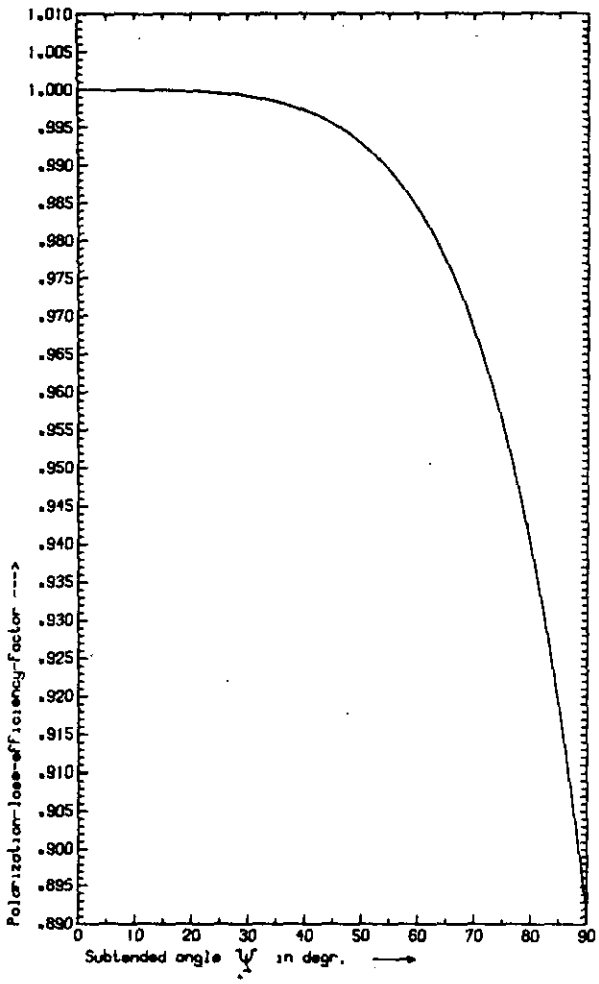

Fig. 6.12 Polarization loss efficiency factor of a parabolic reflector

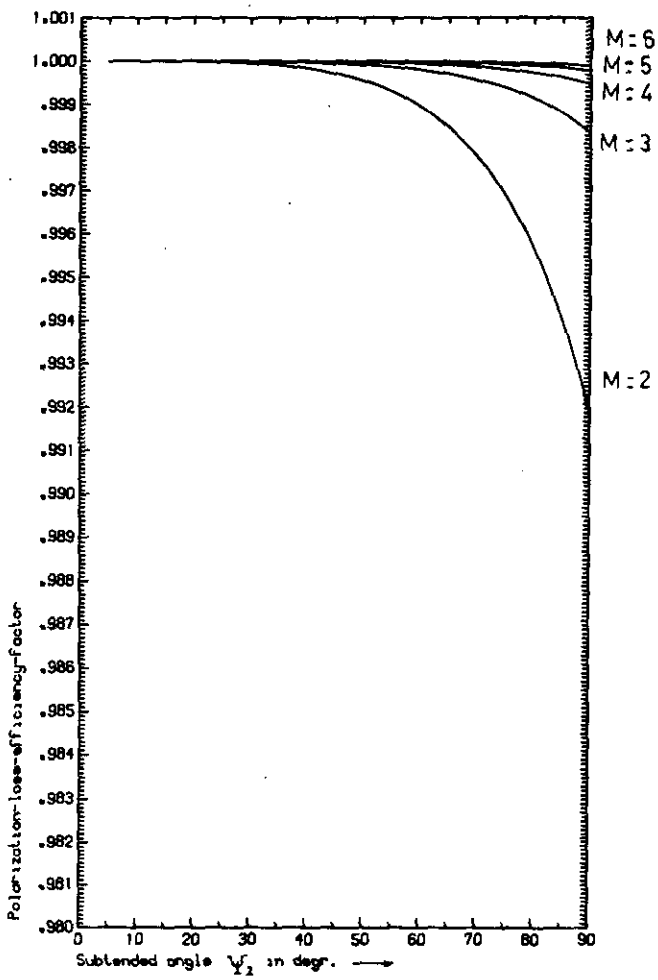

Fig. 6.13 Polarization loss efficiency factor of a classical cassegrain antenna

Fig. 6.13 shows the computed results, where the polarization efficiency is given in relation to the subtended angle of the main reflector with the magnification ratio $M = (e + 1)/(e - 1)$ as a parameter.
When an offset paraboloid antenna is investigated Eq. 6.26 may still be used, however, the integration limits will differ. As explained before [34] ψ will have to be integrated between $\Psi_0 - \Psi$ and $\Psi_0 + \Psi$. The integration limits of ξ, ξ_L and ξ_R are

$$\xi_L = -\text{arc cos } (\cos\Psi - \cos\Psi_0\cos\psi)/(\sin\Psi_0\sin\psi) \tag{6.32}$$

$$\xi_R = +\text{arc cos } (\cos\Psi - \cos\Psi_0\cos\psi)/(\sin\Psi_0\sin\psi) \tag{6.33}$$

where Ψ_0 is the offset angle and Ψ the angular aperture of the main reflector. (In the open cassegrain antenna Ψ is called Ψ_2).
Eq. 6.26 is then written as

$$\eta_p = \frac{\left| \int_{\Psi_0-\Psi}^{\Psi_0+\Psi} \int_{\xi_L}^{\xi_R} E_{mp}(\psi,\xi)/E_0 \tan\tfrac{1}{2}\psi \, d\psi d\xi \right|^2}{\left| \int_{\Psi_0-\Psi}^{\Psi_0+\Psi} \int_{\xi_L}^{\xi_R} (E^2_{mp} + E^2_{cp})^{\frac{1}{2}}/E_0 \tan\tfrac{1}{2}\psi \, d\psi d\xi \right|^2} \qquad (6.34)$$

where the main and cross polarized fields for the offset paraboloid and open cassegrain antenna have been discussed in the previous sections for various illuminations.
In the case of an open cassegrain antenna the efficiency factor becomes a little more complicated. It is readily shown that the factor E_0 in the aperture fields is equal to that of the classical cassegrain antenna and that the integration limits are the same as for the offset antenna. Fig. 6.14 shows the polarization efficiency of an offset paraboloid illuminated by an electric dipole oriented along the positive x'-axis and positive y'-axis respectively, as well as illuminated by a Huygens source.
The results obtained with an open cassegrain antenna are given in Fig. 6.15. The eccentricity of the hyperboloid subreflector was 1.5. For both offset and open cassegrain antennas the offset angle served as a parameter.

6.4.5. A practical example

In the previous section a Huygens source was presented with equal intensities of a magnetic and an electric dipole. However, many feed patterns may be divided in electric and magnetic dipoles with unequal intensities. In this section we work out a practical example.
A popular feed system used to illuminate a reflector surface is the open waveguide excited with the TE_{10} mode described by Silver [108,p.343] and Jones [57] and discussed in Sec. 4.2.2.

If we want to study the cross-polarization properties of antennas illuminated by this feed, we must know the waveguide dimensions, frequency range and cut-off frequency.

If we study a rectangular waveguide in the X-band (8,200 - 12,400 MHz) the dimensions a and b are 0.900 x 0.400 inches and the cut-off frequency is 6560 MHz. The proportions of the lowest and highest frequencies to the cut-off frequency are 1.25 and 1.90, a relationship which is also found for waveguides in other frequency bands. Let λ_1 be the longer wavelength = 3.66 cm and λ_2 the shorter = 2.42 cm. The wavelength in the waveguide is then for λ_1

$$\lambda_{g_{10}} = 3.66/\sqrt{1 - (3.66/4.57)^2} = 6.11 \text{ cm},$$

and for λ_2

$$\lambda_{g_{10}} = 2.42/\sqrt{1 - (2.42/4.57)^2} = 2.85 \text{ cm}$$

From Eq. 6.38 we then obtain for $\beta_{10}/k = \lambda_1/\lambda_{g_{10}} = 3.66/6.11 = 0.60$

and $\beta_{10}/k = \lambda_2/\lambda_{g_{10}} = 2.42/2.85 = 0.85$

The polarization vector is now for λ_1

$$\bar{a}_i = \frac{\cos\xi}{\rho}(1 + 0.60\cos\psi)\bar{a}_\psi - \frac{\sin\xi}{\rho}(0.60 + \cos\psi)\bar{a}_\xi \qquad (6.35)$$

and for λ_2

$$\bar{a}_i = \frac{\cos\xi}{\rho}(1 + 0.85\cos\psi)\bar{a}_\psi - \frac{\sin\xi}{\rho}(0.85 + \cos\psi)\bar{a}_\xi \qquad (6.36)$$

The polarization properties apparently depend on the frequency. If such a feed is used to illuminate a front-fed paraboloid antenna, it is readily found by means of the theory developed in Sec. 6.4.2. that the aperture field

$$\bar{E}_A = E_0\frac{\cos\xi}{1 + \cos\psi}(1 + m\cos\psi)\,(\cos\xi, \sin\xi, 0)_x$$
$$-E_0\frac{\sin\xi}{1 + \cos\psi}(m + \cos\psi)\,(-\sin\xi, \cos\xi, 0)_x$$

or

$$\bar{E}_A = \frac{E_0}{1 + \cos\psi} [\{(1 + m\cos\psi)\cos^2\xi + (m + \cos\psi)\sin^2\xi\}\bar{x} + \\ + \{(1 + m\cos\psi)\cos\xi\sin\xi - (m + \cos\psi)\cos\xi\sin\xi\}\bar{y}] \tag{6.37}$$

where $m = \beta_0/k$ is any value between 0.60 and 0.85.
E_0 is the amplitude factor of the feed system and is in accordance with Silver [108, p.343]

$$E_0 = \frac{\cos[(\pi a/\lambda)\sin\psi\cos\xi]}{[(\pi a/\lambda)\sin\psi\cos\xi]^2 - \frac{1}{4}\pi^2} \times \frac{\sin[(\pi b/\lambda)\sin\psi\sin\xi]}{(\pi b/\lambda)\sin\psi\sin\xi} \tag{4.3}$$

The results for three different values of m are given in Fig. 6.16.

6.4.6. Conclusions

It has been demonstrated in the foregoing that by calculating the aperture electric fields of antennas with a paraboloid (main) reflector, expressions may be derived for the polarization efficiency or polarization loss. These expressions are found not only for front-fed paraboloids, but also for classical cassegrain antennas, front-fed offset paraboloids, and open cassegrain antennas. Both electric dipole excitation and excitation by a Huygens source are investigated as they give a good insight into the problems and facilitate comparative studies. Moreover, there are a number of realistic feeds, such as a rectangular horn excited in the TE_{10} mode, having polarization properties close to the Huygens source. An example of this kind has been worked out, showing that the polarization losses decrease considerably if the polarization vector approach that of a Huygens source. If investigations are required for feeds with polarization properties different from those as discussed here, the same techniques may be used.

After the electric aperture field has become known, an expression may be found for the polarization efficiency η_p. Carrying out the computation, it is readily seen that the front-fed paraboloid has very bad polarization properties, becoming worse for deep paraboloids. In the case that the focus falls within the aperture plane ($\Psi_2 \gg 90^0$), the polarization efficiency falls to 89% (Fig. 6.12). On the other hand, the true cassegrain antenna has much better properties, which not only depend upon the subtending angle

of the main reflector, but also on the magnification ratio $M = (e+1)/(e-1)$, which has been introduced as a parameter (Fig. 6.13). The results become worse for low M values and deep main paraboloids; however, for $M = 2$ and $\Psi_2 = 90$ degrees, the true cassegrain antenna still retains a polarization efficiency of 99%, being considerably more than in the case of front-fed paraboloids with equal Ψ_2. Offset paraboloid antennas show an increase in the losses at increasing subtending angle and increasing offset angle. If we compare the front-fed paraboloid with the offset paraboloid, it appears that the former shows better results at equal subtending angles than the offset antenna with an electric dipole polarized along the x'-axis; e.g. a front-fed paraboloid with a subtending angle of 60 degrees has a polarization efficiency of 98,5%, while an offset paraboloid with subtending and offset angles of 60 degrees shows an efficiency of only 91% (Fig. 6.14). If the dipole is polarized along the y'-axis, the efficiency even drops to 89%.

If we study the results obtained with an open cassegrain antenna illuminated by an electric dipole, it appears that not much difference is noticed if the dipole is oriented along the x"-axis or y"-axis. At offset angles and subtending angles of about 60 degrees it appears that the efficiency drops to 90% which is of the same order as for offset front-fed paraboloids (Fig. 6.15). The results obtained by illumination by a Huygens source are, both for offset antennas and open cassegrain antennas, similar to those obtained by illumination by an electric dipole. The results clearly depend on the offset and subtending angles rather more than on the polarization of the feed. At offset angles and main reflector subtending angles of ca. 60 degrees an efficiency of ca. 90% is noticed again.

We also investigated the losses of open cassegrain antennas in relation to the eccentricity of the hyperboloid subreflector. Using eccentricities of 2.0 and 2.5, the results are very similar to those with eccentricities of 1.5.

Compared with the symmetrical front-fed paraboloid antenna and the classical cassegrain antenna, offset antennas are very unfavourable when illuminated by a Huygens source. The Huygens source gives zero polarization losses for symmetrical paraboloid reflector antennas, but the losses of offset antennas

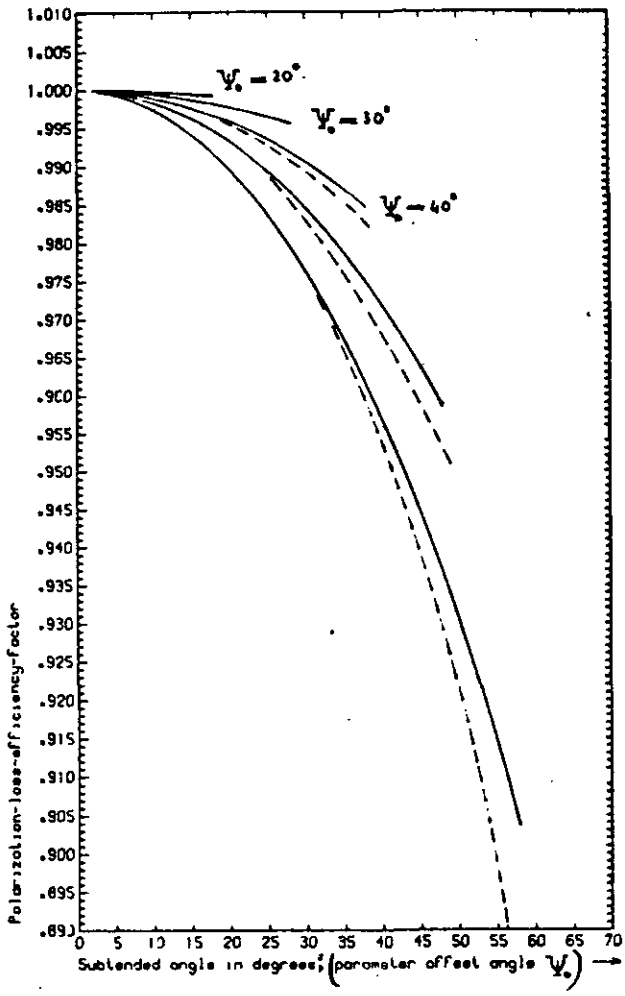

Fig. 6.15 Polarization loss efficiency factor of an open cassegrain antenna, the offset angle Ψ_0 being a parameter, illuminated by
_____ E dipole oriented along x'-and y'-axis
_ _ _ Huygens source

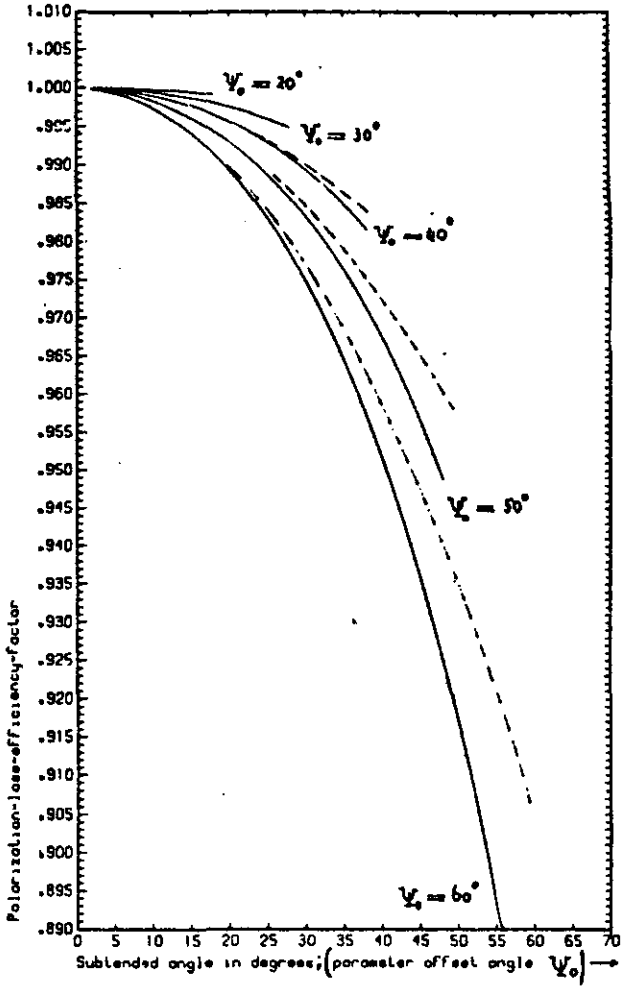

Fig. 6.14 Polarization loss efficiency factor of an offset paraboloid reflector, the offset angle Ψ_0 being a parameter, illuminated by _____ E dipole oriented along x'-axis and Huygens source
_ _ _ E dipole oriented along y'-axis

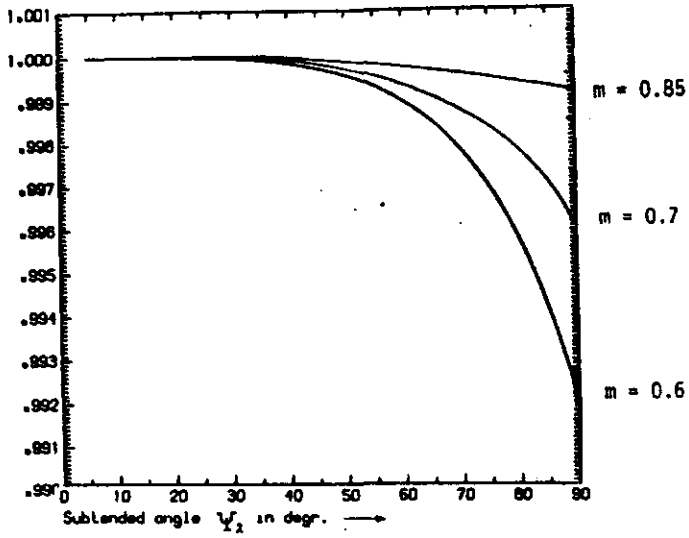

Fig. 6.16 Polarization loss efficiency factor of a circularly symmetrical paraboloid antenna illuminated by an open waveguide excited with the TE_{10} mode

are of the same order as those calculated for offset antennas illuminated by an electric dipole. This conclusion is supported by the fact that for eccentricities differing from $e = 1.5$ similar results are obtained.

More study is required to find out whether feeds may be designed having polarization properties which may improve the polarization losses of offset antennas. However, the present study makes the use of offset antennas for purposes where a polarization discrimination of more than 30 dB is required, very questionable.

References

1. Abramowitz, M. and Stegun I.A., "Handbook of Mathematical Functions", Dover Publications, New York 1965.

2. Afifi M.S., "Scattered radiation from microwave antennas and the design of a paraboloid-plane reflector antenna", Doctor's Thesis, Delft University of Technology, Netherlands, July 1967.

3. Baars J.W.M., "Dual beam parabolic antennae in radio astronomy", Doctors Thesis, Delft University of Technology,Netherlands, March 1970

4. Born, M., and Wolf, E., "Principles of Optics", Pergamon Press, Oxford, 1964.

5. Carberry T.F., "Analysis theory for a shaped beam doubly curved reflector antenna", IEEE Trans. on Antennas and Propagation, Vol. AP 17, pp.131-138, March 1969.

6. Carter D., "Wide angle radiation in pencil beam antennas", Journal of Applied Physics, Vol. 26, Nr. 6, pp.645-652, June 1955.

7. Champeney D.C., "Fourier transforms and their physical applications", Academic Press, London 1973.

8. Chu T.S. and Turrin R.H., "Depolarization properties of offset reflector antennas", IEEE Trans. Antennas and Propagation, Vol. AP 21, pp.339-345, May 1973.

9. Clarricoats P.J.B and Lim S.H., "High efficiency spherical reflector antennas for portable earth stations", Conference on Earth Station Technology, pp.140-143, London, 14-16 Oct.1970.

10. Clarricoats P.J.B and Lim S.H., Almoayyed T.A. and Shaw J.A., "New techniques for high efficiency reflector antennas", 2nd European Microwave Conference, pp. B4/1:1-B4/1:4, Stockholm, 23-28 Aug. 1971.

11. Condon E.U., "Theory of radiation from paraboloid reflectors",Westinghouse Report nr.15, Sept. 24, 1941.

12. Cook J.S., Elam E.M. and Zucker H., "The open cassegrain antenna", Bell System Technical Journal, pp.1255-1300, Sept. 1965.

13. Coolen L., Private Communication, Eindhoven, August 1972.

14. Cornbleet S., "Radiation patterns of circular aperture with structural shadows", Proc. IEE, Vol. 117, pp.1620-1626, Aug. 1970.

15. Cutler C.C., "Parabolic antenna design for microwaves", Proc. IRE, pp.1284-1294, Nov. 1947.

16. Davidson C.F. and Ravenscroft I.A., "Design considerations for a centre fed paraboloidal aerial system for a satellite-communication earth station", Conference on large steerable aerials, pp.289-303, London, June 6-8 1966.

17. Dickieson A.C., "Project Telstar, its aims and purposes", Bell Lab. Record, Vol. 41, nr. 4, pp. 117-121, April 1963.

18. van Diepenbeek, C.T.W., Report graduate work TH Eindhoven, Sept. 1971 (in dutch).

19. Doidge E.G., "Antenna gain as it applies to satellite communication earth stations", A seminar on satellite earth station technology, Washington 16-27 May 1966.

20. Dijk J., Jeuken M.E.J. and Maanders E.J., "An antenna for a satellite communication ground station", T.H. Report 68-E.01 (1968) 120 pp.

21. Dijk J., Jeuken M.E.J., and Maanders E.J., "Blocking and diffraction effects in cassegrainian antenna systems", De Ingenieur, Vol. 80, pp. 79-91, July 1968.

22. Dijk J. and Maanders E.J., "Optimising the blockage efficiency in shaped cassegrain systems", Electronic Letters, Vol. 4, pp.372-373, Sept. 1968.

23. Dijk J., Jeuken M.E.J. and Maanders E.J., "On antenna noise temperature", Proc.I.E.E. Vol.115, pp. 1403-1410, Oct. 1968.

24. Dijk J. and Maanders E.J., "Telecommunicatie via satellieten, elektrische problemen van de grondstation antenne", De Ingenieur, Vol.81, nr.47, pp.E121-E133, 21st November 1969.

25. Dijk J. and Maanders E.J., "De elektrische eigenschappen van grondstations voor satelliet-communicatie", Elektrotechniek, Vol. 47, pp.657-668, 27th November 1969.

26. Dijk J., Koop H.E.M. and Maanders E.J., "On conical horn antennas", TH Report, 70-E-10 (1970) 63 pp.

27. Dijk J., Groothuis H.H.H., and Maanders E.J., "Some improvements in antenna noise temperature calculation", IEEE Transactions on Antennas and Propagation, Vol.AP.18, nr.5, pp.690-692, Sept. 1970.

28. Dijk J., and Maanders E.J., "Aperture blockage in dual reflector antenna systems --- a review", TH Report 71-E-23, 50 pp. Eindhoven University of Technology, September 1971.

29. Dijk J., Kramer C., Maanders E.J., and van der Vorst A.C.A., "Digitized antenna measurements", IEEE Transactions on Microwave Theory and Techniques, Vol. MIT 20-20, nr.1, pp.48-51, January 1972.

30. Dijk J., Maanders E.J., and Sniekers J.P.F., "On the efficiency and radiation patterns of mismatched shaped cassegrain systems", IEEE Transactions on Antennas and Propagation, Vol. AP-20 pp. 653-655, September 1972.

31. Dijk J., Berends J.M. und Maanders E.J., "Die Nebenzipfel einer Cassegrain Antenna in der Umgebung der Hauptachse", Archiv für Elektronik und Uebertragungstechnik, Band 26 pp.362-364, August 1972.

32. Dijk J. and Maanders E.J., "Some aspects of near and far angle sidelobes in double reflector systems", paper presented at AGARD conference, 7-10 May 1973, Rome.

33. Dijk J. and Maanders E.J., "Some errors in calculating radiation patterns of reflector antennas using Kirchhoff integration", Electronic Letters, Vol. 9, pp.510-512, 18 Oct. 1973.

34. Dijk J., van Diepenbeek C.T.W., Maanders E.J., and Thurlings L.F.G., "The polarization losses of offset paraboloid antennas",
a) IEEE Transactions on Antennas and Propagation, Vol.AP 22, pp.513-520, July 1974,
b) TH report 73-E-39, June 1973, 46 pages.

35. Dijk J., Coolen L., and Maanders E.J., "Reply to comment on calculation of the radiation patterns of reflector antennas, using Kirchhoff integration", Electronic Letters, Vol.10, pp.184-185, 16 May 1974.

36. Filipowsky R.F., and Muehldorf E.I., "Space communication systems", Prentice Hall Inc., Englewood Cliffs, N.J., USA 1965.

37. Freeman R., "An approach to earth station technology", Telecommunication Journal, Vol. 38, pp. 470-478 June 1971.

38. Galindo V., "Synthesis of dual reflector antennas", Report 64-22, Electronics Research Laboratory, University of California, Berkely, July 30, 1964.

39. Galindo V., "Design of dual reflector antennas with arbitrary phase and amplitude distributions", IEEE Trans. on Antennas and Propagation, pp.403-408, 1964.

40. Gillitzer E., "Die Cassegrain-Parabolantenne und andere Antennes für Breitband-Richtfunk bei 6 GHz", Frequenz, 16, nr. 11, pp.459-468, Nov. 1962.

41. Graham R., "The polarization characteristics of offset cassegrain aerials", European Microwave Conference, pp.352, London 8-12 Sept. 1969.

42. Graham R., "The polarization characteristics of offset cassegrain aerials". International Conference on Radar and Future, IEE, London 23-25 October 1973.

43. Gray C.L., "Estimating the effect of feed support member blocking on antenna gain and sidelobe level", The Microwave Journal, pp.88-91, March 1964.

44. Green K.A., "Modified cassegrain antenna for arbitrary phase and amplitude illumination", IEEE Transactions of Antennas and Propagation, pp. 589-590, Sept. 1963.

45. Hanfling J.D., "Aperture fields of paraboloidal reflectors by stereographic mapping of feed polarization", IEEE Trans. on Antennas and Propagation, Vol. AP 18, nr. 3, pp.392-396, May 1970.

46. Hannan P.W., "Microwave antennas derived from the cassegrain telescope", Trans. IRE AP-9, nr.2, pp.140-153, March 1961.

47. Hartsuyker A.P., Baars J.W.M., Drenth S., and Gelato-Volders Louise.,"Interferometric measurement at 1415 MHz of the radiation pattern of the paraboloid antenna at Dwingelo Radio Observatory", IEEE Transactions on Antennas and Propagation, Vol. AP-20, nr. 2, pp.166-176, March 1972.

48. Hines J.N., Tingye Li and Turrin R.H., "The electrical characteristics of the conical horn-reflector antenna", Bell Syst. Techn. Journal, pp.1187-1211, July 1963.

49. Hoffman M., "Antenna noise temperature", U.S. Seminar on satellite communications earth station technology, May 16-27, 1966 Washington D.C.

50. Hogg D.C., and Mumford W.W., "The effective noise temperature of the sky", The Microwave Journal, pp.81-84, March 1960.

51. van Hoof H.A.J.M., "Comment on calculation of the radiation patterns of reflector antennas using Kirchhoff integration", Electronic letters, Vol. 10, pp.70-71, 1974.

52. IEEE Test procedure for antennas, number 149, IEEE Std. 145-1973 Aug.2, 1973.

53. Jakes W.C., "Participation of Bell Telephone Laboratories in project Echo and experimental results", Bell Syst.Techn. J., Vol. 40, nr. 4, pp.975-1028, July 1961.

54. James G.L. and Kerdemelidis V., "Reflector antenna radiation patterns analysis by equivalent edge currents", IEEE Trans. on Antennas and Propagation, Vol. AP-21, pp.19-24, Jan. 1973.

55. Jeuken M.E.J., "Frequency independence and symmetry properties of corrigated horn antennas with small flare angles", Doctor's Thesis, Eindhoven University of Technology, Netherlands, 1970.

56. Johnson J.A., "The Intelsat System", Telecommunication Journal Vol. 38, pp.270-278, May 1971.

57. Jones E.M.T., "Paraboloid Reflector and Hyperboloid Lens Antennas", IRE Trans. on Antennas and Propagation, pp.119-127, July 1954.

58. Kampinsky A. and Ritt R.K., "Experimental and theoretical evaluation of a passive communication satellite (Echo II)", Electromagnetic Wave Theory Pt.2, Oxford Pergamon Press, pp.633-660 1967.

59. Kay A.F., "Electrical design of metal space frame radomes", IEEE Trans. AP-13, nr. 2, pp.188-202, March 1965.

60. Keller J., "Geometrical theory of diffraction", J.Opt. Soc. Amer.,Vol. 52, pp.116-130, 1962.

61. Kiesling J.D., "The NASA Relay I experimental communication satellite", RCA Rev., Vol. 25, nr. 2, pp.232-261, June 1964.

62. Kinber B.E., "The condition of shadowing and diffraction correction to current distribution", Radio Engineering and Electronic Phys, Vol. 5, pp.75-89, 1960.

63. Kinber B.E., "Sidelobe radiation of reflector antennae", Radio Engng and Electronic Phys., Vol. 6, pp.481-492, 1961.

64. Kinber B.E., "On two reflector antennas", Radio Engng Electronic Phys. Vol. 7, pp.914-921, June 1962.

65. Kinber B.E. and Tseytlin V.B., "Phase centers of parabolic antennas", Radio Engng and Electronic Phys., Vol. 15, pp.218-229, 1970.

66. Kinber B.E. and Tischenko V.A., "Polarization of radiation of axisymmetric reflector antennas", Radio Engng. and Electronic Phys., Vol. 17, pp.528-534, April 1972.

67. Kington C.N., Shearman E.D.R., Prime H.A., "A 20 ft offset cassegrain aerial for radio propagation control and communication research at 3-30 GHz", Conference on Earth Station Technology, pp.233-239, London 14-16 Oct. 1970.

68. Kofman I., "Feed Polarization for parallel currents in reflectors generated by conic sections", IEEE Trans. on Antennas and Prop. Vol. AP-14, pp.37-40, Jan. 1966.

69. Korbanski J.N., "Electric field of a Hertz dipole on the axis of an ideally conducting paraboloid of revolution", Radio Engng and Electronic Phys., Vol.13, pp.1460-1462, 1968.

70. Kouyoumjian R.G., "Asymptotic high frequency methods", Proc. IEEE, Vol. 53, pp.864-876, August 1965.

71. Kouyoumjian R.G., and Pathak P.H., "The dyadic diffraction coefficient for a perfectly conducting edge structure", URSI Meeting, UCLA, Los Angeles, California, 1971.

72. Kritikos H.N., "The extended aperture method for the determination of the shadow region radiation of parabolic reflectors", IEEE Trans. on Antennas and Propagation, Vol. AP-11, pp.400-404, July 1963.

73. Lass H., "Vector and Tensor analysis", Mc Graw-Hill, New York, 1950.

74. Lo Y.T., Private Communication, Eindhoven, May 1973.

75. Ludwig A.C., "Calculation of scattered patterns from asymmetrical reflectors", Jet Propulsion Lab, Pasadena, California, Report 21-1430, Febr. 1970.

76. Ludwig A.C., "The definition of cross polarization", IEEE Trans. Antennas and Propagation, Vol. AP-21, nr. 1, pp.116-119, January 1973.

77. Maanders E.J., "Einige Neuentwicklungen bei Doppelreflektor Systemen", Seminar über Antennentechnik, Internationales Elektronik Zentrum, Munchen 22-23 Nov. 1973.

78. Martin E.J., "Commercial satellite communications experience" IEEE Norteast Electronics Research and engineering meeting NEREM pp.104-105, Boston 1966.

79. Mei K.K., and van Bladel J., "Scattering by perfectly conducting rectangular cylinders", IEEE Trans. AP-11, nr. 2, pp.185-192, March 1963.

80. Morgan S.P., "Some examples of generalized cassegrainian and gregorian antennas", IEEE Trans. Antennas and Propagation, pp.685-694, November 1964.

81. Oshiro F.K. and Mitzner K., "Digital computer solutions of three dimensional scattering problems", G-AP Int. Record, Ann Arbor, Michigan, pp.257-263, 1967.

82. Pagones M.J., "Gain factor of an offset-fed paraboloidal reflector", IEEE Trans. on Antennas and Propagation, Vol. AP-20, pp.653-655, Sept. 1968

83. Pinney E., "Electromagnetic fields in a paraboloidal reflector" Journal of Mathematics and Physics, Vol. 26, pp.42-55, 1947.

84. Plonsey R., "Aperture Fields", IRE Trans. on Antennas and Propagation, Vol. AP-9, p.577,1961.

85. Potter P.D., "The aperture efficiency of large paraboloidal antennas as a function of their feed system radiation characteristics", Technical-Report, nr. 32-149, Jet Propulsion Lab., Pasadena, California U.S.A., Sept. 15, 1961.

86. Potter, P.D., "Unique feed system improves space antennas", Electronics, pp.36-40, June 22, 1962.

87. Potter P.D., "Aperture illumination and gain of a cassegrainian system", IEEE Transactions on Antennas and Propagation, pp.373-375, May 1963.

88. Potter P.D., "Design and performance of the NASA/JPL 210 ft steerable paraboloid", Design and construction of large steerable aerials, IEE Conference, June 6-8, 1966.

89. Rao E.L.J. and Chen S.N.C., "Illumination effieciency of a shaped cassegrain system", IEEE Trans. on Antennas and Propagation, pp.411-412, May 1970.

90. Reinders M., "Eine 10 meter Parabolantenne met einem Rillhornstrahler für Satellitenfunk oberhalb 10 GHz", Seminar über Antennentechnik, Internationales Elektronik Zentrum, Munchen 22-23 Nov. 1973.

91. Romeiser K.P., Private communication, Munchen, Jan. 1972.

92. Romeiser K.P., Rebhand W. und Leupelt U., "Nahfeld-Cassegrain-Antennen hohen Flächen-wirkungsgrades für Nachrichten-Verbindungen über Satellieten", NTG-Fachtagung, Darmstadt, 22-24 Februar 1972, pp.103-109, VDE-Verlag, 1000 Berlin 12, Bismarckstrasse 33.

93. Ross R.A., "Radar cross-section of rectangular flat plates as a function of aspect angle", IEEE Trans. on Antennas and Propagation, Vol. AP-14, pp.329-335, May 1966.

94. Ruck G.T., Barrick D.E., Stuart W.D. and Kirchbaum C.K., "Radar cross-section handbook", Plemun Press, New York, 1970.

95. Rusch W.V.T., "Scattering of a spherical wave by an arbitrary truncated surface of revolution", Technical Report Jet Propulsion Lab. Pasadena, California, nr. 32-434, May 1963.

96. Rusch W.V.T., "Scattering from a hyperboloidal reflector in a cassegrainian feed system", IEEE Trans. Antennas and Propagation, Vol. 11, nr. 4, pp.414-421, July 1963.

97. Rusch W.V.T. and Potter P.D., "Analysis of reflector antennas", Academic Press 1970, New York - London.

98. Rusch W.V.T., Private communication, Sorento, Sept. 1972.

99. Rusch W.V.T., Private communication, Birmingham, March 1974.

100. Ruze J., "Antenna tolerance theory - a review", Design and construction of large steerable aerials IEE conference, June 6-8 1966.

101. Ruze J., "Feed support blockage loss in parabolic antennas", Microwave Journal, pp.76-78, December 1968.

102. Ryan C.E. and Peters L., "Evaluation of edge-diffracted fields including equivalent currents for the caustic regions", IEEE Trans. on Antennas and Propagation, Vol. AP 17, pp.292-299, May 1969.

103. Sciambi A., "The effect of the aperture illumination on the circular aperture antenna pattern characteristics", Microwave Journal, pp.79-84, Aug. 1965.

104. Sciambi A., "Instant antenna patterns", Microwaves, pp.48-60 June 1966.

105. Sheftman F.J., "Experimental study of subreflector support structures in a cassegrainian antenna", M.I.T. Technical Report 416, 23 September 1966.

106. Siegel V.M., "Far field scattering from bodies of revolution", Appl. Sci. Res. Vol. 7, pp.293-328, 1959.

107. Siglin P.W. and Senn G.F., "The Courier Satellite", Proc. Symp. on Communication satellites, London, 12 May 1961.

108. Silver S., "Microwave antenna theory and design", Mc Graw Hill, New York, 1949.

109. Sletten C.J. and Blacksmith P., "The paraboloid mirror", Applied Optics, Vol. 4, pp.1239-1251, October 1965.

110. Smith J.M., "A note on diffraction theory and polarization", Proc. IEE, Vol.110, pp.88-90, January 1963.

111. Steinberg R.A.,"Report gaduate work",Eindhoven University of Technology,November 1970

112. Tandit V.L. and Tartakovski L.B., "The radiation of a reflector antenna in the shadow region", Radio Engng and Electron. Phys. Vol. 6, pp.61-74, 1961.

113. Tanner R.L. and Andreasen M.G., "Numerical solution of electromagnetic problems", IEEE Spectrum Vol. 4, pp.53-61, September 1967.

114. Tartakovski L.B., "Side radiation from ideal paraboloid with circular aperture", Radio Engng and Electron. Phys. Vol. 4, pp.14-28, 1959.

115. Tartakovski L.B. and Tandit V.L., "Current distribution on the reflector of a reflector antenna", Radio Engng and Electr. Phys. Vol. 5, pp.53-64, 1960.

116. Taylor F., "The Goonhilly project", The Inst. of Electrical Engineers, Savoy Place, London 1964.

117. Thourel L., "The antenna", Chapman and Hall, London, 1960.

118. von Trentini G., "Erregersysteme für Cassegrain-Antennen", Frequenz/Sonderausgabe, 17, S.491-499, Dec. 1963.

119. von Trentini G., Romeiser K.P. und Jatsch E., "Dimensioniering und Elektrische Eigenschaften der 25 M.Antenne der Erdefunkstelle Raisting usw.", Frequenz, 19, Nr.12, S.402-421,Dec.1965.

120. von Trentini G., Romeiser K.P. und Reitzig R., "Aenderungs- und Verbesserungsmöglichkeiten im Aufbau grosser Cassegrain-Antennen mit Hornparabolspeisung", Frequenz 22, 5, S.216-223, Aug. 1968.

121. Thurlings L.F.G., Private communication, Eindhoven, June 1973.

122. Watson P.A. and Ghobrial S.I., "Off-axis polarization characteristics of cassegrainian and front-fed antennas", IEEE Trans. on Antennas and Prop., Vol. AP 20, nr. 6, pp.691-699, November 1972.

123. Wested J.H., "Shadow and diffraction effects of spars in a cassegrainian system", IEE Conference nr. 21; Design and Contribution of large steerable aerials, London 6-8 June 1966.

124. Williams W.F., "High efficiency antenna reflector", Microwave Journal, pp.79-82, July 1965.

125. Woodbury D.O., "The glass giant of Palomar", Dodd Head and Co., New York N.Y. 1957.

126. Yen R., "Polarization characteristics of parabolic mirror antennas", Radio Engng and Electronics, Phys. Vol. 13, nr. 2, pp.179-184, 1968.

127. Poisson J., "Extrait d'une lettre de M.Poisson a M.Fresnel", Annales de Chimie et de Physique, Vol.22, pp.270-280, 1823

EINDHOVEN UNIVERSITY OF TECHNOLOGY
EINDHOVEN (THE NETHERLANDS)
DEPARTMENT OF ELECTRICAL ENGINEERING

Reports:

1: Dijk, J., M. Jeuken and E.J. Maanders
AN ANTENNA FOR A SATELLITE COMMUNICATION GROUND STATION (PROVISIONAL ELECTRICAL DESIGN). TH-Report 68-E-01. March 1968. ISBN 90-6144-001-7

2: Veefkind, A., J.H. Blom and L.H.Th. Rietjens
THEORETICAL AND EXPERIMENTAL INVESTIGATION OF A NON-EQUILIBRIUM PLASMA IN A MHD CHANNEL. (Submitted to the Symposium on a Magnetohydrodynamic Electrical Power Generation, Warsaw, Poland, 24-30 July, 1968. TH-Report 68-E-2. March 1968. ISBN 90-6144-002-5

3: Boom, A.J.W. van den and J.H.A.M. Melis
A COMPARISON OF SOME PROCESS PARAMETER ESTIMATING SCHEMES. TH-Report 68-E-03. September 1968. ISBN 90-6144-003-3

4: Eykhoff, P., P.J.M. Ophey, J. Severs and J.O.M. Oome
AN ELECTROLYTIC TANK FOR INSTRUCTIONAL PURPOSES REPRESENTING THE COMPLEX-FREQUENCY PLANE. TH-Report 68-E-04. September 1968. ISBN 90-6144-004-1

5: Vermij, L. and J.E. Daalder
ENERGY BALANCE OF FUSING SILVER WIRES SURROUNDED BY AIR. TH-Report 68-E-05. November 1968. ISBN 90-6144-005-X

6: Houben, J.W.M.A. and P. Massee
MHD POWER CONVERSION EMPLOYING LIQUID METALS. TH-Report 69-E-06. February 1969. ISBN 90-6144-006-8

7: Heuvel, W.M.C. van den and W.F.J. Kersten
VOLTAGE MEASUREMENT IN CURRENT ZERO INVESTIGATIONS. TH-Report 69-E-07. September 1969. ISBN 90-6144-007-6

8: Vermij, L.
SELECTED BIBLIOGRAPHY OF FUSES. TH-Report 69-E-08. September 1969. ISBN 90-6144-008-4

9: Westenberg, J.Z.
SOME IDENTIFICATION SCHEMES FOR NON-LINEAR NOISY PROCESSES. TH-Report 69-E-09. December 1969. ISBN 90-6144-009-2

10: Koop, H.E.M., J. Dijk and E.J. Maanders
ON CONICAL HORN ANTENNAS. TH-Report 70-E-10. February 1970. ISBN 90-6144-010-6

11: Veefkind, A.
NON-EQUILIBRIUM PHENOMENA IN A DISC-SHAPED MAGNETOHYDRODYNAMIC GENERATOR. TH-Report 70-E-11. March 1970. ISBN 90-6144-011-4

12: Jansen, J.K.M., M.E.J. Jeuken and C.W. Lambrechtse
THE SCALAR FEED. TH-Report 70-E-12. December 1969. ISBN 90-6144-012-2

13: Teuling, D.J.A.
ELECTRONIC IMAGE MOTION COMPENSATION IN A PORTABLE TELEVISION CAMERA. TH-Report 70-E-13. November 1970. ISBN 90-6144-013-0

EINDHOVEN UNIVERSITY OF TECHNOLOGY
EINDHOVEN (THE NETHERLANDS)
DEPARTMENT OF ELECTRICAL ENGINEERING

Reports:

14: Lorencin, M.
AUTOMATIC METEOR REFLECTIONS RECORDING EQUIPMENT. TH-Report 70-E-14. November 1970. ISBN 90-6144-014-9

15: Smets, A.J.
THE INSTRUMENTAL VARIABLE METHOD AND RELATED IDENTIFICATION SCHEMES. TH-Report 70-E-15. November 1970. ISBN 90-6144-015-7

16: White, Jr., R.C.
A SURVEY OF RANDOM METHODS FOR PARAMETER OPTIMIZATION. TH-Report 70-E-16. February 1971. ISBN 90-6144-016-5

17: Talmon, J.L.
APPROXIMATED GAUSS-MARKOV ESTIMATORS AND RELATED SCHEMES. TH-Report 71-E-17. February 1971. ISBN 90-6144-017-3

18: Kalášek, V.
MEASUREMENT OF TIME CONSTANTS ON CASCADE D.C. ARC IN NITROGEN. TH-Report 71-E-18. February 1971. ISBN 90-6144-018-1

19: Hosselet, L.M.L.F.
OZONBILDUNG MITTELS ELEKTRISCHER ENTLADUNGEN. TH-Report 71-E-19. March 1971. ISBN 90-6144-019-X

20: Arts, M.G.J.
ON THE INSTANTANEOUS MEASUREMENT OF BLOODFLOW BY ULTRASONIC MEANS. TH-Report 71-E-20. May 1971. ISBN 90-6144-020-3

21: Roer, Th.G. van de
NON-ISO THERMAL ANALYSIS OF CARRIER WAVES IN A SEMICONDUCTOR. TH-Report 71-E-21. August 1971. ISBN 90-6144-021-1

22: Jeuken, P.J., C. Huber and C.E. Mulders
SENSING INERTIAL ROTATION WITH TUNING FORKS. TH-Report 71-E-22. September 1971. ISBN 90-6144-022-X

23: Dijk, J. and E.J. Maanders
APERTURE BLOCKING IN CASSEGRAIN ANTENNA SYSTEMS. A REVIEW. TH-Report 71-E-23. September 1971. ISBN 90-6144-023-8

24: Kregting, J. and R.C. White, Jr.
ADAPTIVE RANDOM SEARCH. TH-Report 71-E-24. October 1971. ISBN 90-6144-024-6

25: Damen, A.A.H. and H.A.L. Piceni
THE MULTIPLE DIPOLE MODEL OF THE VENTRICULAR DEPOLARISATION. TH-Report 71-E-25. October 1971. ISBN 90-6144-025-4

26: Bremmer, H.
A MATHEMATICAL THEORY CONNECTING SCATTERING AND DIFFRACTION PHENOMENA, INCLUDING BRAGG-TYPE INTERFERENCES. TH-Report 71-E-26. December 1971. ISBN 90-6144-026-2

EINDHOVEN UNIVERSITY OF TECHNOLOGY
EINDHOVEN (THE NETHERLANDS)
DEPARTMENT OF ELECTRICAL ENGINEERING

Reports:

27: Bokhoven, W.M.G. van
METHODS AND ASPECTS OF ACTIVE RC-FILTERS SYNTHESIS. TH-Report 71-E-27. March 1972. ISBN 90-6144-027-0

28: Boeschoten, F.
TWO FLUIDS MODEL REEXAMINED FOR A COLLISIONLESS PLASMA IN THE STATIONARY STATE. TH-Report 72-E-28. February 1972. ISBN 90-6144-028-9

29: REPORT ON THE CLOSED CYCLE MHD SPECIALIST MEETING. Working Group of the Joint ENEA/IAEA International MHD Liaison Group. Eindhoven, The Netherlands, September 20,21 and 22, 1971. Edited by L.H.Th. Rietjens. TH-Report 72-E-29. April 1972. ISBN 90-6144-029-7

30: Kessel, C.G.M. van and J.W.M.A. Houben
LOSS MECHANISMS IN AN MHD GENERATOR. TH-Report 72-E-30. June 1972. ISBN 90-6144-030-0

31: Veefkind, A.
CONDUCTING GRIDS TO STABILIZE MHD GENERATOR PLASMAS AGAINST IONIZATION INSTABILITIES. TH-Report 72-E-31. September 1972. ISBN 90-6144-031-9

32: Daalder, J.E. and C.W.M. Vos
DISTRIBUTION FUNCTIONS OF THE SPOT DIAMETER FOR SINGLE- AND MULTI-CATHODE DISCHARGES IN VACUUM. TH-Report 73-E-32. January 1973. ISBN 90-6144-032-7

33: Daalder, J.E.
JOULE HEATING AND DIAMETER OF THE CATHODE SPOT IN A VACUUM ARC. TH-Report 73-E-33. January 1973. ISBN 90-6144-033-5

34: Huber, C.
BEHAVIOUR OF THE SPINNING GYRO ROTOR. TH-Report 73-E-34. February 1973. ISBN 90-6144-034-3

35: Bastian, C., F. Boeschoten, H. Hekman, H.P. Riske and A. van Iersel
THE VACUUM ARC AS A FACILITY FOR RELEVANT EXPERIMENTS IN FUSION RESEARCH. Annual Report 1972. Euratom-T.H.E. Group "Rotating Plasma". TH-Report 73-E-35. February 1973. ISBN 90-6144-035-1

36: Blom, J.A.
ANALYSIS OF PHYSIOLOGICAL SYSTEMS BY PARAMETER ESTIMATION TECHNIQUES. TH-Report 73-E-36. May 1973. ISBN 90-6144-036-X

37: This number was cancelled.

38: Andriessen, F.J., W. Boerman and I.F.E.M. Holtz
CALCULATION OF RADIATION LOSSES IN CYLINDRICAL SYMMETRICAL HIGH PRESSURE DISCHARGES BY MEANS OF A DIGITAL COMPUTER. TH-Report 73-E-38. August 1973. ISBN 90-6144-038-6

39: Dijk, J., C.T.W. van Diepenbeek, E.J. Maanders and L.F.G. Thurlings
THE POLARIZATION LOSSES OF OFFSET ANTENNAS. TH-Report 73-E-39. June 1973. ISBN 90-6144-039-4